Theses and Dissertations   1. Thesis and Dissertation Collection, all items

1966-05

Experimental determination of heat transfer and flow friction characteristics for several plate fin type compact heat exchanger surfaces

Ball, Stuart Franklin, Jr.

Monterey, California. Naval Postgraduate School

http://hdl.handle.net/10945/9509

EXPERIMENTAL DETERMINATION OF HEAT
TRANSFER AND FLOW FRICTION
CHARACTERISTICS FOR SEVERAL PLATE FIN
TYPE COMPACT HEAT EXCHANGER SURFACES

STUART FRANKLIN BALL, JR.

5-24

EXPERIMENTAL DETERMINATION OF HEAT TRANSFER

AND FLOW FRICTION CHARACTERISTICS FOR SEVERAL

PLATE FIN TYPE COMPACT HEAT EXCHANGER

SURFACES

by

Stuart Franklin Ball, Jr.
Lieutenant, United States Navy
B.S., United States Naval Academy, 1959

Submitted in partial fulfillment
for the degree of

MASTER OF SCIENCE IN MECHANICAL ENGINEERING

from the

UNITED STATES NAVAL POSTGRADUATE SCHOOL
May 1966

ABSTRACT

In this report, the heat transfer and isothermal flow friction characteristics for seven compact heat exchanger surfaces are presented and compared. Five of the surfaces were of a similar triangular fin configuration, differing in material and method of construction, and two of the surfaces, having been tested previously, were of a modified rectangular passage configuration. The modified rectangular passage surfaces showed better overall performance than the triangular fin sur- faces, and matrices constructed from perforated material showed better overall performance than similar surfaces constructed from non-perforat- ed material. For similar matrix configurations, small variations in manufacturing procedure had little effect upon heat transfer and flow friction performance.

The heat transfer data was obtained by means of the single-blow transient testing technique. A cylic method of transient testing was also investigated, and found to be both reliable and useful in that the additional method of testing extends the Reynolds number range for the experimental apparatus.

TABLE OF CONTENTS

LIST OF ILLUSTRATIONS

4

LIST OF TABLES

NOMENCLATURE

English Letter Symbols

A	Matrix total heat transfer area	sq ft
A_b	Base area (plane surface area)	sq ft
A_c	Matrix minimum free flow area	sq ft
A_{fr}	Matrix total frontal area	sq ft
A_o	Open area of matrix material due to perforations ·	sq ft
A_s	Matrix solid cross sectional area available for thermal conduction	sq ft
A_k	Matrix solid cross sectional conduction area considering effect of matrix material perforations	sq ft
c_p	Specific heat (gas) at constant pressure	Btu/(lbm deg F)
c_s	Matrix material specific heat	Btu/(lbm deg F)
C_f	Flow stream capacity rate (mc_p)	Btu/(hr deg F)
C_s	Matrix heat capacity ($W_s c_s$)	Btu/(deg F)
D_H	Hydraulic diameter of internal passage	ft
E	Friction power expended per unit of surface heat transfer area	hp/sq ft
F	Frequency of sinusoidal temperature oscillation	cycles/sec
G	Matrix flow stream mass velocity (m/Ac)	lbm/(hr sq ft)
g_c	Proportionality factor in Newton's second law	32.2(lbm ft)/(lbf sec^2)
h	Thermal convection surface heat transfer coefficient; heat transfer power per unit area per degree temperature difference	Btu/(hr sq ft deg F)
K_c	Loss coefficient for sudden flow contraction at matrix entrance	dimensionless

7

K_e	Loss coefficient for sudden flow expansion at matrix exit	dimensionless
k	Unit thermal conductivity	Btu/(hr sq ft deg F/ft)
k_s	Matrix material thermal conductivity	Btu/(hr sq ft deg F/ft)
L	Total matrix flow length	ft
m	Mass flow rate	lbm/hr
P	Pressure	lbf/sq ft
p	Matrix porosity (A_c/A_{fr})	dimensionless
q	Heat transfer rate	Btu/hr
R	Universal gas constant (53.35 for air)	(ft lbf)/(lbm deg R)
r	Electrical resistance	ohm
r_H	Hydraulic radius $(A_c L/A_b)$	ft
t	Temperature	deg F
u	Flow velocity	ft/sec
V_m	Matrix volume	cu ft
V_s	Matrix material volume (corrected for effects of perforations)	cu ft
W_s	Matrix mass	lbm
x	Distance from matrix inlet in flow direction	ft

8

Greek Letter Symbols

β	Area density; compactness (ratio of matrix total heat transfer area to core volume-A/V)	sq ft/cu ft
Δ	Difference or change (time, distance, temperature)	-
η_f	Fin efficiency	-
θ	Time	Sec, hr.
μ	Fluid viscosity (dynamic)	lbm/hr ft
ν	Open area ratio due to matrix material perforations	-
ρ	Density	lbm/cu ft
σ	Ratio of free flow to frontal area (A_c/A_{fr})	dimensionless
φ	Denotes "function of"	-
ω_0	Angular frequency of temperature oscillation	rad/sec

Subscripts

atm	Local atmosphere
ave	Average
f	Fluid (gas, air)
i	Initial, inlet, individual
k	Equilavent
m	Mean, matrix
o	At orifice
s	Solid (matrix material), static
STD	Standard (temperature and pressure)
w	Wall (solid surface)
x	Local conditions
1	At inlet (upstream of heating elements)
2	At matrix inlet (downstream of heating)
3	At matrix exit

Dimensionless Groupings

f   Fanning friction factor (Ratio of wall shear stress to the fluid dynamic head). This factor is plotted versus N_R to illustrate the flow friction characteristics of a matrix surface.

j   Colburn Factor ($N_{St} N_{Pr}^{2/3}$), a generalized heat transfer grouping. This factor is plotted versus N_R to illustrate heat transfer characteristics of a matrix surface

M   Flow parameter ($\dot{m} c_p / W_s c_s \omega_o$)

N_{Nu} Nusselt number ($h D_H / k$), a heat transfer modulus

N_{Pr} Prandtl number ($\mu c_p / k$), a fluid properties modulus

N_R Reynolds number ($D_H G / \mu$), a flow modulus

N_{St} Stanton number ($h / G c_p$), a heat transfer modulus

Ntu   Number of heat transfer units ($h A / \dot{m} c_p$), a heat transfer parameter

R_A Ratio of matrix outlet temperature amplitude to matrix inlet temperature amplitude during cyclic temperature variation

λ Longitudinal heat conduction parameter for solid matrix material ($K_s A_s / \dot{m} L c_p$).

λ_K Longitudinal heat conduction parameter for perforated matrix material ($K_s A_K / \dot{m} L_K c_p$).

ξ Distance parameter (x/L)

τ Time parameter ($h A / W_s c_s$) used in Locke's analysis

$\bar{\tau}$ Time parameter ($u \theta / L$) used in Cyclic technique

ω Frequency parameter ($\omega_o L / u$) used in cyclic technique

1. INTRODUCTION

A compact heat exchanger may be defined as a heat exchanger having a large heat transfer surface area per cubic foot of core volume. Arbitrarily, heat exchangers with more than 200 square feet of heat transfer area per cubic foot of core volume are considered compact. Applications of particular interest for compact heat exchangers, are gas turbine power plants in aircraft, automobiles, and small seagoing craft. In all these applications the designer is limited by weight, flow frontal area, core volume, and pressure drop across the heat exchanger. An effective basis for presentation and comparison of heat transfer and flow friction data for various heat transfer surfaces and core configurations is by plotting the dimensionless groupings- Colburn's heat transfer factor, "j", and the Fanning friction factor, "f", versus Reynolds number for heat exchanger surfaces.

The data presented in this report was obtained by means of the single-blow transient testing technique described in the two sections following, and in reference [24]. The objectives of this thesis were to obtain and compare flow friction and heat transfer data for compact heat exchanger matrices of different configuration, to correlate this data obtained with data obtained for identical surfaces by means of a steady state steam-to-air testing technique, and to develop a testing technique that will extend the range of transient testing to higher Reynolds numbers.

13

2. SUMMARY OF THEORY

    A. BACKGROUND

        Analytical development of the theory for the single-blow or transient heating/cooling problem was performed in the 1920's by Anzelius (1926), Nusselt (1927), Hausen (1927-1929), and Schumann (1929).

        There was some duplication of effort in that Nusselt did not know of Anzelius' publication, and Schumann was unaware of the work of Anzelius and Nusselt. Anzelius and Schumann used similar procedures. Anzelius represented the gas and solid temperatures as unsolved, relatively simple integrals, where Schumann derived and solved explicitly two infinite series utilizing Bessel functions. Schumann's solution was for a liquid flowing through a porous solid, however, dimensional analysis may be used to make his analysis applicable to gasses [24]. Hausen's derivation was similar to Schumann's, and in addition Hausen also solved the equations for cyclic heating and cooling. Nusselt's derivation was more simplified than Hausen's or Schumann's, but it is worth noting that Nusselt was the only one who considered the problem as part of a regenerator theory [10]. A summary of the single blow theory as it applies to a gas flowing through a porous solid is presented below.

    B. THEORY

        A homogeneous, porous solid has a fluid flowing through it. Both fluid and solid are at the same constant, uniform temperature. After a step change in the entering fluid temperature, the temperature of the solid and the fluid are to be determined as functions of time and position (along the flow length of the solid).

14

Starting with an energy balance in the matrix:

$$\dot{m}\, c_P\, t_F$$

$$\dot{m}\, c_P\left(t_F + \frac{\partial t_F}{\partial x}dx\right)$$

$$hb(t_F - t_s)dx$$

$$-K_s A_s \frac{\partial t_s}{\partial x}$$

A_s | Solid | b

$$-K_s A_s\left(\frac{\partial t_s}{\partial x} + \frac{\partial^2 t_s}{\partial x^2}dx\right)$$

$$\longleftarrow dx \longrightarrow$$
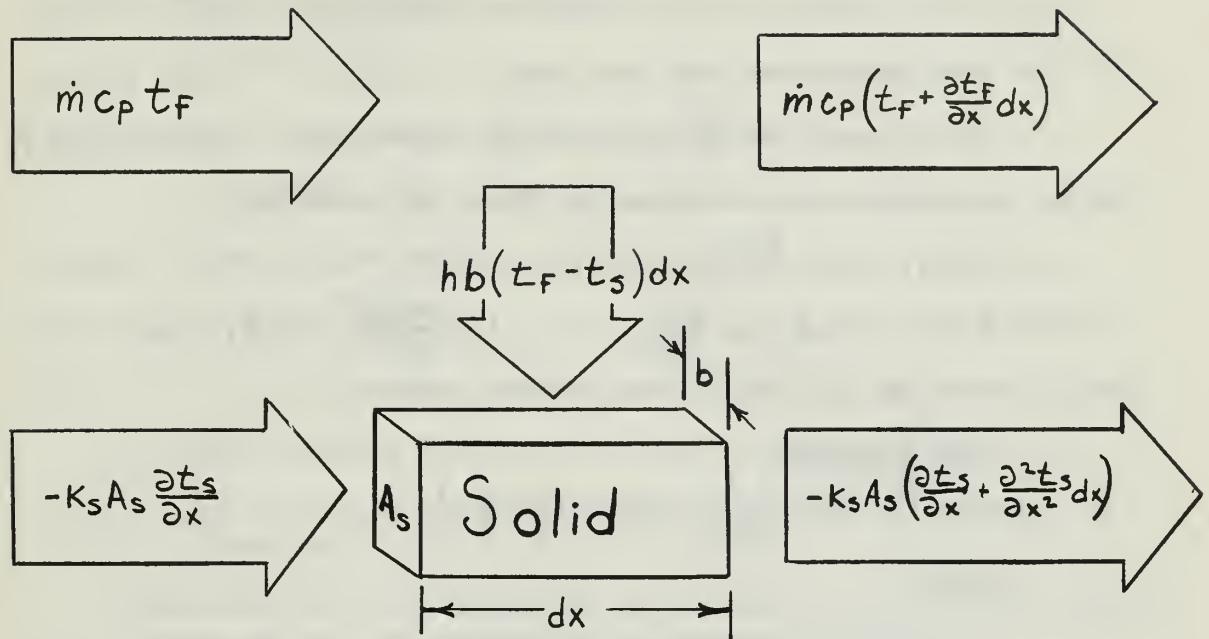
Assumptions:

(1) The fluid properties are temperature independent.

(2) The fluid flow is steady.

(3) The porous solid is homogeneous.

(4) The thermal conductivities of the solid and the fluid are
infinite in the direction perpendicular to the fluid flow.

(5) The thermal conductivity of the fluid is zero in the flow
direction.

Boundary conditions:

(1) The matrix is initially at uniform temperature.

(2) At time zero, there is a step change in the entering fluid
temperature.

(3) The matrix boundaries are adiabatic.

15

Heat rates from the above energy diagram are:

(1) Heat absorbed by the solid: $\rho_s A_s c_s \frac{\partial t_s}{\partial \theta} dx$

(2) Heat transferred to the solid by convection: $hb(t_F - t_s)dx$

(3) Heat transferred from the fluid: $\dot{m} c_p \frac{\partial t_F}{\partial x} dx$

(4) Heat transferred in the solid by conduction: $-K_s A_s \frac{\partial^2 t_s}{\partial x^2} dx$

The net resulting energy balances for fluid and solid are:

(1) Fluid: $\dot{m} c_p \frac{\partial t_F}{\partial x} dx + hb(t_F - t_s)dx = 0$ (2-1)

(2) Solid: $\rho_s A_s c_s \frac{\partial t_s}{\partial \theta} dx = K_s A_s \frac{\partial^2 t_s}{\partial x^2} dx + hb(t_F - t_s)dx$ (2-2)

Now introduce the following dimensionless parameters:

(1) <u>Time parameter</u>

$$\tau = \frac{hA}{W_s c_s}\left(\theta - \frac{W_f}{\dot{m}}\frac{x}{L}\right)$$ (2-3)

    Where:

h = unit conductance for convective heat transfer

A = matrix heat transfer area (sq ft)

$W_s c_s$ = matrix capacity (Btu/deg F)

θ = time (hours)

W_F = mass of fluid contained within matrix (lb m)

$\dot{m}$ = fluid mass flow rate (lbm/hr)

x = distance from matrix inlet in flow direction (ft)

L = matrix flow length (ft)

Introducing the fluid specific heat, and regrouping, (2-3) becomes:

$$\tau = \frac{hA}{W_s c_s}\theta - \frac{hA}{\dot{m} c_p}\frac{x}{L}\frac{W_F c_p}{W_s c_s}$$ (2-4)

The term $\frac{W_F c_p}{W_s c_s}$ is very small since the thermal capacity of the matrix is much greater than the thermal capacity of the fluid contained within it. Thus, the dimensionless time parameter can be reduced to:

16

$$\tau \approx \frac{hA}{W_s c_s} \theta \tag{2-5}$$

(2) <u>Position parameter</u>:

$$z = \frac{hA}{\dot{m} c_p} \frac{x}{L} \tag{2-6}$$

Since the Number of Transfer Units, $N_{tu} = \frac{hA}{\dot{m} c_p}$:

$$z = N_{tu} \frac{x}{L} \tag{2-7}$$

(3) <u>Conduction parameter</u>:

$$\lambda = \frac{k_s A_s}{\dot{m} c_p L} \tag{2-8}$$

Where:

k_s = matrix thermal conductivity (Btu/hr sq ft deg F/ft)

A_s = solid matrix cross sectional area available for thermal conduction (sq ft)

Introducing the above dimensionless parameters into the heat balance equations for the fluid and solid, and rearranging yields:

Fluid: $\quad \dfrac{\partial t_F}{\partial z} = t_s - t_F \tag{2-9}$

Solid: $\quad \dfrac{\partial t_s}{\partial \tau} = t_F - t_s + \lambda N_{tu} \dfrac{\partial^2 t_s}{\partial z^2} \tag{2-10}$

If thermal conduction in the solid is assumed zero in the direction of flow, the above equations simplify:

$$\frac{\partial t_F}{\partial z} = t_s - t_F \tag{2-11}$$

$$\frac{\partial t_s}{\partial \tau} = t_F - t_s \tag{2-12}$$

From equations (2-11) and (2-12), Schumann, utilizing Bessel functions, developed his temperature-time-distance relationships:

$$\frac{t_F - t_i}{t_{f_1} - t_i} = 1 - e^{-(z+\tau)} \sum_{n=1}^{\infty} z^n \frac{d^n [J_0(2i\sqrt{\tau z})]}{d[\tau z]^n} \tag{2-13}$$

$$\frac{t_s - t_i}{t_{F_1} - t_i} = 1 - e^{-(z+\tau)} \sum_{n=0}^{\infty} z^n \frac{d^n [J_0(2i\sqrt{\tau z})]}{d[\tau z]^n} \tag{2-14}$$

Plots of these functions versus z appear in Figure 1. Using these curves to determine N_{tu} from experimental data would be a tedious task

involving infinite series computations and curve comparisons. However, in his maximum slope technique, Locke [15] differentiated the theoretical curves, plotting slope versus τ/Ntu for various values of Ntu. Locke's expression for slope is:

$$\frac{d\left(\frac{t_{F_2}-t_i}{t_{F_1}-t_i}\right)}{d\left(\tau/Ntu\right)} = \frac{Ntu^2}{\sqrt{\tau \, Ntu}}\left[-J_1\left(2i\sqrt{\tau \, Ntu}\right)e^{-(Ntu+\tau)}\right] \quad (2\text{-}15)$$

The downstream fluid temperature is taken at x = L so that $\bar{z}$ becomes Ntu and $t_f = t_{f_2}$. Locke also evaluated the maximum slope of the temperature curve for each Ntu, and plotted maximum slope versus Ntu, a single curve. Figures 2 and 3 show Locke's curves.

Both Schumann and Locke assumed thermal conductivity of the solid, in the flow direction, to be zero. The effect of longitudinal thermal conductivity is small in the high Reynolds number range, but it is considerable and should be taken into account in the low Reynolds range. To account for longitudinal thermal conduction, equations (2-9) and (2-10) must replace equations (2-11) and (2-12). Thus, the maximum slope will depend upon both Ntu and λ . Howard [9], utilizing a digital computer and finite difference technique, tabulated and plotted Ntu versus maximum slope for various values of λ . Howard's curves appear in Figures 4 through 6. By means of a properly designed experimental apparatus which satisfies Howard's idealizations and boundary conditions, the maximum slope of the heating or cooling curve and the conduction parameter can be determined. Ntu can then be found using Howard's data shown in Figure 5.

In the vicinity of Ntu = 2, it can be seen from Figure 6 that there can be considerable error in Ntu for a small error in maximum slope.

18

In addition, it is more difficult to accurately determine maximum slope in the high Reynolds number region, as the maximum slope occurs earlier in time as Ntu decreases, and the determination of the maximum slope becomes difficult, having large uncertainties due to the inherent time response of the instrumentation.

Another theory for determining the heat transfer characteristics of a porous solid, based upon a sinusoidally varying fluid temperature at the matrix inlet, was developed by Bell and Katz [2]. Starting as before with an energy balance in the matrix:

$$\dot{m}c_p t_F \qquad\qquad \dot{m}c_p\!\left(t_F + \frac{\partial t_F}{\partial x}dx + \frac{\partial t_F}{\partial \theta}d\theta\right)$$

$$hb(t_F - t_s)dx$$

Solid

$$\vert\!\!\leftarrow \quad b \quad \rightarrow\!\!\vert$$

$$\vert\!\!\leftarrow \quad dx \quad \rightarrow\!\!\vert$$
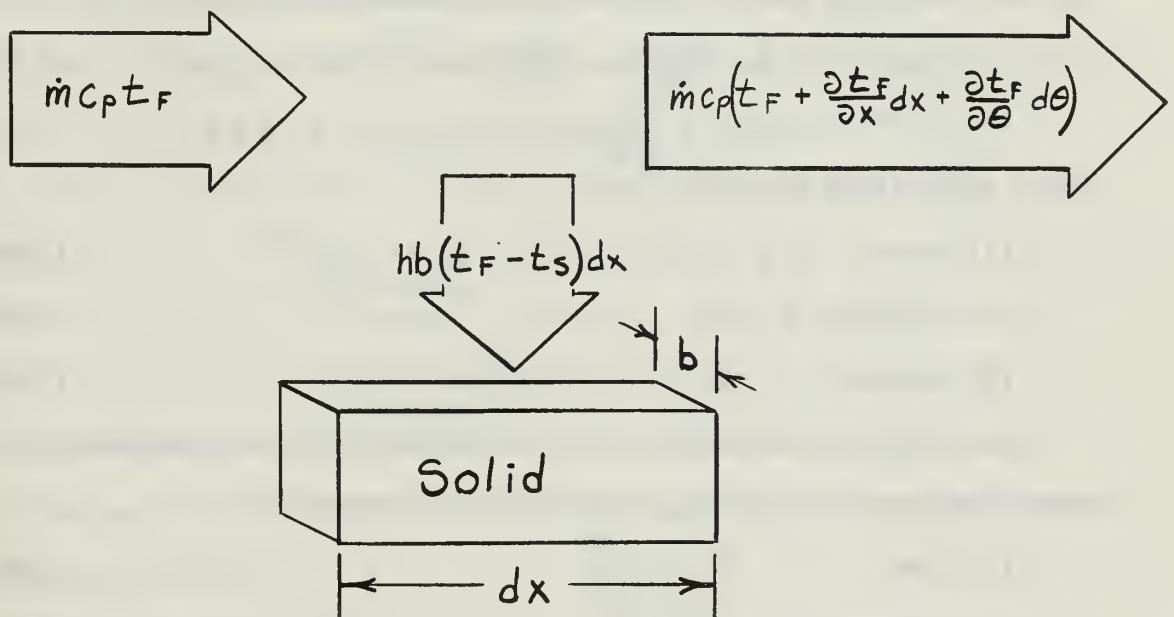
Assumptions:

(1) All cross sections of the solid normal to the flow direction are uniform.

(2) The fluid velocity is uniform throughout the matrix.

(3) The fluid properties are temperature independent.

(4) Thermal conductivity of the solid and fluid is infinite in the direction normal to fluid flow.

(5) Thermal conductivity of the fluid and solid is zero in the direction parallel to the fluid flow.

(6) The matrix boundaries are adiabatic.

(7) The convective heat transfer coefficient remains constant.

Heat rates from the above heat balance are:

(1) Heat absorbed by the solid: $\rho_s A_s c_s \frac{\partial t_s}{\partial \theta}$

(2) Heat transferred to the solid by convection: $hb(t_F - t_s)dx$

(3) Heat absorbed by the fluid: $\dot{m} c_p \left(\frac{\partial t_F}{\partial x} dx + \frac{\partial t_F}{\partial \theta} d\theta \right)$

(4) Heat transferred in the solid by conduction: 0

The net resulting energy balances for fluid and solid are:

(1) Fluid: $\dot{m} c_p \left(\frac{\partial t_F}{\partial x} dx + \frac{\partial t_F}{\partial \theta} d\theta \right) = hb(t_F - t_s)dx$ (2-16)

(2) Solid: $\rho_s A_s c_s \frac{\partial t_s}{\partial \theta} dx = hb(t_F - t_s)dx$ (2-17)

Inlet and initial conditions are:

(1) Inlet: $t_F(0, \theta) = t_m + \Delta \sin \omega_o \theta$ (2-18)

(2) Initial: $t_s(0) = t_{s_o}$ (2-19)

(3) Initial: $t_F(x, 0) = t_o(x)$ (2-20)

where Δ is the amplitude of the sinusoidally varying temperature.

Now introduce the following dimensionless parameters:

(1) Time: $\tau = \frac{u\theta}{L}$ (2-21)

(2) Distance: $\xi = \frac{x}{L}$ (2-22)

(3) Frequency: $\omega = \frac{\omega_o L}{u}$ (2-23)

(4) Flow: $M = \frac{\dot{m} c_p}{W_s c_s \omega_o}$ (2-24)

(5) Heat transfer: $N_{tu} = \frac{hA}{\dot{m} c_p}$ (2-25)

Where:

u = flow velocity   (ft/sec)

θ = time   (sec)

L = matrix flow length   (ft)

20

X = distance from matrix inlet in flow direction   (ft)

ω_o = angular frequency of temperature oscillation   (rad/sec)

Introducing the above dimensionless parameters into equations (2-16) through (2-20) and rearranging yields:

(1) $\dfrac{\partial t_F}{\partial \xi} + \dfrac{\partial t_F}{\partial \tau} + Ntu\left(t_F - t_s\right) = 0$ (2-26)

(2) $\dfrac{\partial t_s}{\partial \tau} - M\omega Ntu\left(t_F - t_s\right) = 0$ (2-27)

(3) $t_F(0,\tau) = t_m + \Delta \sin \omega \bar{\tau}$ (2-28)

(4) $t_s(0) = t_{s_o}$ (2-29)

(5) $t_F(\xi,0) = t_o(\xi)$ (2-30)

This system has the periodic solution:

$$t_F(\xi,\bar{\tau}) = t_m + \Delta e^{-\alpha \xi} \sin\left(\omega \bar{\tau} - \beta \xi\right) \qquad (2\text{-}31)$$

$$t_s(\xi,\bar{\tau}) = t_m + \Delta \alpha e^{-\alpha \xi}\left[M Ntu \sin\left(\omega \bar{\tau} - \beta \xi\right) - \cos\left(\omega \bar{\tau} - \beta \xi\right)\right] \qquad (2\text{-}32)$$

Where:

$$\alpha = \frac{Ntu}{1 + (M Ntu)^2}$$

$$\beta = \frac{M Ntu^2}{1 + (M Ntu)^2} + \omega$$

A simple quantity to determine experimentally is R_A, the ratio of the amplitude of outlet and inlet gas temperatures. Straightforward calculation shows:

$$R_A = \frac{\Delta e^{-\alpha}}{\Delta} = e^{-\frac{Ntu}{1+(M Ntu)^2}} \qquad (2\text{-}33)$$

A plot of Ntu versus R_A for various values of M is shown in Figure 7. The same experimental apparatus can be used for this cyclic operation as is used for the maximum slope method. The only addition needed is a method to sinusoidally vary the temperature of the air entering the matrix.

Thus, heat transfer data can be determined for a wide range of

21

Reynolds numbers utilizing two testing methods on a single experimental apparatus; the single-blow technique producing heat transfer data for low Reynolds numbers, and the cyclic technique producing data for high Reynolds numbers.

3. EXPERIMENTAL TECHNIQUES

A. Single Blow Technique

For Reynold's numbers up to approximately 1,000, the results of Howard's work [9] were used in determining the heat transfer data, Ntu and j, appearing in this report. In order to utilize Howard's theoretical data, the experimental apparatus had to conform to the idealizations stated in reference [9].

Idealizations:

(1) The fluid flowing through the matrix remains steady and uniform in velocity and temperature at any cross section. The matrix thermal conductivity is infinite in the direction normal to fluid flow, and finite in the direction parallel to fluid flow. Thus the problem is one-dimensional in space.

(2) The thermal capacity of the matrix is large compared with the fluid contained within it. This restricts the fluid to a gas, and means that there will be no time dependent terms in the equations for the fluid.

(3) The thermal properties of the fluid and matrix are constant and uniform.

(4) The convective heat transfer coefficient is some suitable average and remains constant.

(5) At time zero, the change in fluid temperature is a step change, with the matrix and its entrained fluid initially at uniform and equal temperatures.

The test apparatus utilized for this report satisfies the above idealizations as described below:

(1) A square cross section contracting cone and screen type flow straighteners provided the necessary uniform velocity profile. In addition, the matrix test section was located as far upstream as possible to take advantage of this uniform velocity profile. The flow rate measuring apparatus was located downstream. The heater configuration, Figure 10, insured a uniform temperature profile due to even distribution of heat over the flow cross section. The thermal conductivity in the direction parallel to fluid flow is taken care of by the use of the conduction parameter λ.

(2) The use of a gas as the fluid flowing satisfies idealization (2).

(3,4) A small temperature variation will insure uniform solid and fluid physical properties. At 80°F, a temperature variation of $\pm$ 10°F will result in an air viscosity variation of approximately $\pm$ 1.5%. The changes in specific heats and thermal conductivities are negligible for a $\pm$ 10°F change in temperature.

(5) Various methods have been devised to produce a step change in matrix inlet temperature. The electric heater arrangement used in this report appears to produce the closest approximation to the desired step change with a minimum effect on flow properties [24].

A schematic diagram of the experimental apparatus is shown in Figure 8. Photographs of various components are shown in Figures 9 through 14. The system is comprised of an entrance section with a contracting cone and a screen flow straightener, a heat section consisting of 28 resistance type wire heaters made of nichrome wire in grid fashion, a matrix test section, an orifice metering section, a flow control valve and prime mover, and pressure and temperature measuring and recording

24

systems. Each of these components are further described in Appendix A. The experimental procedure for the single blow technique is as follows:

Air is drawn through the system by means of a 30 horsepower Spencer Turboblower. The heater section is designed to heat the air to approximately twenty degrees above ambient temperature. The mass flow rate is measured by means of an ASME orifice meter with removable orifice plates.

Flow friction data is obtained by measuring the isothermal pressure drop across the matrix and the mass flow rate through the orifice meter.

Heat transfer data is obtained as follows: the heaters are energized to heat the air to approximately twenty degrees above ambient temperature. When the matrix has been heated to a uniform temperature, the heaters are quickly de-energized and the time-temperature history of the air leaving the matrix is recorded on a Minneapolis Honeywell "Brown" strip chart recorder.

The following data is recorded for each test run:

(1) Atmospheric pressure $\quad\quad\quad\quad\quad\quad P_{atm}$

(2) Static pressure upstream of matrix $\quad\quad\quad P_s$

(3) Pressure drop across the matrix $\quad\quad\quad \Delta P_m$

(4) Static pressure upstream of orifice $\quad\quad P_o$

(5) Pressure drop across the orifice $\quad\quad\quad \Delta P_o$

(6) Temperature upstream of orifice $\quad\quad\quad t_o$

(7) Orifice diameter $\quad\quad\quad\quad\quad\quad\quad d_o$

(8) Time-temperature cooling curve

(9) Recorder chart speed

B. Cyclic Technique:

To obtain heat transfer data by means of the cyclic temperature variation method, the same testing apparatus can be used, the only modification being in the power input to the heaters. The idealizations set forth by reference [2] are the same as those imposed by reference [9] and shown on the previous pages with two exceptions:

(a) The thermal conductivity of the solid is zero in the direction parallel to the fluid flow.

(b) The temperature of the matrix inlet varies sinusoidally. To satisfy idealization (a), this testing method is restricted to the high Reynolds number ranges ($N_R > 500$), where Ntu is small (Ntu $<$ 5), and the effect of longitudinal thermal conduction is small and can be neglected.   (See Figure 15 and Chapter 5).

To satisfy idealization (b), sinusoidally varying power is applied to the heaters by means of a 1.5 KW Amplidyne receiving field excitation from a variable frequency function generator. This system is described further in Appendix B.

To obtain heat transfer data, the temperatures of the matrix inlet and exit are recorded on the strip chart recorder. The amplitudes of the cyclic variation of these two temperature curves are then measured and Ntu is determined from the ratio of the amplitudes and the dimensionless parameter, M. Figure 15 shows a sample chart trace for a cyclic test.

The same data are recorded as for the maximum slope technique.

Data reduction relationships for both of these transient testing techniques are described in Appendix B.

26

4. DESCRIPTION OF MATRICES

The surfaces investigated in this report are of two major varieties modified rectangular passage and triangular fin.

The modified rectangular passage surfaces, previously examined by Bannon [1], and Piersall [22], are constructed of formed sheets separated by flat splitter plates as shown below. The matrix approximates one made up of rectangular passages. The rectangular passages have an aspect ratio, α , of approximately 7:
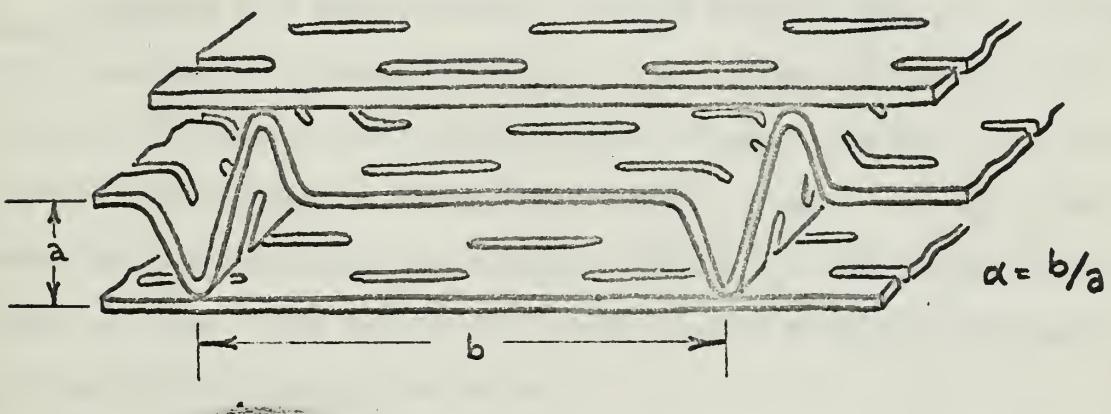
One parallel plate matrix is made from .0022 inch thick perforated nickel and the other from .002 inch thick solid nickel. The perforations are of type 160/40 TV and are described further in Appendix C.

The five triangular fin matrices, provided by Solar, A Division of International Harvester, San Diego, were of varied material and method of construction. Geometric and physical data for these matrices appear in Figures 16 through 22. Two were made from nickel; one had fins made from .005 inch thick solid material, the other had fins made from type 80/20 T perforated nickel material .0047 inches thick. The other three triangular fin matrices were made from .005 inch thick type 430 stainless steel, and had no perforations. Of these stainless steel matrices, one had fins with very sharp bends, (all others had approximately sinusoidal corrugations), one had maximum fillet braze joints where fins and

splitters touched, (all others were not bonded by any means), and the last stainless steel surface was similar in shape and construction to its solid nickel finned counterpart. All of the triangular fin matrices had a fin height of .1 inches and 10 fins per inch. All of the matrices measured 3-1/16 inch high X 3-1/16 inch wide. The modified rectangular passage matrices were 2 inches in flow length, while the triangular finned ones were 3 inches long. Geometric and physical data for all matrices appear in Figures 16 through 22.

5. PRESENTATION OF RESULTS

Heat transfer and flow friction data for all surfaces tested are shown in TABLES I through VII and Figures 23 through 35. In Figures 23 through 31 the Colburn heat transfer modulus, j, and Fanning friction factor, f, are plotted versus Reynolds number. The Reynolds number was based on hydraulic diameter. In Figure 32, all surfaces are compared by a plot of j/f versus Reynolds number, and Figure 33 is a plot, for all surfaces, of heat transfer power versus flow friction power on a unit area basis.

Figure 34 is a plot of Colburn j versus Reynolds number for the brazed stainless steel triangular fin surface. The j values for this plot were obtained by means of both the single-blow technique, and the cyclic temperature variation technique described in Chapters 2 and 3. For $N_R <$ 1000 the single-blow technique was employed, and for $N_R >$ 500 the cyclic technique was used. This was the only surface tested by means of the cyclical temperature variation technique.

Figure 15 shows a plot of Colburn j versus Reynolds number for the perforated nickel rectangular passage matrix. This plot shows the effects of varying the longitudinal conduction parameter, λ . One curve results from assuming $\lambda = 0$, the second curve results from the calculated in reference [22] and described in Appendix C, and the third curve results from an electrical analogy method calculation of λ which is also described in Appendix C.

Figure 35 is a plot of Colburn j versus Reynolds number for the perforated nickel triangular fin matrice. the data for this curve was obtained by means of both the single blow technique and a steady state steam to air technique described in reference [29].

In Figure 36, experimental and theoretical data are compared for the brazed triangular fin matrix.

30

6. EXPERIMENTAL UNCERTAINTIES

The experimental uncertainties for the heat transfer and friction data appearing for this report were determined by the method described in reference [13] and shown in Appendix D. These uncertainties arise from possible errors in:

(1) <u>Physical constants</u> - These physical constants were obtained from references [6], [7], and [8], and their uncertainties are estimated to be as follows:

$$k_s \quad \pm\ .5\%$$
$$c_s \quad \pm\ .5\%$$
$$c_p \quad \pm\ .5\%$$
$$N_{Pr} \quad \pm\ 2.0\%$$
$$\mu \quad \pm\ 1.0\%$$

(2) <u>Geometric measurements</u> - These errors are due to construction inaccuracies and errors in linear measurement and are estimated to be as follows:

$$A_c\ ,\ A_{fr},\ A\ ,\ A_s \quad \pm\ 1.0\%$$
$$L \quad \pm\ .5\%$$
$$W_s \quad \text{negligible}$$

(3) <u>Instrumentation</u> - Assuming adequate manufacturer's calibration a manometers and thermocouple wire, instrumentation errors will be assumed to be due to instrument fluctuations (manometers), and size of scale divisions (manometers and potentiometer).

<u>Pressures</u>:

$$P_s \quad \pm\ 1.0\%$$
$$\Delta P_m \quad \pm\ 1.0\%$$

31

$$P_o \quad \pm \ 1.0\%$$

$$\Delta P_o \quad \pm \ 1.0\%$$

$$P_{ATM} \quad \text{negligible}$$

The error for the manometers depends upon the range of the pressure being read. In the range 1 to 3 inches of water, the error is .17% to .5% in the range 3 to 5 inches of water, the error is 1.0% to 1.7%.

Temperatures:

$$t_o \pm 1.5 \ deg \ F$$

Maximum Slope:

The measurement of maximum slope involves the drawing of a tangent and the linear measurement of three quantities x , y , and m , as described in Appendix A. The percent error in maximum slope is estimated as $\pm$ 2.0%. Entering Figure (7) with this value at Ntu = 3.0 and λ = 0, obtain Ntu error as $\pm$ 7.2%. At Ntu = 25 and λ = .05, Ntu error is $\pm$ 10.0% for a 2.0% error in maximum slope.

A summary of extreme values of uncertainty intervals calculated by the method shown in Appendix D is given below:

$$\dot{m} \quad \pm \ 1.0\%$$

$$N_R \quad \pm \ 2.3\%$$

$$j \quad \pm \ 10\%$$

$$f \quad \pm \ 4\%$$

7.   DISCUSSION OF RESULTS

Heat transfer and flow friction results appear in Figures 23 through 36, with comparisons of all surfaces in Figures 31 through 33.

In general, the triangular fin surfaces all had similar j and f curves; the nickel matrices having higher j and j/f values than the stainless steel matrices. The high j and j/f for the nickel surfaces are due chiefly to the high thermal conductivity of nickel - 36.0 compared to 12.8 for 430 stainless steel (at 80°F). The j,f, and j/f characteristics for the triangular fin surfaces are in agreement with the theory presented in reference [16] for laminar flow through idealized cross sections (see Figure 36).

The three stainless steel cores were quite similar in cross section, however, one might expect to find small differences in their heat transfer and flow friction characteristics due to slight differences in geometry. The rounded corners produced by the sine wave corrugations in two of the surfaces should reduce the effective surface area for heat transfer and wall friction as mentioned in reference [16]. The experimental results seem to agree in part with the above - the sharp cornered triangular passage geometry yielded higher friction factors than the sinusoidal fin geometry, with the brazed sinusoidal fin core producing intermediate friction factors. The heat transfer characteristics, however, showed the j curve for the brazed core slightly higher than the j curves for the unbrazed ones. There are two reasons for this: First of all, the heat transfer area calculations for the brazed core took into account the loss of metal surface area due to brazing. In the unbrazed sinusoidal fin core, a portion of surface area similar to the "lost area" was relatively ineffective for heat transfer, but not accounted for in

33

calculating j. Secondly, the fin shape and matrix construction for the brazed core actually produced a geometry that is a cross between a triangular passage and a rectangular passage, with a rectangular passage having higher values of j and j/f than a triangular passage as shown in reference [16].

It should be noted that these three stainless steel matrices yielded heat transfer and flow friction results that differed only slightly, indicating that small deviations in manufacturing procedure may have little effect upon heat transfer and flow friction performance.

The rectangular passage cores had heat transfer and friction characteristics similar to the triangular fin cores; however, their heat transfer curves (j versus N_R) were less steep, the perforated material producing a markedly higher curve than the solid material. The j/f flow area "goodness" factors for these surfaces increased as N_R increased, while j/f for the triangular fin surfaces decreased with increasing Reynolds number (See Figure 32). On the h_{STD} versus E_{STD} plot, Figure 33, rectangular passage surfaces showed definite superiority over the triangular fin surfaces, with the perforated material producing the best results.

Figure 15 demonstrates the influence of conduction parameter upon the heat transfer modulus, j. Curves such as those shown dotted can result from an improper assumption ($\lambda = 0$ in low Reynolds range), approximations for λ (Appendix C), or an inaccurate value for k_s.

Referring to Figure 7, it can be seen that there are areas where a small error in Amplitude Ratio, R_A, would result in a large corresponding error in Ntu. However, the frequency of temperature oscillation, ω_0, can be chosen so as to produce a flow parameter, M, $(M = mc_p / A_s c_s \omega_0)$

that will result in Ntu being determined with minimum error for a given error in R_A. For instance, at Ntu = 1.5, ω_o should be chosen so that M is less than .35, since values of M near .7 in this case result in a high uncertainty of Ntu. This flexibility is not inherent in the single-blow technique (where Ntu $\approx$ 2).

Figure 35 shows heat transfer data for the brazed triangular fin matrix. Both the single-blow and cyclic techniques were employed, thus producing data up to a Reynolds number of 1850 with an area of overlap between Reynoldd numbers 380 and 560. There seems to be fairly good correlation between the two testing methods with the exception of the data points at Reynolds numbers 450 and 560. These points were the result of employing the single-blow technique in the area of high N_R and low Ntu (1.65 and 1.44), where Ntu is subject to error as explained in Chapter 2. The data from the cyclic technique was also subject to some error due chiefly to the cyclic power input to the heaters. As can be seen on the sample chart trace in Figure 37, there was some distortion in the temperature waveforms making them slightly different than true sinusoids. This distortion is due to inaccurate signal reproduction in the amplidyne. There was also a problem in instrumentation - the temperature waveforms were recorded separately by means of the same instrument instead of simultaneously. Bell and Katz [2] utilized a dual channel instrument recording both temperatures simultaneously, reversing the input connections midway through each run so as to record each temperature on both channels, thus eliminating the effects of unequal channel sensitivities. The thermocouple configuration described in Appendix B does not allow for simultaneous temperature measurement and recording.

In Figure 35 data from the single-blow technique is plotted with data from a steady state stream to air technique. In both tests the identical type 80/20T perforated nickel triangular fin surface was investigated. The steam to air test was conducted on a cross flow heat exchanger with the surface to be tested on the air side. The core configuration for the single-blow test is described in Chapter 4 and Figure 17. Theoclitus in reference [28] utilized a dual testing technique similar to this in determining fin efficiency, η_f, and total surface temperature effectiveness η_o, for various surfaces. Theoclitus found for simple finned surfaces, that the theories for fin efficiency and total surface temperature effectiveness are reliable since he obtained a close correlation of data from the two methods of testing. For the steady state technique, theoretical values of η_f and η_o are used in determining the heat transfer characteristics, Ntu and j, while η_f and η_o have values of unity when the transient technique is employed, due to lack of a temperature gradient in the fin in the direction perpendicular to fluid flow (See Chapter 3).

Figure 35 indicates a fairly good correlation of data for the two testing methods.

Conclusions:

(1) For matrices of the same geometry and material, small deviations in manufacturing procedure have little effect upon overall heat transfer and friction performance.

(2) The single-blow and cyclic transient testing techniques utilized for this report are reliable in that the experimental results obtained agree with results obtained by means of steady state testing

36

and with theory.

(3) The single-blow and cyclic techniques supplement each other in producing heat transfer data over a wide range of Reynolds numbers.

8. RECOMMENDATIONS FOR FURTHER WORK

Refinement of the cyclic method of testing is needed both in theory and in testing apparatus. The theory could be extended to include the effect of longitudinal thermal conduction, this involving the use of another non-dimensional parameter in place of M, and a theoretical solution using methods similar to Howard's [9] or Moreland's [20].

There are a number of areas for improvement in the test apparatus:

(1) A modification is needed if higher flow rates are to be employed. Either a larger pipe diameter at the orifice meter, or another means of measuring flow rate is needed to increase the flow rates employed.

(2) A more reliable power source is needed for the heaters so that a truer sinusoidal temperature variation results.

(3) The temperature measuring system could be modified so that the matrix inlet and exit temperatures can be recorded simultaneously.

It is also recommended that more surfaces be made available for testing by both transient and steady state methods so that data is available for a wider range of Reynolds numbers, and the reliability of the two methods may be compared.

9. BIBLIOGRAPHY

(1) Bannon, John M. "An Experimental Determination of Heat Transfer and Flow Friction Characteristics of Perforated Material for Compact Heat Exchanger Surfaces." Master's Degree Thesis U. S. Naval Postgraduate School, Monterey, California. 1964.

(2) Bell, J. C. and Katz, E. F. "A Method for Measuring Surface Heat Transfer Using Cyclic Temperature Variations", _Heat Transfer and Fluid Mechanics Institute_, Berkeley, California, 1949.

(3) Carslaw, H. S. and Jaeger, J. C. _Conduction of Heat in Solids_, Second Edition, Oxford: Clarendon Press, 1959.

(4) Coppage, J. E. "Heat Transfer and Flow Friction Characteristics of Porous Media", T.R. No. 16, _Department of Mechanical Engineering, Stanford University_, Stanford, California, December 1, 1952.

(5) Creswick, F. A. "A Digital Computer Solution of the Equations for the Transient Heating of a Porous Solid Including the Effects of Longitudinal Conduction", _Industrial Mathematics_, Volume 8, 1957.

(6) Elridge, E. A. and Deem, H. W. _Report on Physical Properties of Metals and Alloys from Cryogenic to Elevated Temperatures._ Philadelphia: American Society for Testing Materials, 1961.

(7) Goldsmith, A., _et. al._ _Handbook of Thermophysical Properties of Solid Materials._ Revised Edition, Volume I, Elements, New York: The MacMillan Company, 1961.

(8) Hilsenrath, J., _et al._ _Tables of Thermodynamic and Transport Properties of Air, Argon, Carbon Monoxide, Hydrogen, Nitrogen, Oxygen, and Steam._ New York: Permagon Press, 1960.

(9) Howard, C. P. "The Single Blow Problem Including the Effects of Longitudinal Conduction", _ASME paper_, Number 64-GTP-11

(10) Jakob, M. _Heat Transfer_, Volume II, New York: John Wiley and Sons, Inc., 1957.

(11) Kays, W. M. "Loss Coefficients for Abrupt Changes in Flow Cross Section with Low Reynolds Number Flow in Single and Multiple Tube Systems", TR Number 9, _Department of Mechanical Engineering, Stanford University_, Stanford, California, 1950.

(12) Kays, W. M. and London, A. L. _Compact Heat Exchangers._ Second Edition. New York: McGraw-Hill Book Company, Inc., 1964.

(13) Kline, S. J. and McClintock, F. A. "Describing Uncertainties in Single-Sample Experiments," _Mechanical Engineering_, January 1953, pp 3-8.

(14) Lambertson, T. J. "Performance Factors of a Periodic Flow Heat Exchanger", Trans. ASME, Volume 80, 1958.

(15) Locke, G. L. "Heat Transfer and Flow Friction Characteristics of Porous Solids", TR. No. 10, Department of Mechanical Engineering, Stanford University, Stanford, California, June 1, 1950.

(16) London, A. L. "New Developments in Compact Heat Exchangers-Design Theory, Surfaces, and Applications", lecture presented at the Sixth National ASME-AIC E Heat Transfer Conference, Boston, Massachusetts, August, 1963.

(17) London, A. L., Biancardi, F. R., and Mitchell, "The Transient Response of Gas Turbine Plant Heat Exchangers, Regenerators, Intercoders, Precoolers and Ducting, Trans. ASME, Volume 81, pp. 43, 1959.

(18) McAdams,   Heat Transmission, Third Edition, New York: McGraw-Hill Book Company, Inc., 1954.

(19) Mondt, J. R. "Effects of Longitudinal Thermal Conduction in the Solid on Apparent Convection Behavior, with Data for Plate Fin Surfaces", 1961 International Heat Transfer Conference, Boulder, Colorado, Paper No. 73, Proceedings ASME.

(20) Moreland, F. E. "Solution of the Single Blow Problem, with Longitudinal Conductivity by Numerical Inversion of LaPlace Transforms", Master's Degree Thesis, U. S. Naval Postgraduate School, Monterey, California, 1964.

(21) Murdock, J. W. "Tables for the Interpolation and Extrapolation of ASME Coefficients for Square-Edged Concentric Orifices", ASME paper, Number 64-WA/FM-6.

(22) Piersall, C. H. "Experimental Evaluation of Several High Performance Surfaces for Compact Heat Exchangers". Master's Degree Thesis, U. S. Naval Postgraduate School, Monterey, California, 1965.

(23) Power Test Code Supplements, Instruments and Apparutus, PTC-19.5.4 Flow Measurements, Chapter 4, New York: American Society of Mechanical Engineers, 1959.

(24) Pucci, P. F., Howard, C. P., and Piersall, C. H., "The Single-Blow Transient Testing Technique for Compact Heat Exchanger Surfaces," ASME Paper, Number 66-GT-93.

(25) Raven, F. H. "Automatic Control Engineering," New York: McGraw-Hill Book Company, Inc., 1961.

(26) Schumann, T. E. W. "Heat Transfer: A Liquid Flowing through a Porous Prism", Journal of the Franklin Institute, Volume 208, 1929, pp 405-416.

(27) Solar Aircraft Company, <u>Engineering Report</u> ER 1221, Regnerator core
    Module Tests-T-600 Engine, 18 April, 1962. Rev. A: 25 October,
    1962, AD 290234.

(28) Theoclitus, G. and Ecbrich, T. L. "An Experimental Technique for
    Determining the Effectiveness of Extended Surfaces", presented
    at the <u>Seventh National Heat Transfer Conference</u>, Cleveland,
    Ohio, August, 1964.

(29) Ward, J. P. "Steady State Steam to Air Testing Facility for Compact
    Heat Exchangers". Master's Degree Thesis, <u>U. S. Naval Postgrad-
    ate School</u>, Monterey, California, 1965.
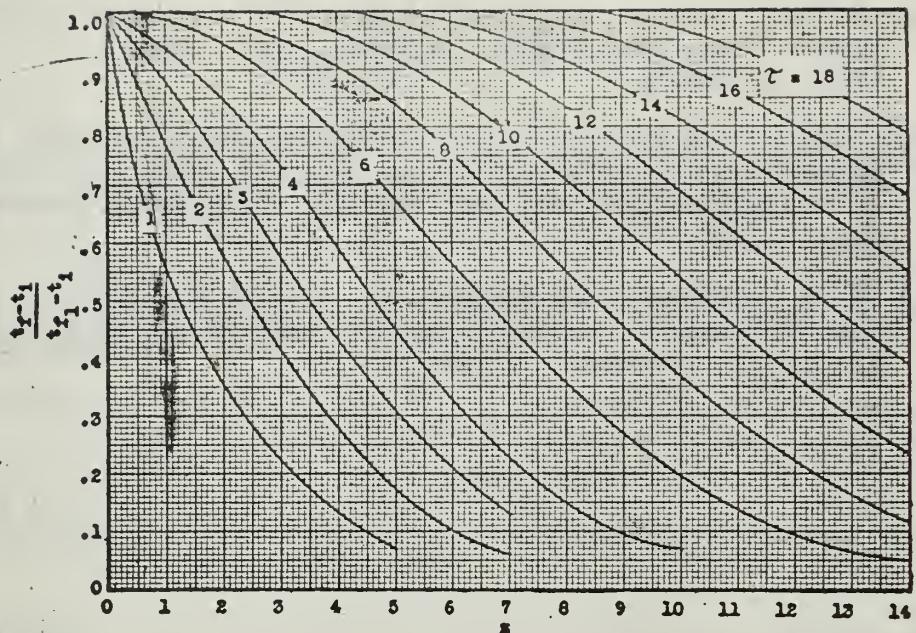
TEMPERATURE AS A FUNCTION OF τ AND z OF A FLUID
FLOWING THROUGH AN INITIALLY UNIFORM TEMPERATURE
POROUS SOLID
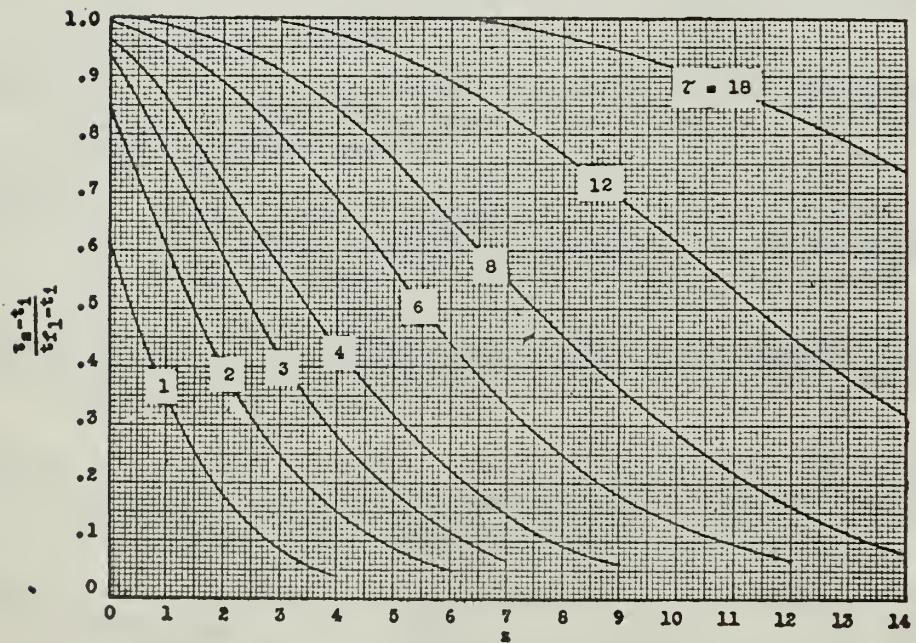
SOLID TEMPERATURE AS A FUNCTION OF τ AND z
OF A POROUS SOLID INITIALLY AT A UNIFORM
TEMPERATURE AND THROUGH WHICH A FLUID FLOWS

Figure 1.   Schumann's Curves
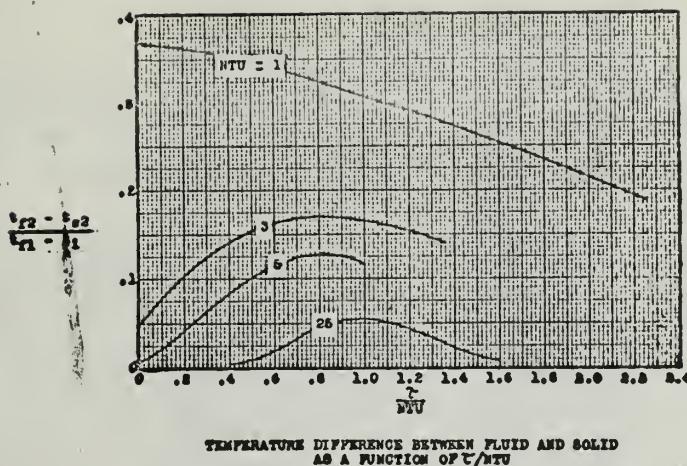
TEMPERATURE DIFFERENCE BETWEEN FLUID AND SOLID
AS A FUNCTION OF τ/NTU
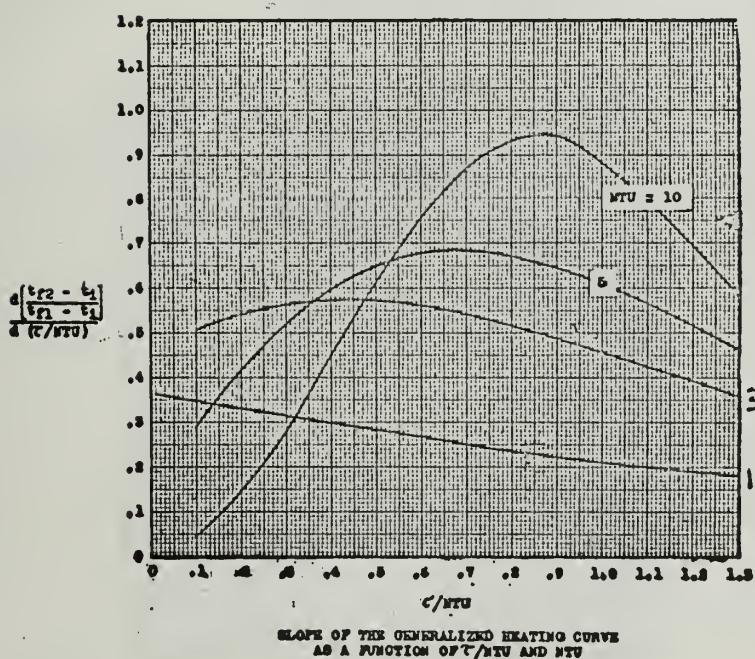
SLOPE OF THE GENERALIZED HEATING CURVE
AS A FUNCTION OF τ/NTU AND NTU

Figure 2. Locke's Curves

43
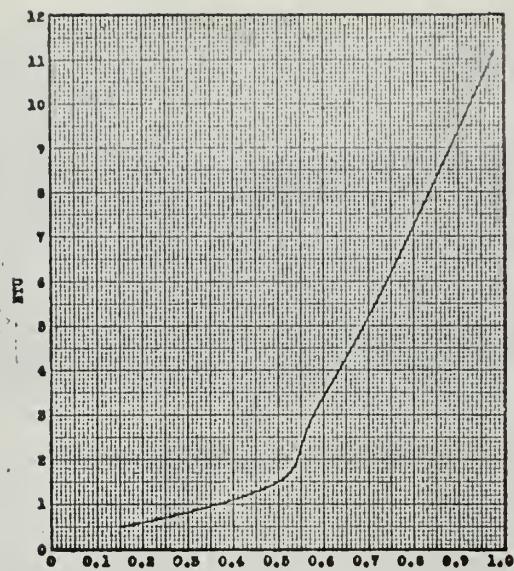
NTU AS A FUNCTION OF THE MAXIMUM SLOPE
OF THE GENERALIZED HEATING CURVE
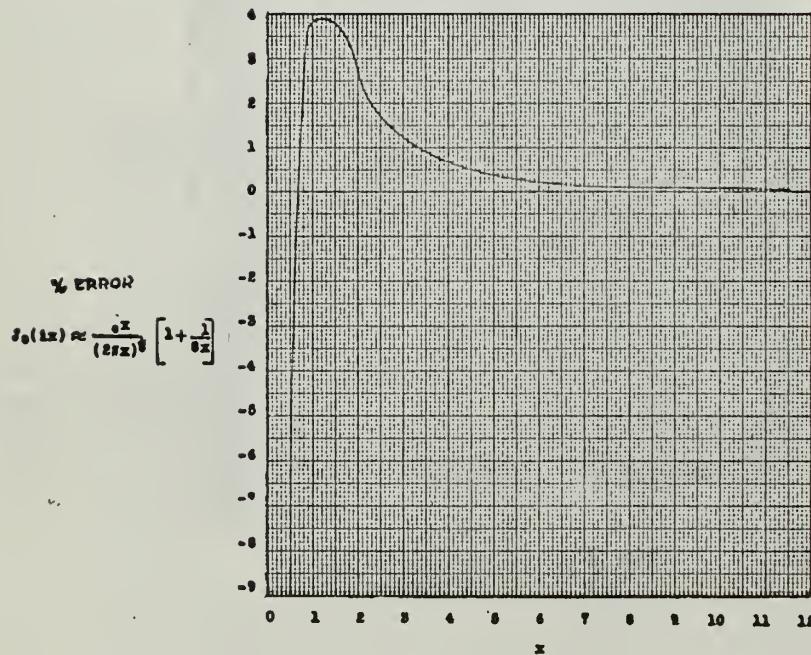
Figure 3.   Locke's Curves

44
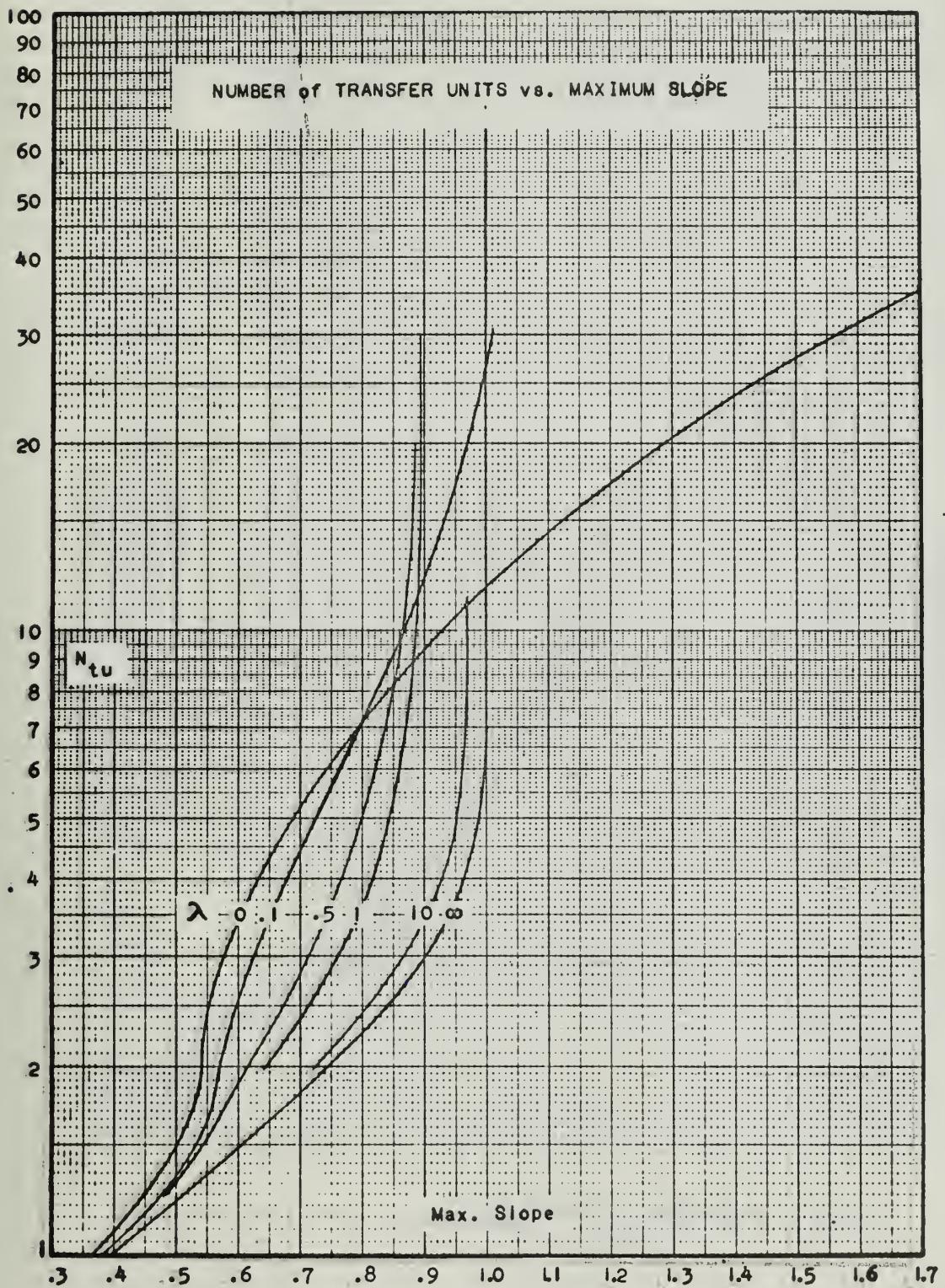
Figure 4. Ntu versus Maximum Slope

45
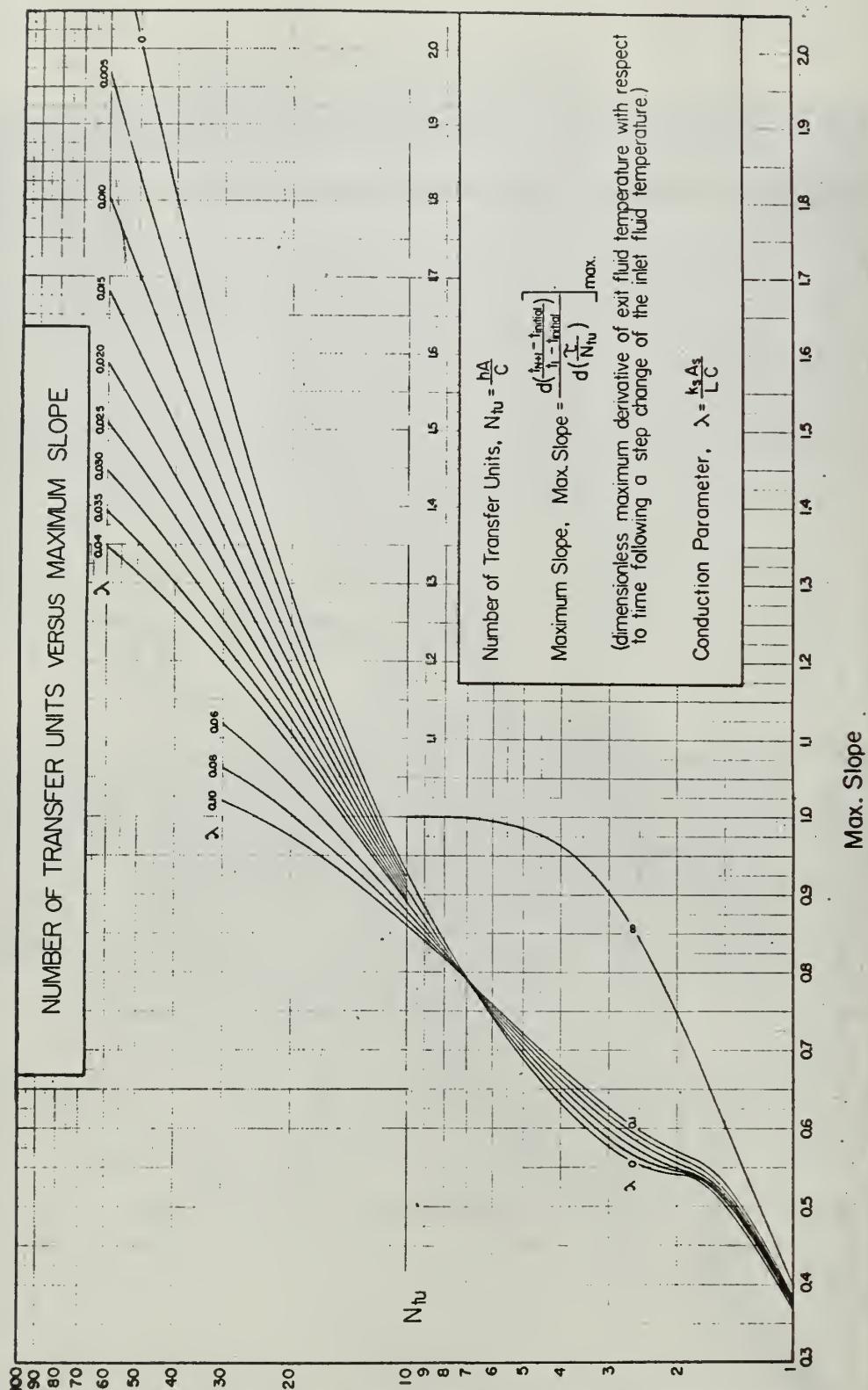
Figure 5. Ntu versus Maximum Slope

46
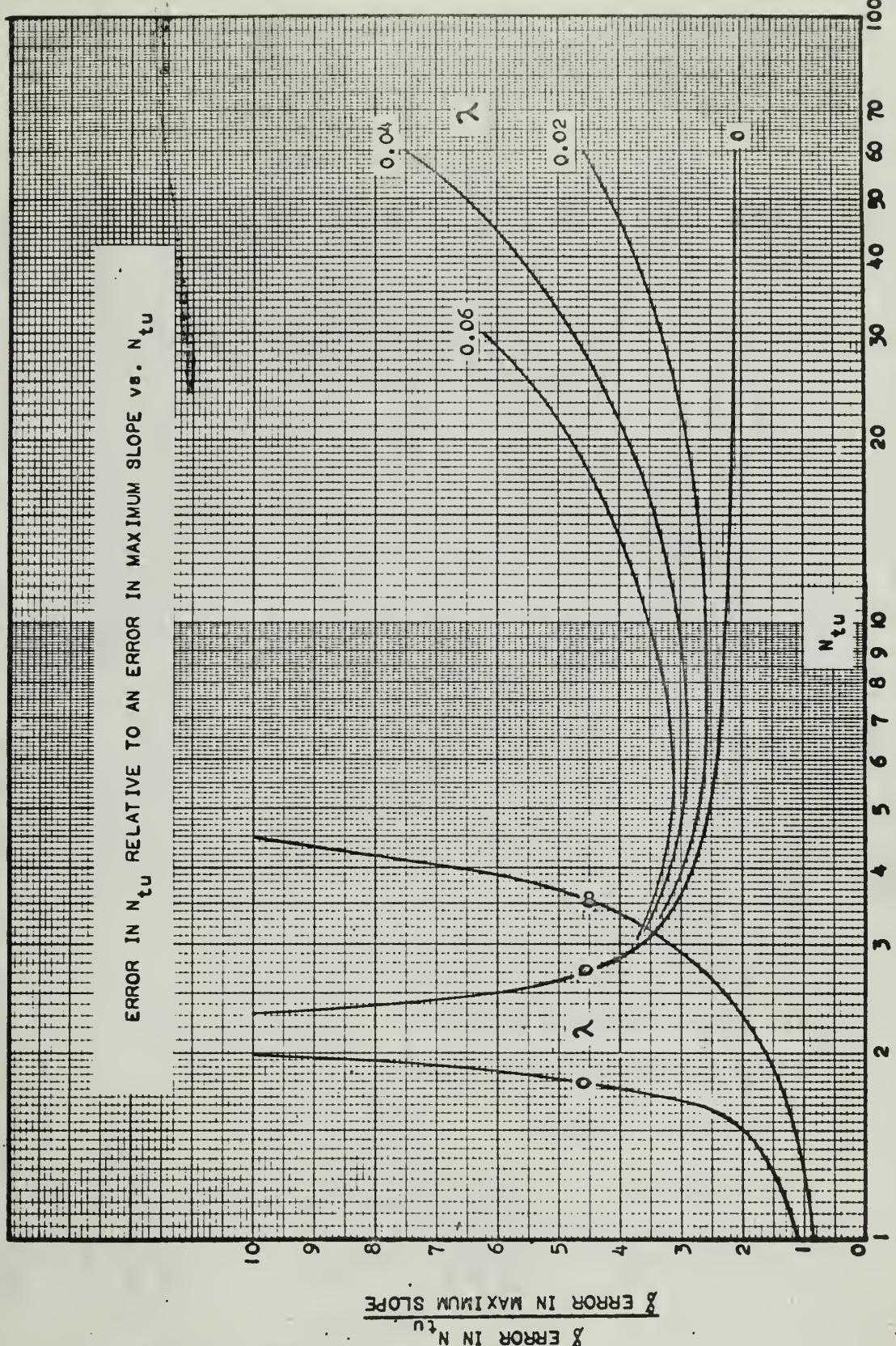
Figure 6. Ntu error versus Ntu

47
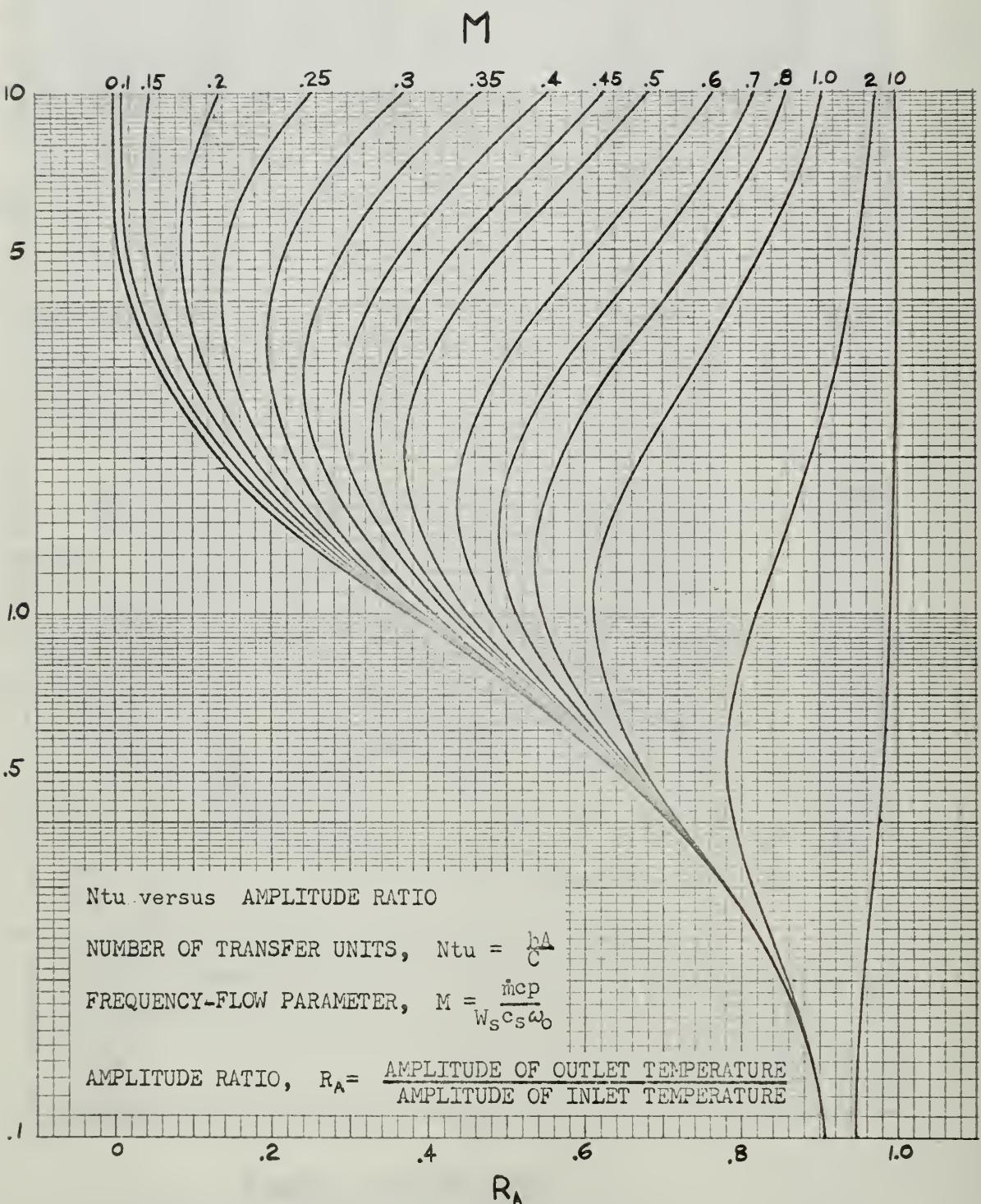
Figure 7. Ntu versus Amplitude Ratio

48
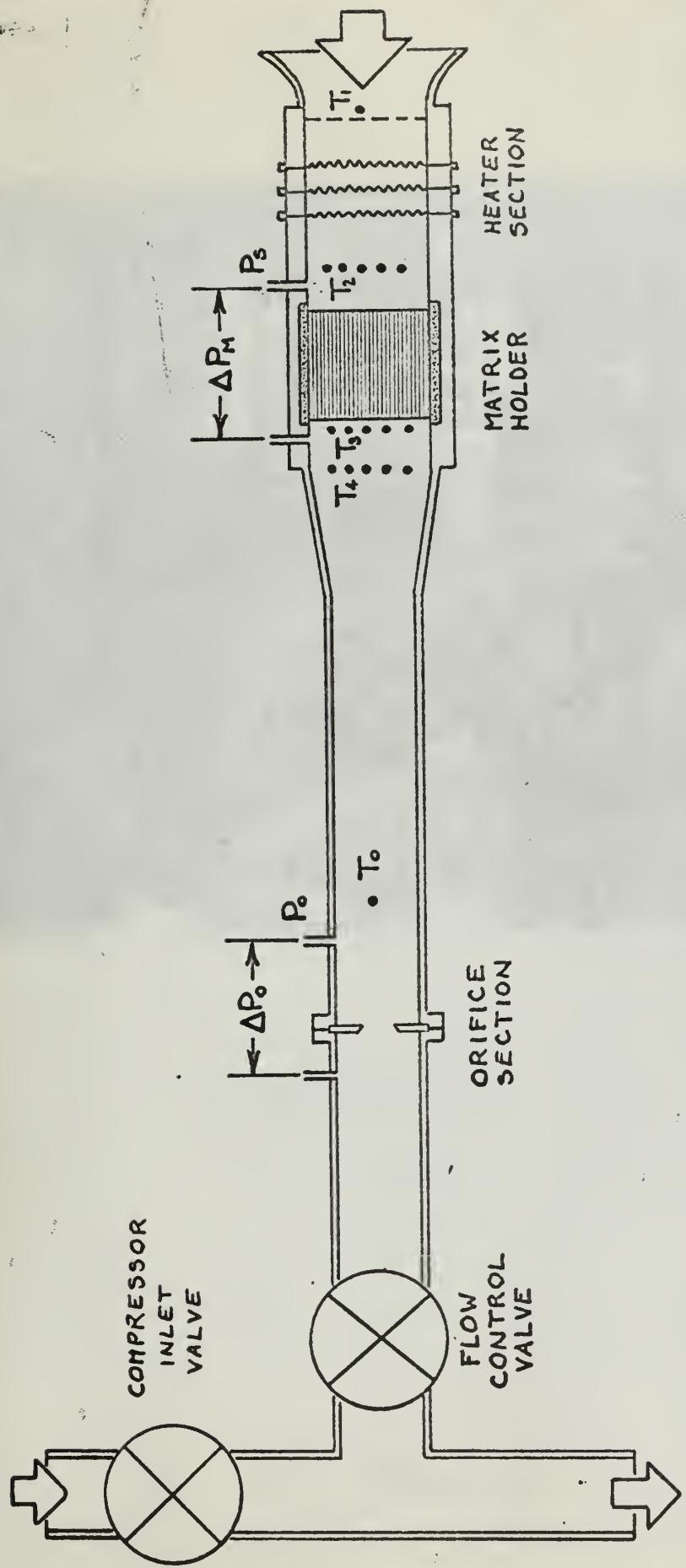
SCHEMATIC OF TEST APPARATUS

FIGURE 8.

TEST APPARATUS

FIGURE 5.

MEMBRANE TYPE HEATER
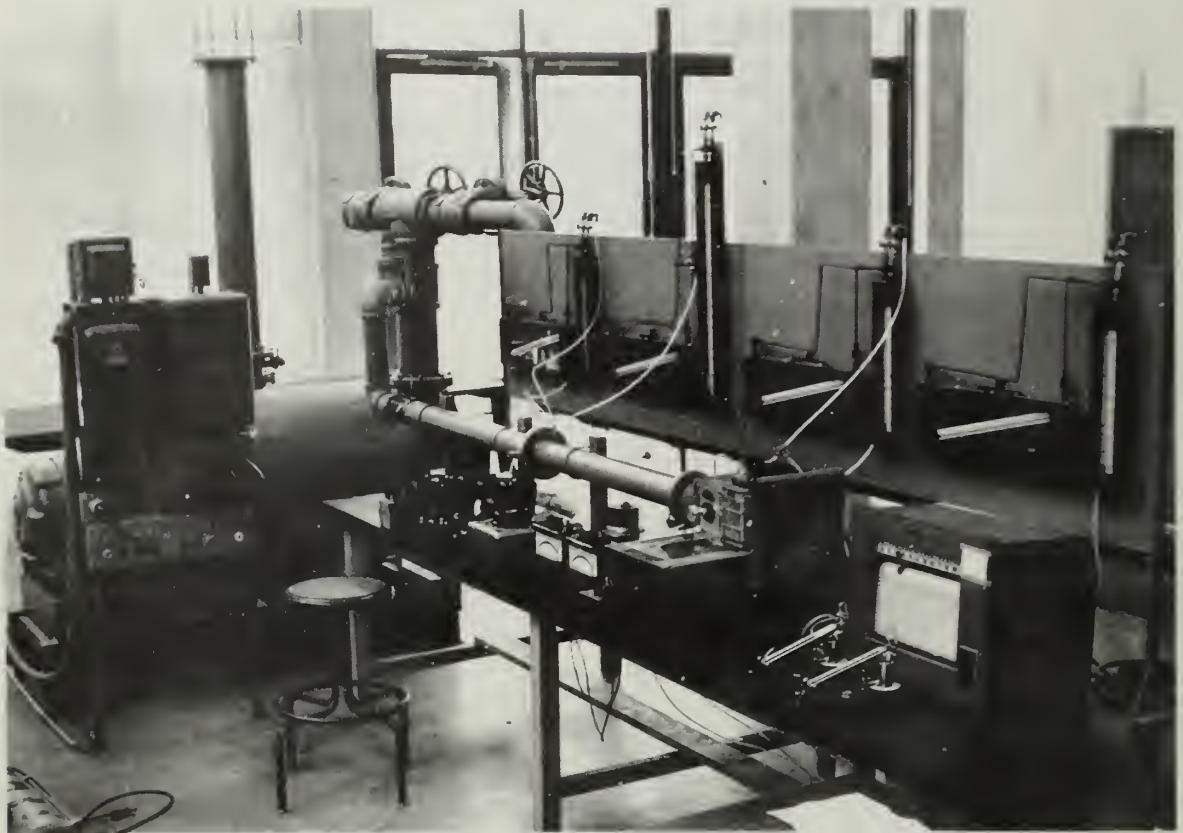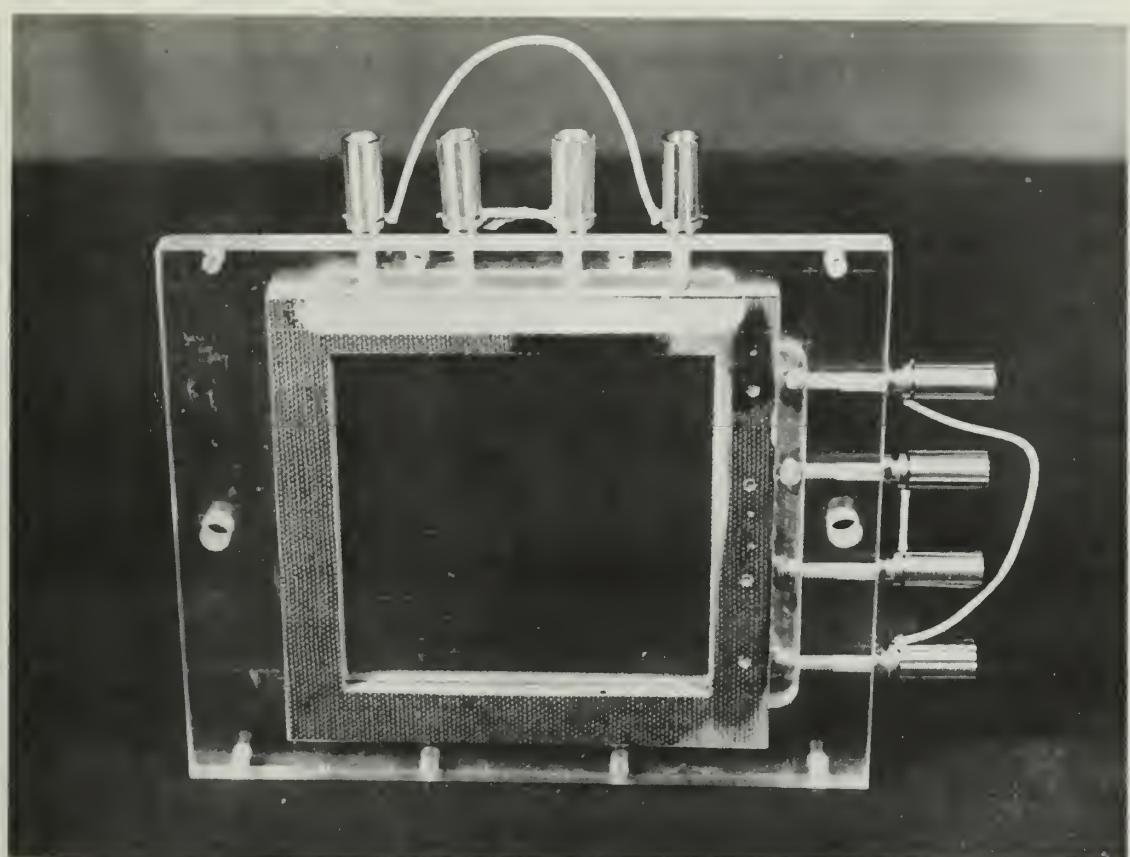
TWO HEATERS PER FRAME

FIGURE 10.
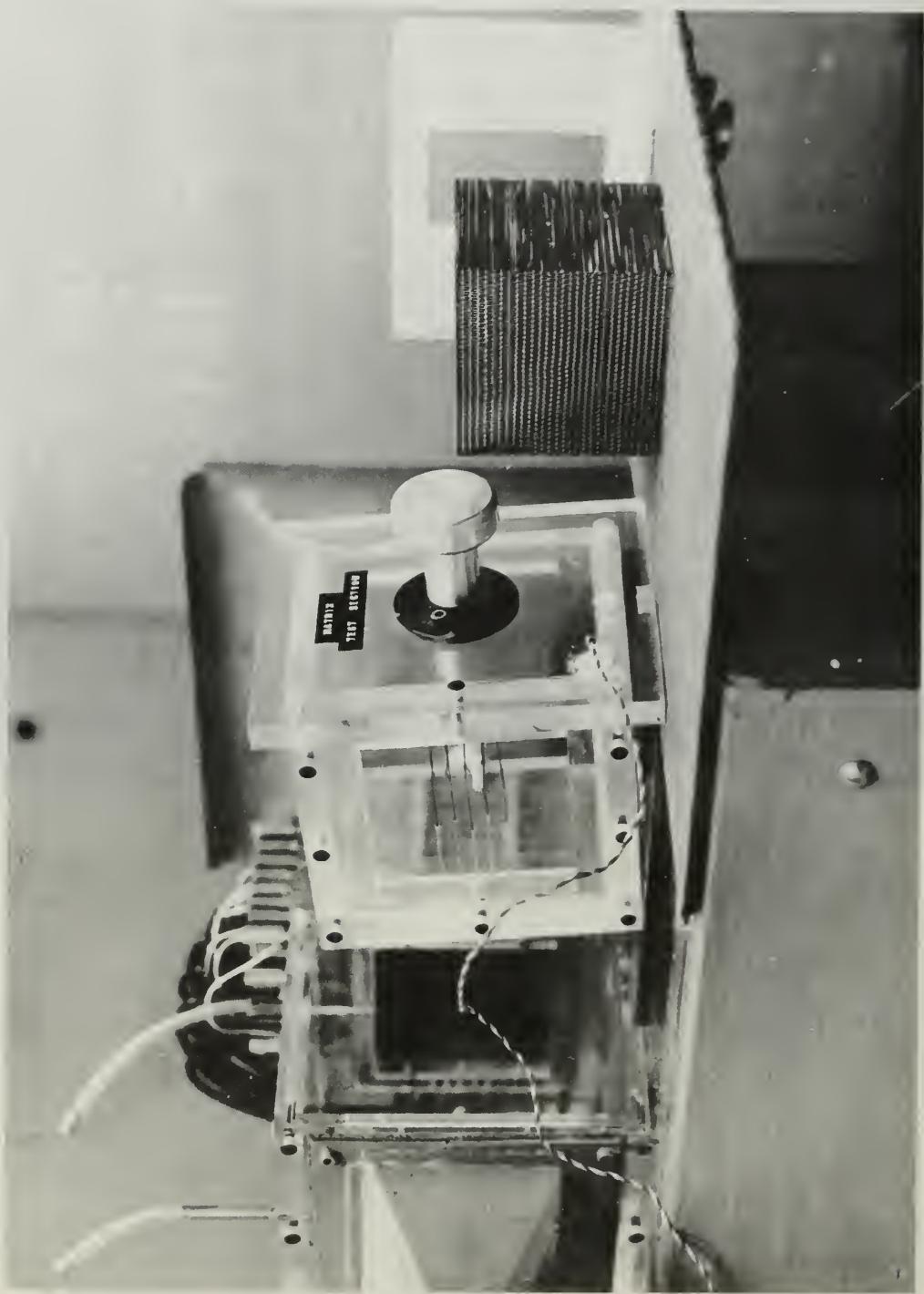
51

52

FIGURE 11. BLOWER AND TEST SECTION

53

PROBE IN MATRIX HOUSING

VIEW FROM UPSTREAM

(Figure 12).

54
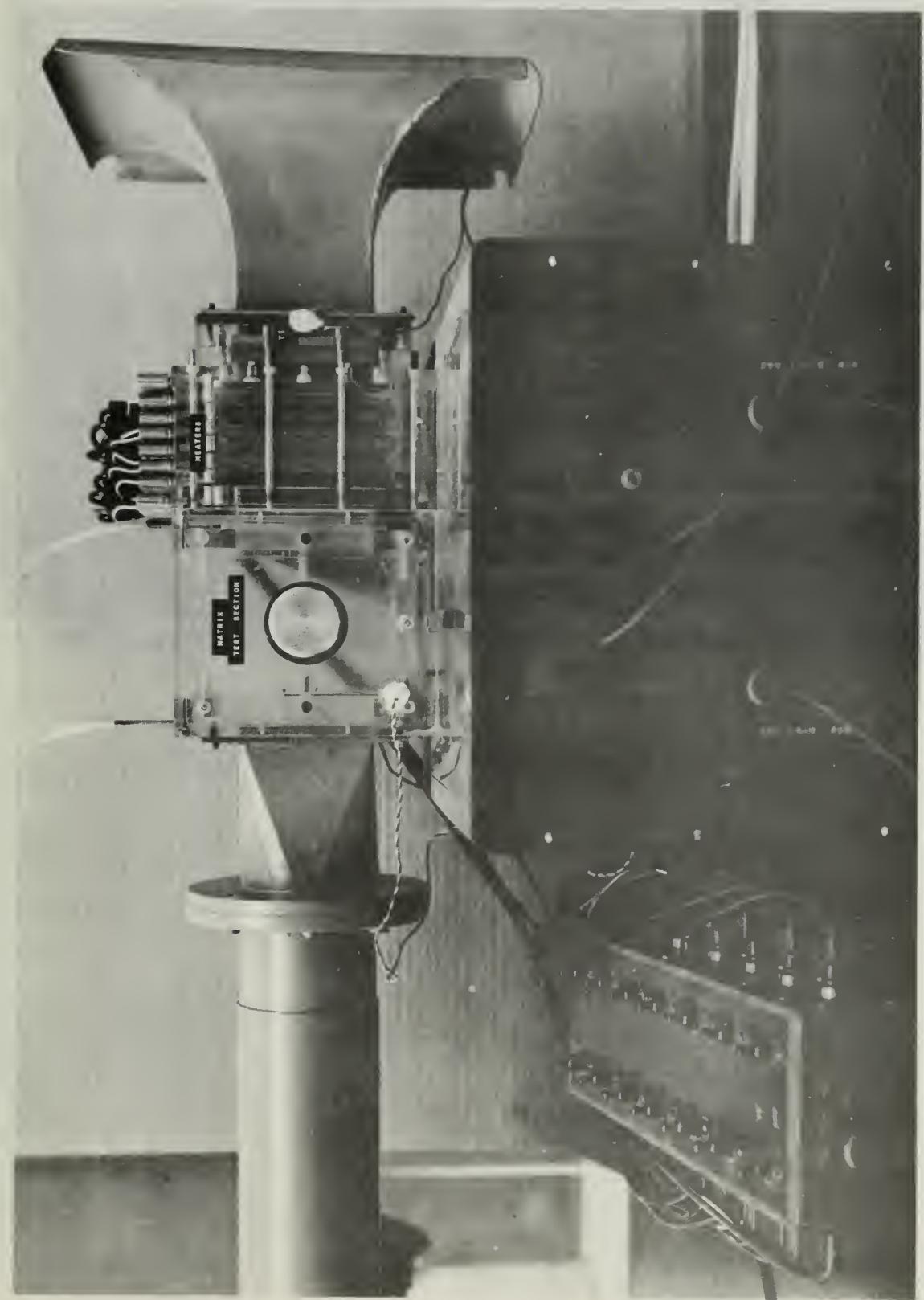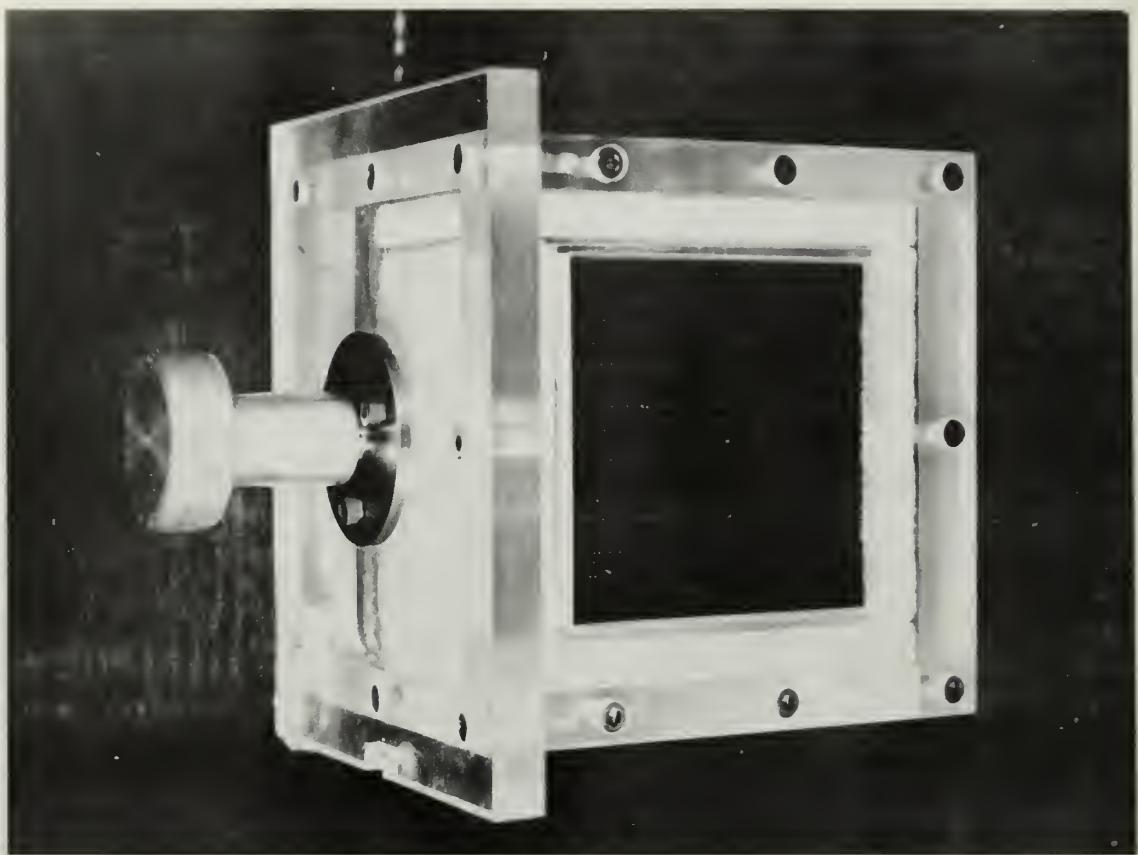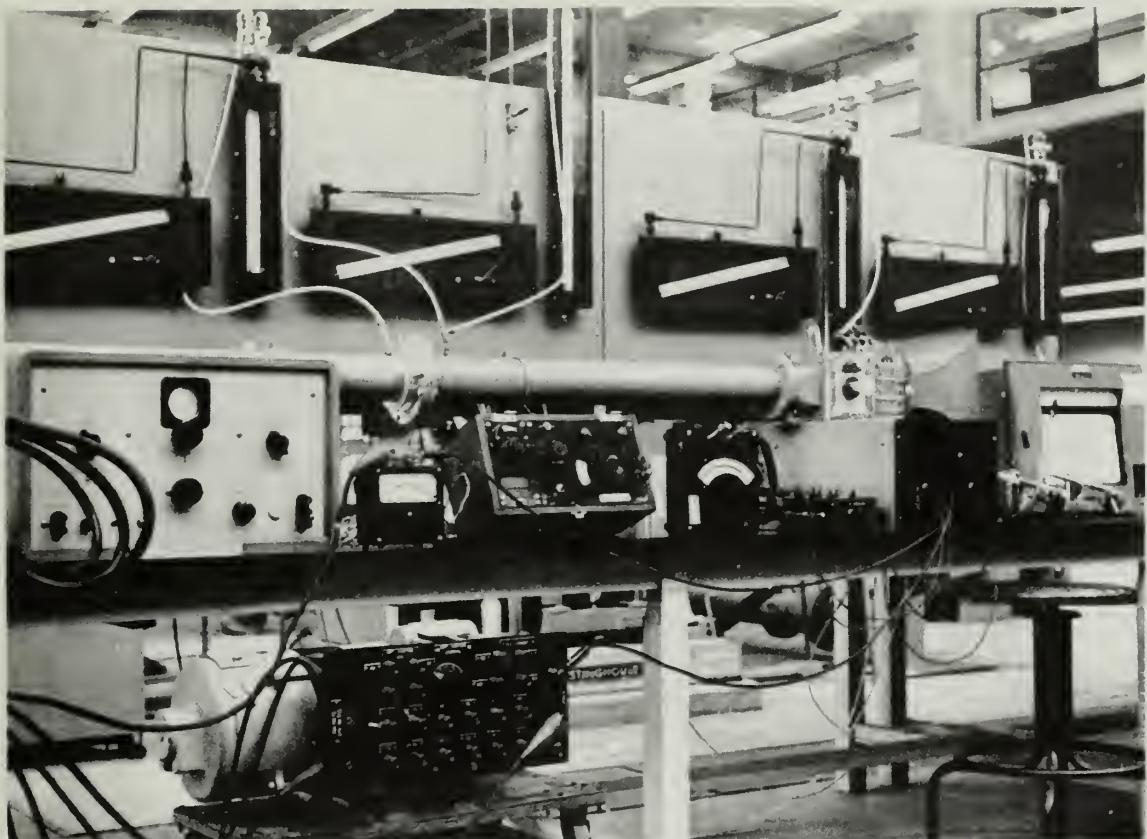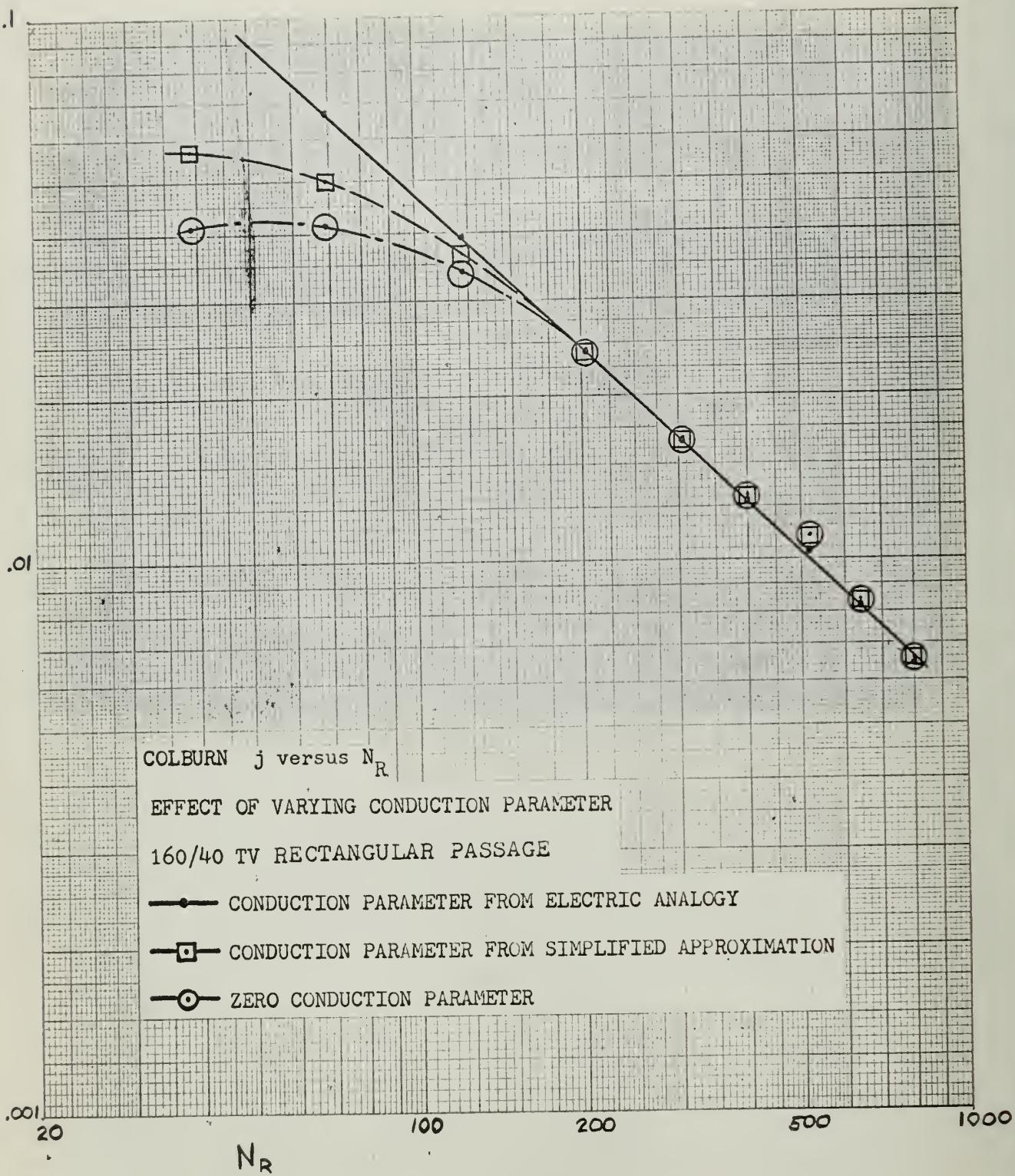
Figure 15. Effects of Longitudinal Conduction Parameter
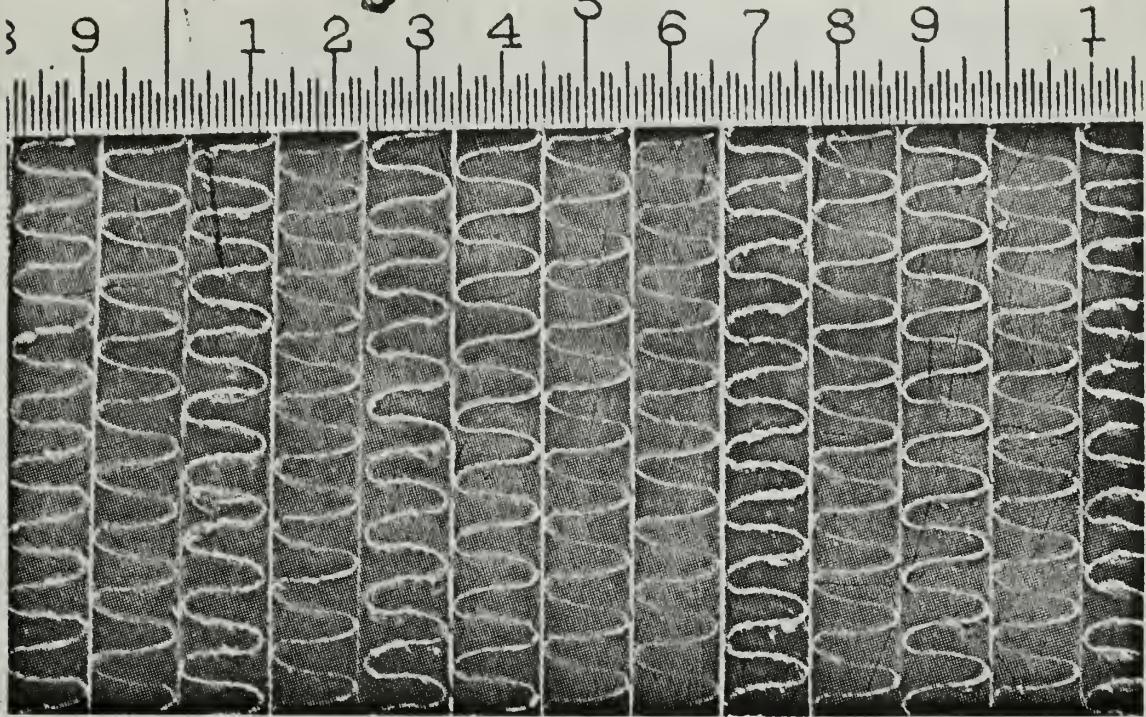
SOLAR #1

Matrix Material		Nickel
Specific Heat, c_s	(Btu/lbm deg F)	.106
Thermal Conductivity, k_s	(Btu/hr ft deg F)	36.0
Material Thickness	(in)	.005
Total Heat Transfer Area ,A	(sq ft)	12.768
Frontal Area, A_{fr}	(sq ft)	.07022
Conductive Area, A_s	(sq ft)	.01078
Free Flow Area, A_c	(sq ft)	.05944
Matrix Flow Length, L_m	(ft)	.24917
Matrix Volume, V_m	(cu ft)	.0175
Matrix Density, ρ_m	(lbm/cu ft)	86.1378
Compactness,	(sq ft/cu ft)	729.7026
Porosity, p		.8464
Hydraulic Diameter	(ft)	.0046395

Figure 16 Geometric and Physical Properties
for Solar #1
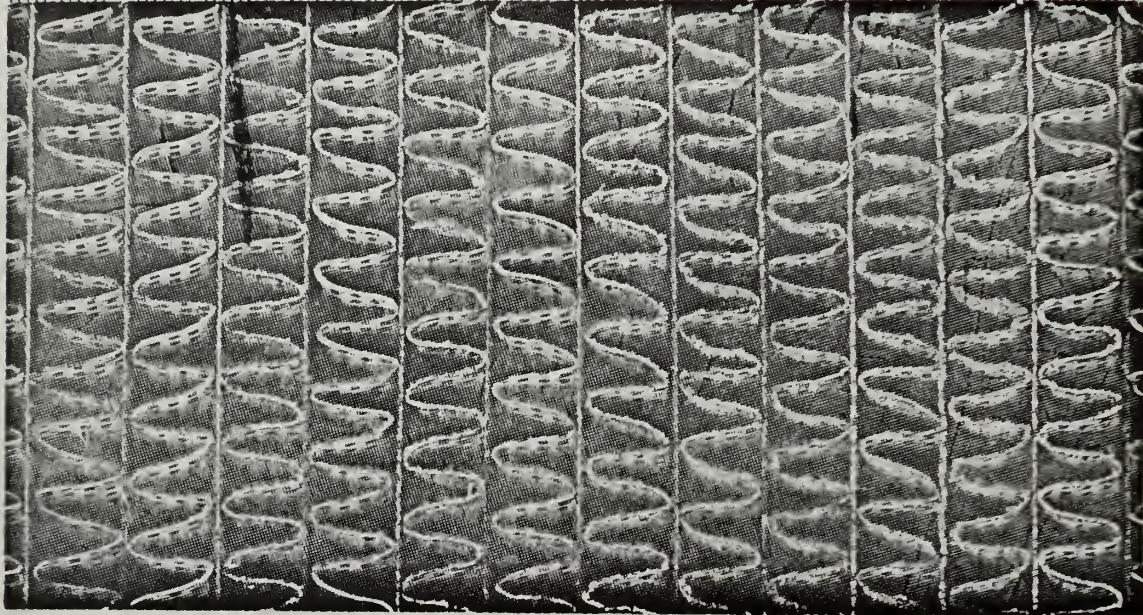
SOLAR #2

Matrix Material		Nickel
Specific Heat, c_s	(Btu/lbm deg F)	.106
Thermal Conductivity, k_s	(Btu/hr ft deg F)	36.0
Material Thickness	(in)	.005
Total Heat Transfer Area, A	(sq ft)	12.093
Frontal Area, A_{fr}	(sq ft)	.07022
Conductive Area, A_s	(sq ft)	.01034
Free Flow Area, A_c	(sq ft)	.05987
Matrix Flow Length, L_m	(ft)	.25583
Matrix Volume, V_m	(cu ft)	.01797
Matrix Density, ρ_m	(1bm/cu ft)	70.3099
Compactness,	(sq ft/cu ft)	673.143
Porosity, p		.85281
Hydraulic Diameter	(ft)	.0046272
Perforated Fin Material	.0047" thick	80/20T

Figure 17   Geometric and Physical Properties
for Solar #2
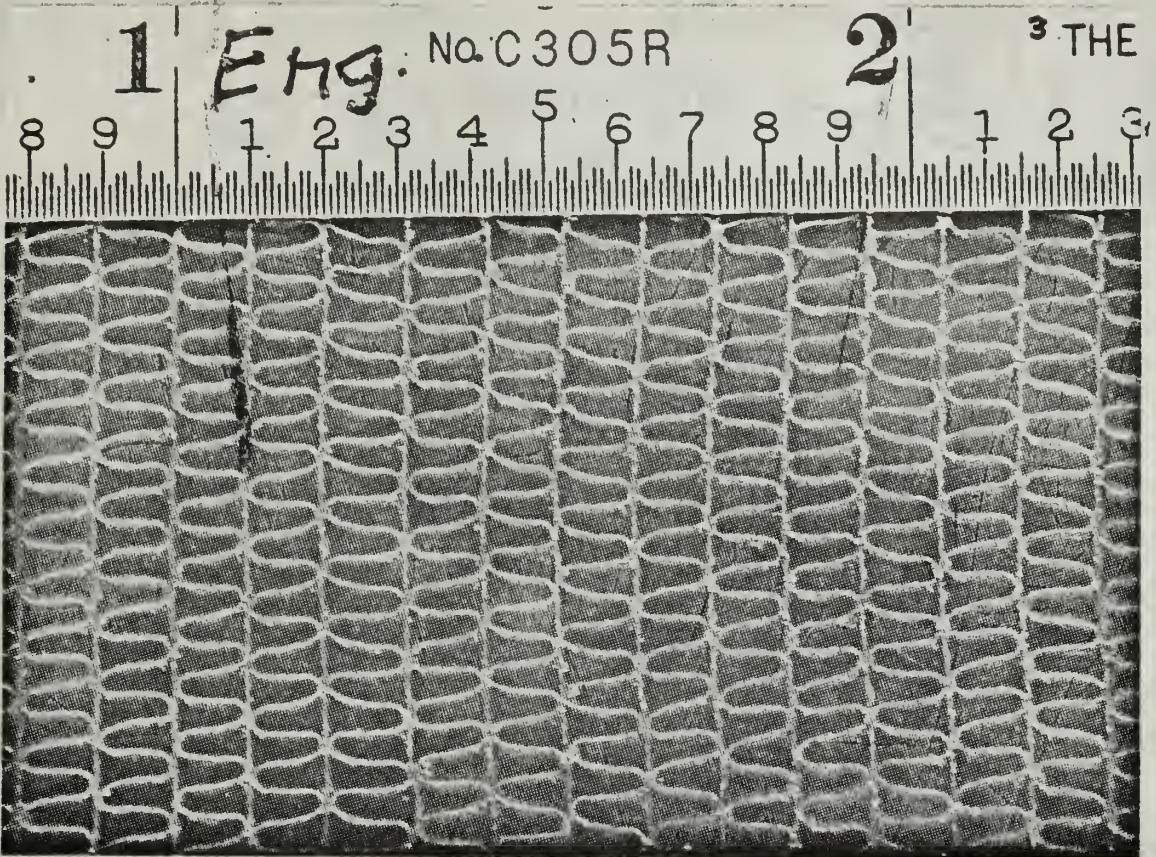
SOLAR #3

Matrix Material		430 Stainless Steel
Specific Heat, c_s	(Btu/lbm deg F)	.11
Thermal Conductivity, k_s	(Btu/hr ft deg F)	12.8
Material Thickness	(in)	.005
Total Heat Transfer Area, A	(sq ft)	14.3588
Frontal Area, A_{fr}	(sq ft)	.06803
Conductive Area, A_s	(sq ft)	.01325
Free Flow Area, A_c	(sq ft)	.05478
Matrix Flow Length, L_m	(ft)	.24833
Matrix Volume, V_m	(cu ft)	.01689
Matrix Density, ρ_m	(lbm/cu ft)	94.2656
Compactness,	(sq ft/cu ft)	849.8962
Porosity, p		.80517
Hydraulic Diameter	(ft)	.0037895

Figure 18. Geometric and Physical Properties
For Solar #3
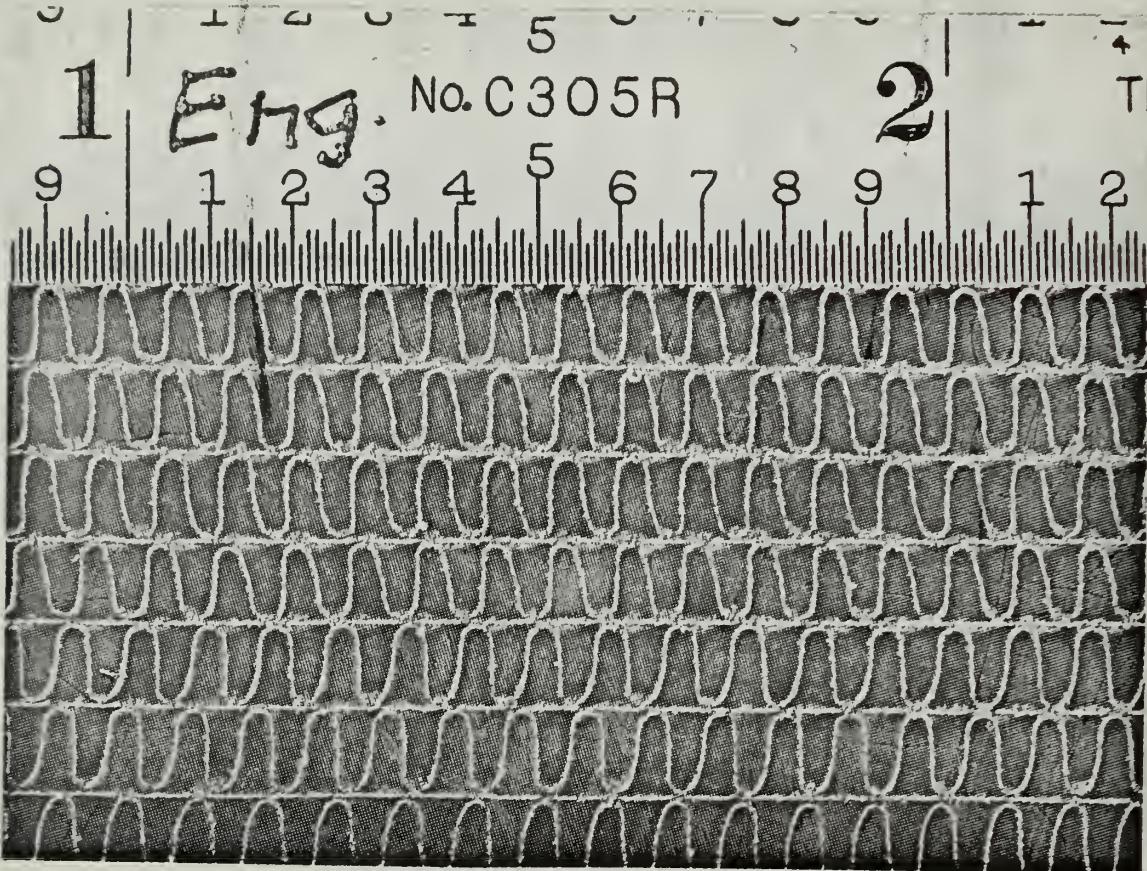
SOLAR #4

Matrix Material		430 stainless steel
Specific Heat, c_s	(Btu/lbm degF)	.11
Thermal Conductivity, k_s	(Btu/hr ft deg F)	12.8
Material Thickness	(in)	.005
Total Heat Transfer Area, A	(sq ft)	14.27694
Frontal Area, A_{fr}	(sq ft)	.06713
Conductive Area, A_s	(sq ft)	.01229
Free Flow Area, A_c	(sq ft)	.05484
Matrix Flow Length, L_m	(ft)	.24417
Matrix Volume, V_m	(cu ft)	.01638
Matrix Density, $_m$	(lbm/cu ft)	88.5918
Compactness,	(sq ft/cu ft)	.81690
Hydraulic Diameter	(ft)	.00375168

Figure 19. Geometric and Physical Properties
for Solar #4
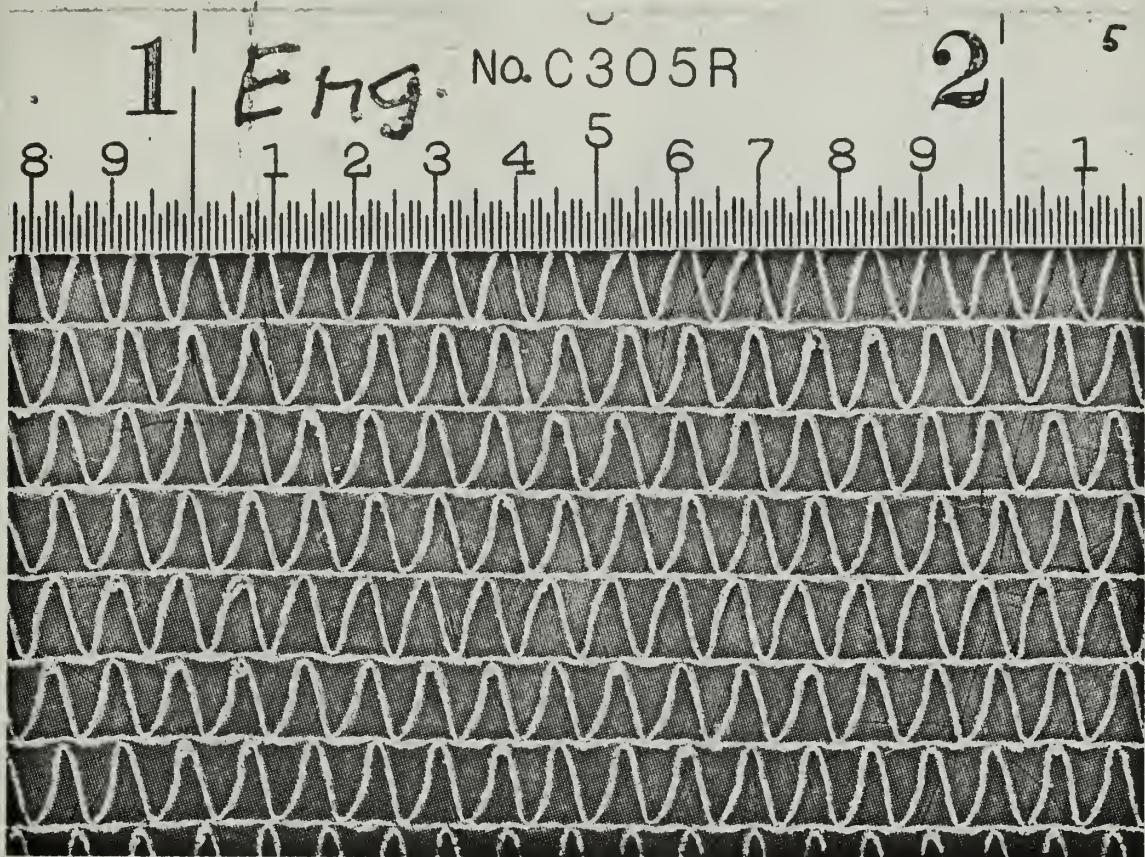
SOLAR #5

Matrix Material		430 stainless steel
Specific Heat, c_s	(Btu/1bm deg F)	.11
Thermal Conductivity, k_s	(Btu/hr ft deg F)	12.8
Material Thickness	(in)	.005
Total Heat Transfer Area ,A	(sq ft)	14.4234
Frontal Area, A_{fr}	(sq ft)	.06781
Conductive Area, A_s	(sq ft)	.01148
Free Flow Area, A_c	(sq ft)	.05633
Matrix Flow Length, L_m	(ft)	.26417
Matrix Volume, V_m	(cu ft)	.0179
Matrix Density, $_m$	(1bm/cu ft)	81.9345
Compactness,	(sq ft/cu ft)	805.13313
Porosity, p		.83066
Hydraulic Diameter	(ft)	.0041269

Figure 20.   Geometric and Physical Properties
for Solar #5

61
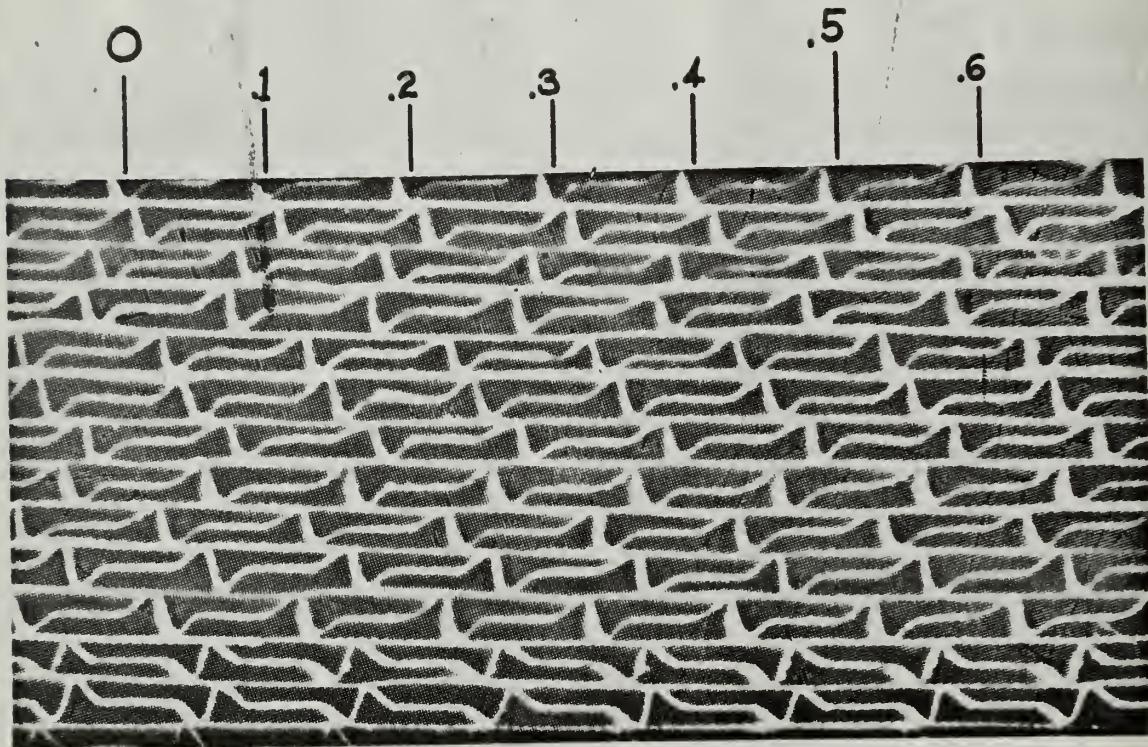
MODIFIED RECTANGULAR PASSAGE

Matrix Material		160/40 Perforated nickel
Specific Heat, c_s	(Btu/lbm deg F)	.106
Thermal Conductivity, k_s	(Btu/hr ft deg F)	36.0
Material Thickness	(in)	.0022
Total Heat Transfer Area ,A	(sq ft)	18.593
Frontal Area, A_{fr}	(sq ft)	.06953
Conductive Area, A_s	(sq ft)	.00424
Free Flow Area, A_c	(sq ft)	.0584
Matrix Flow Length, L_m	(ft)	.16098
Matrix Volume, V_m	(cu ft)	.01159
Matrix Density	(lbm/cu ft)	63.6
Compactness,	(sq ft/cu ft)	1604.5
Porosity, p		.840
Hydraulic Diameter	(ft)	.001929

Figure 21.   Geometric and Physical Properties
for 160/40 TV
Modified Rectangular
Passage
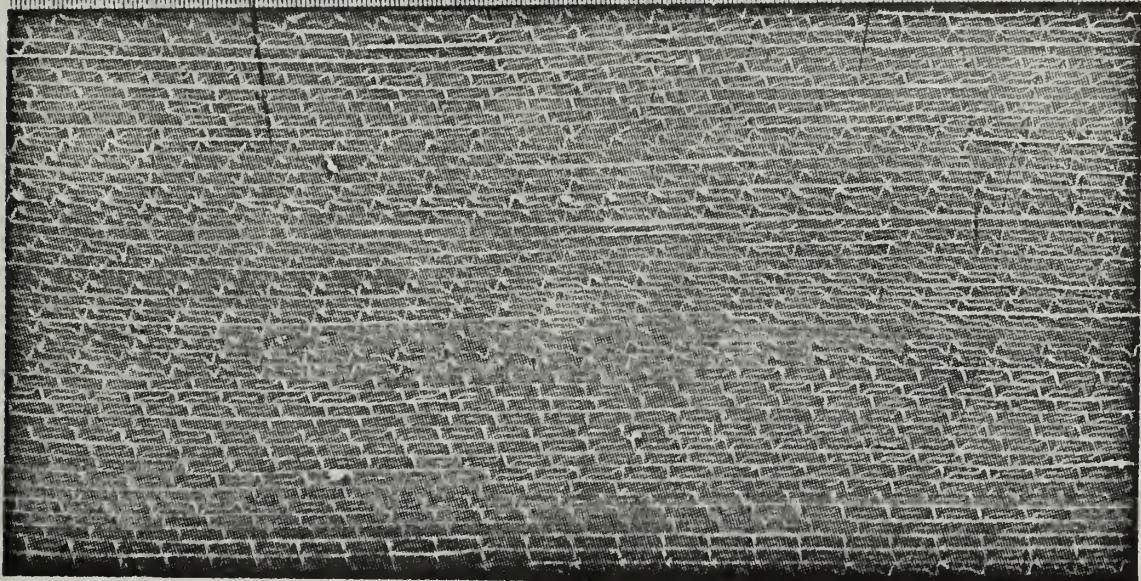
MODIFIED RECTANGULAR PASSAGE

Matrix Material		Solid Nickel
Specific Heat, c_s	(Btu/lbm deg F)	.106
Thermal Conductivity, k_s	(Btu/hr ft deg F)	36.0
Material Thickness	(in)	.002
Total Heat Transfer Area, A	(sq ft)	20.1875
Frontal Area, A_{fr}	(sq ft)	.06953
Conductive Area, A_s	(sq ft)	.01014
Free Flow Area, A_c	(sq ft)	.05939
Matrix Flow Length, L_m	(ft)	.16098
Matrix Volume, V_m	(cu ft)	.011588
Matrix Density, $_m$	(lbm/cu ft)	77.7
Compactness,	(sq ft/cu ft)	1742.1
Porosity, p		.854
Hydraulic Daimeter	(ft)	.001961

Figure 22. Geometric and Physical Properties
for Solid Nickel Modified
Rectangular Passage

Figure 23. Heat Transfer and Flow Friction
Characteristics   Solar #1
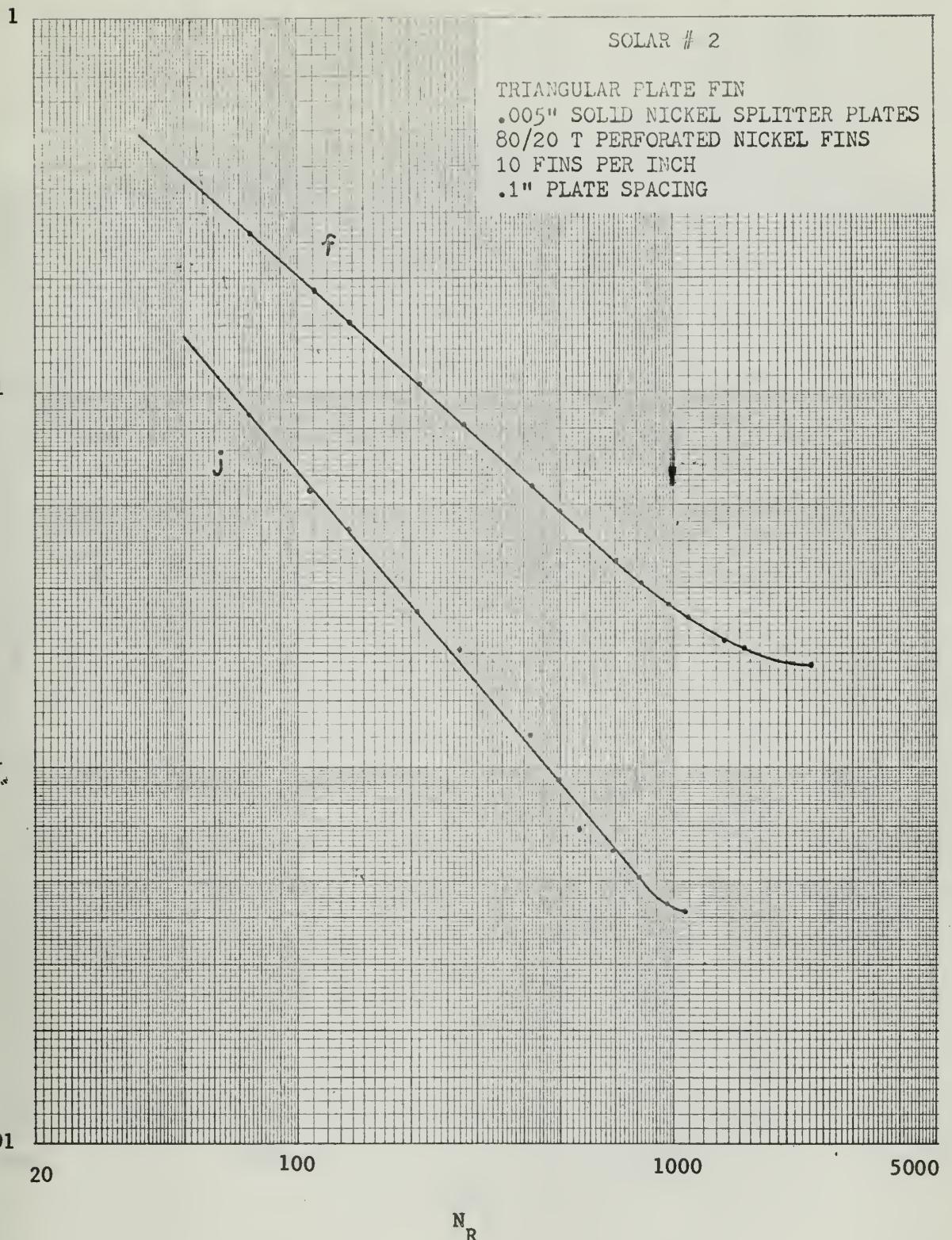
Figure 24. Heat Transfer and Flow Friction
Characteristics Solar #2
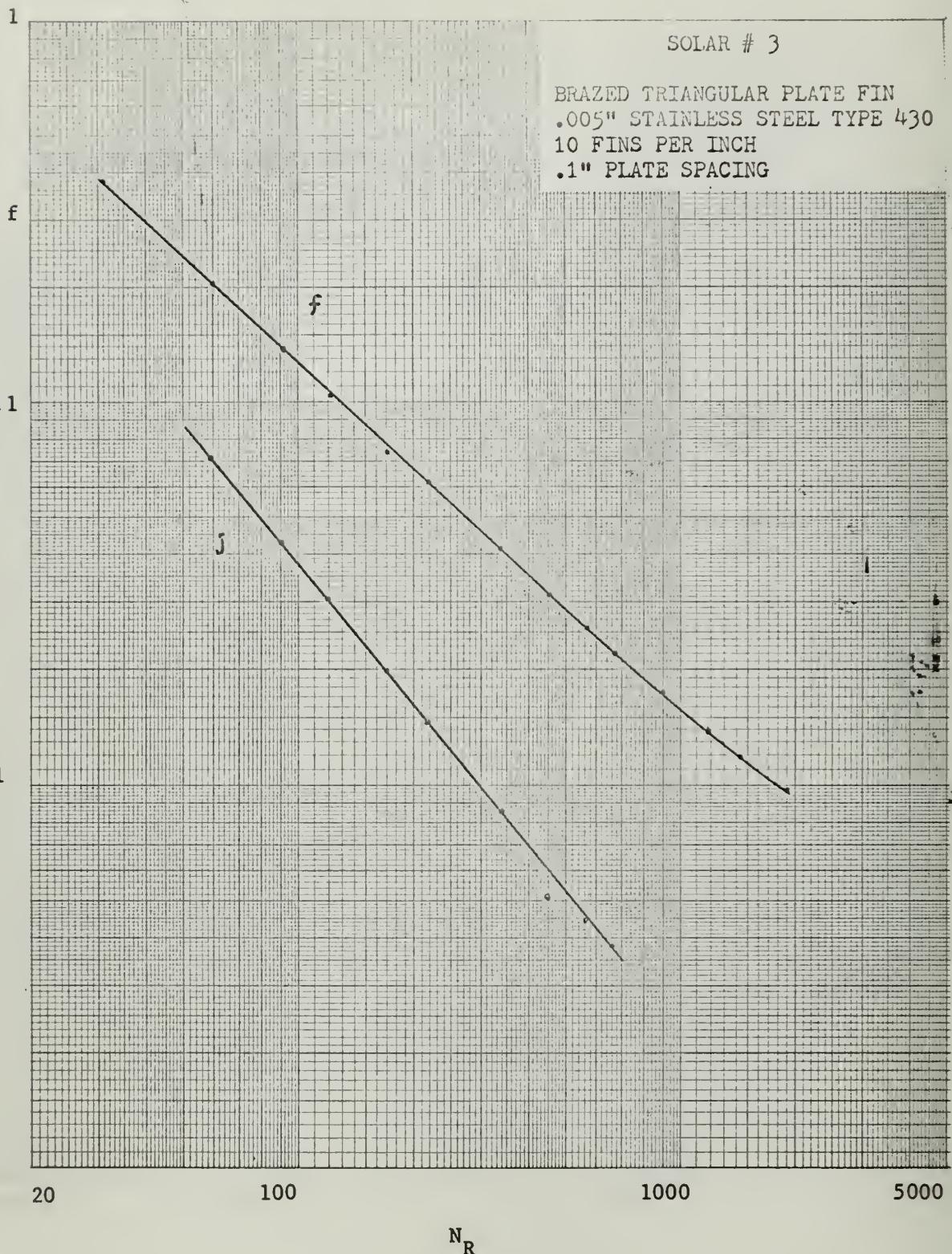
Figure 25. Heat Transfer and Flow Friction
Characteristics Solar #3
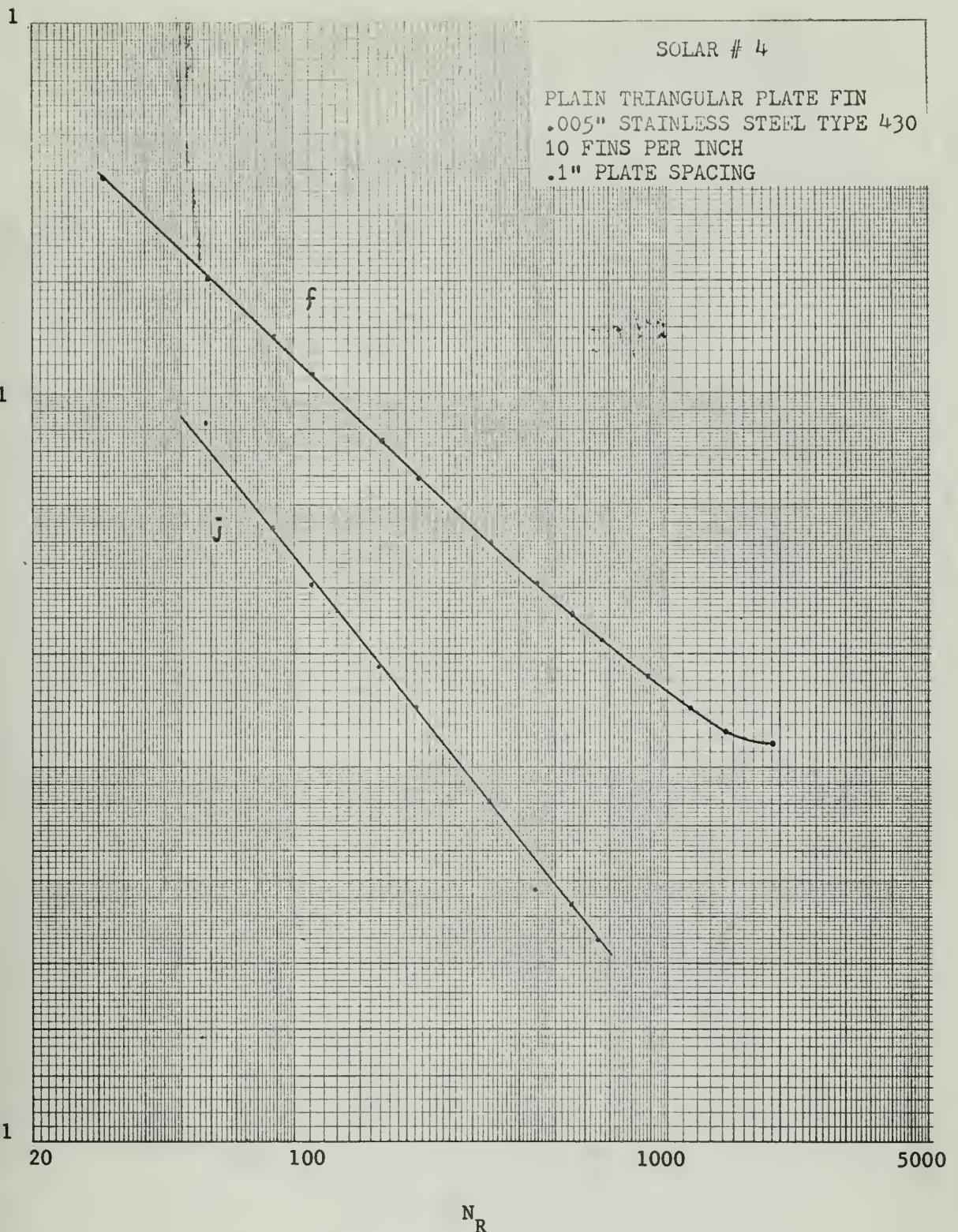
Figure 26. Heat Transfer and Flow Friction
Characteristics Solar #4
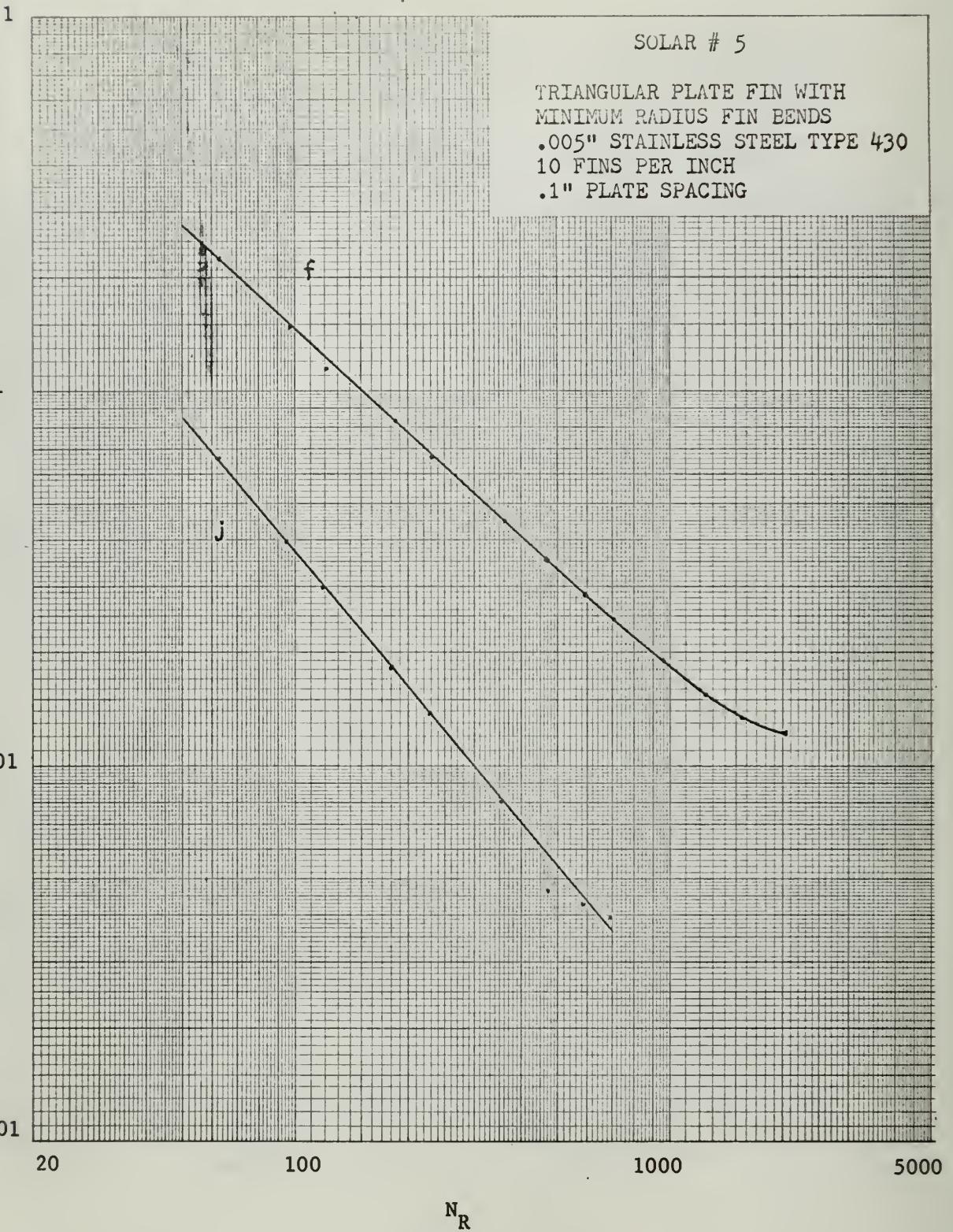
Figure 27.   Heat Transfer and Flow Friction
.. Characteristics Solar #5
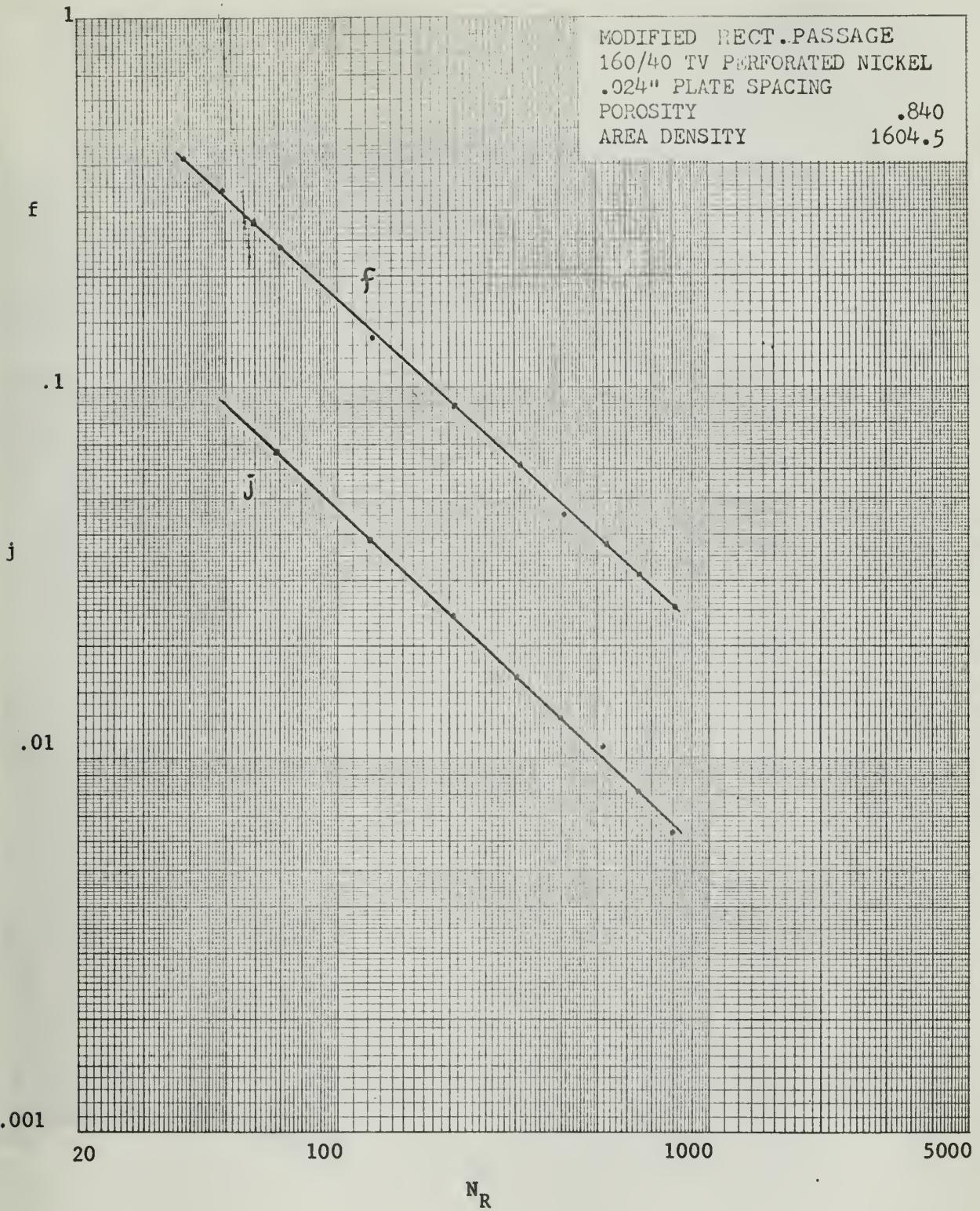
Figure 28. Heat Transfer and Flow Friction
Characteristics 160/40 TV
Modified Rectangular
Passage
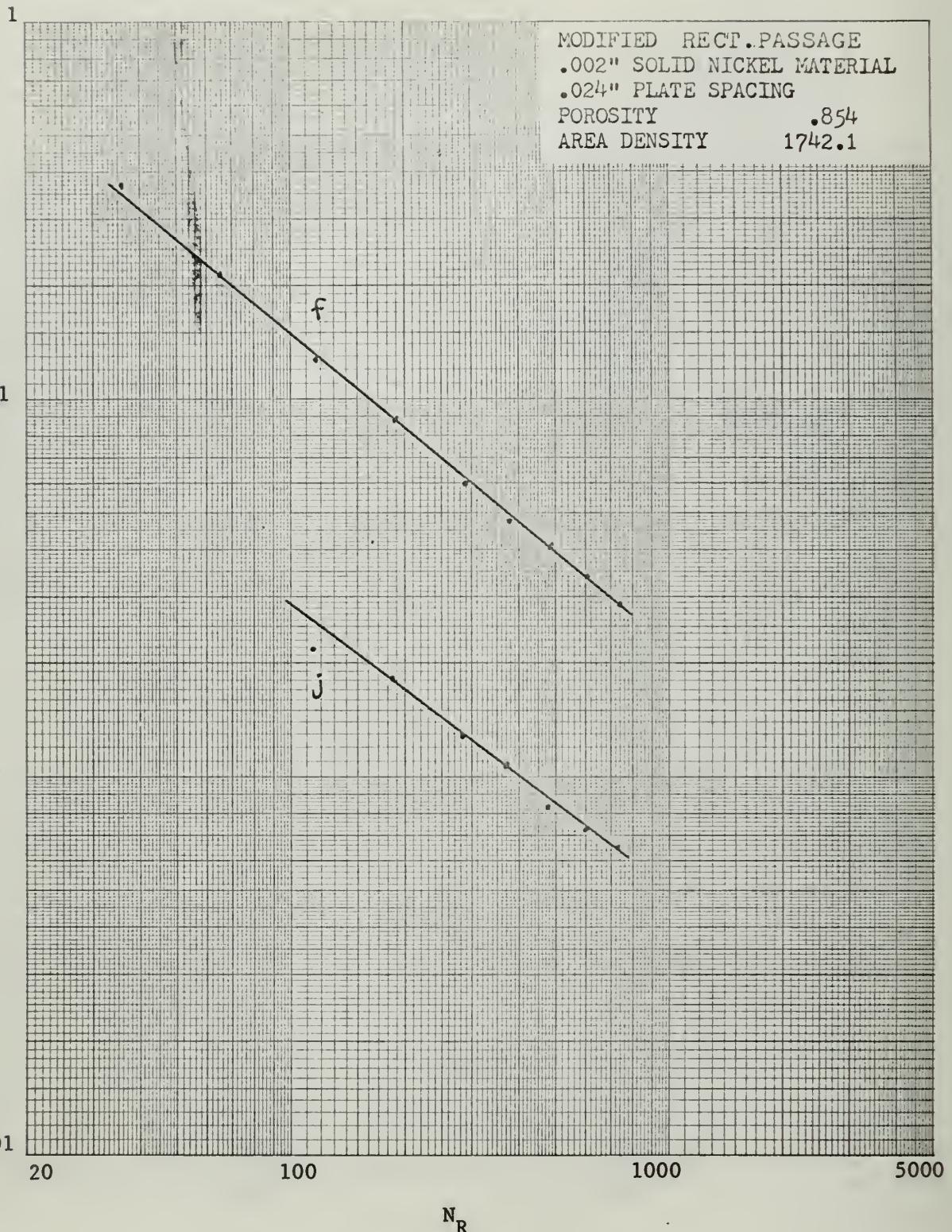
Figure 29.   Heat Transfer and Flow Friction
Characteristics Solid Nickel
Modified Rectangular Passage

COLBURN j   versus N_R

1. SOLAR # 1
2. SOLAR # 2
3. SOLAR # 3
4. SOLAR # 4
5. SOLAR # 5
6. 160/40 TV RECT.PASSAGE
7. SOLID NICKEL RECT.PASSAGE
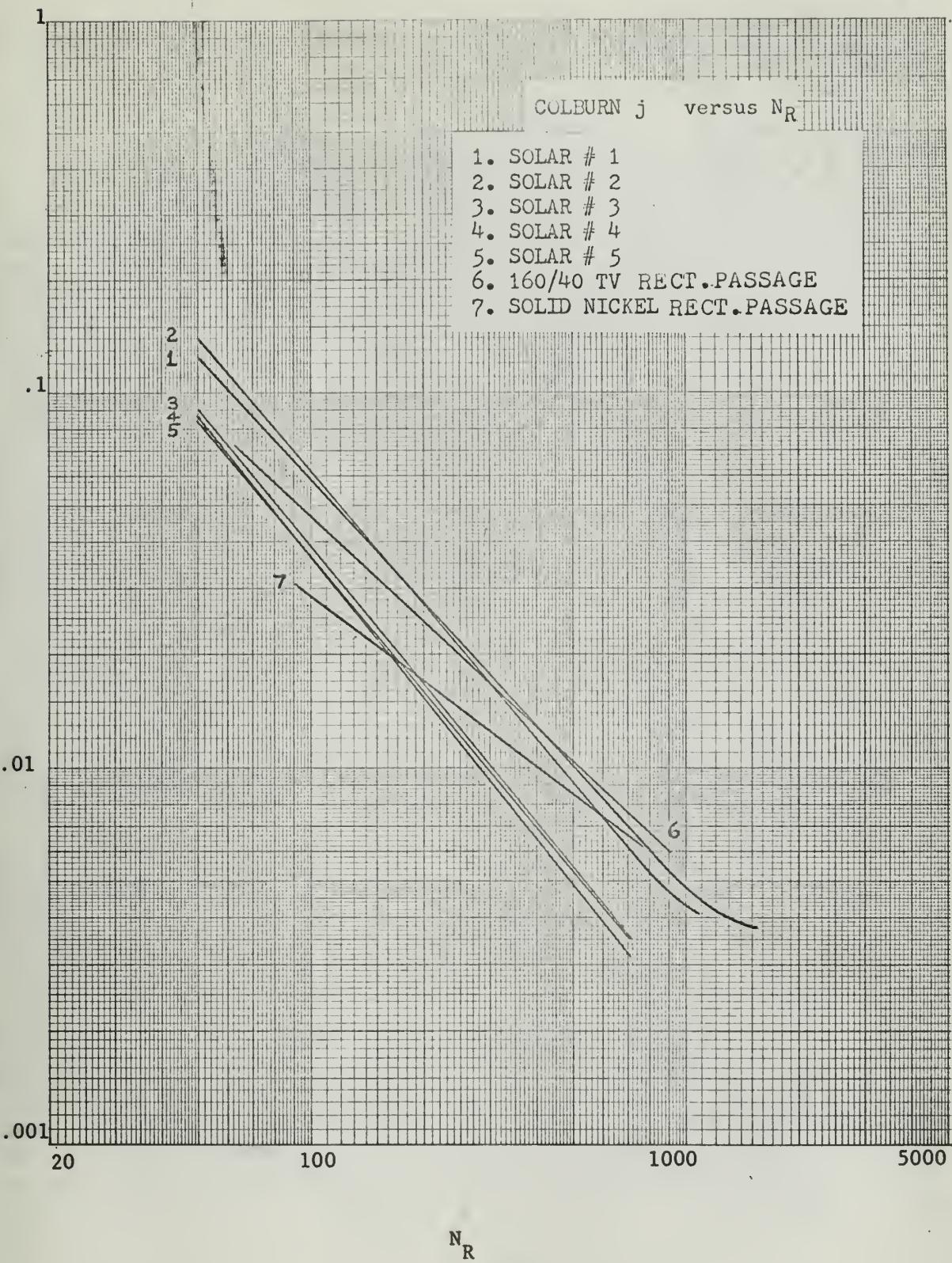
Figure 30. Comparison of Heat Transfer
Characteristics for all Surfaces

71
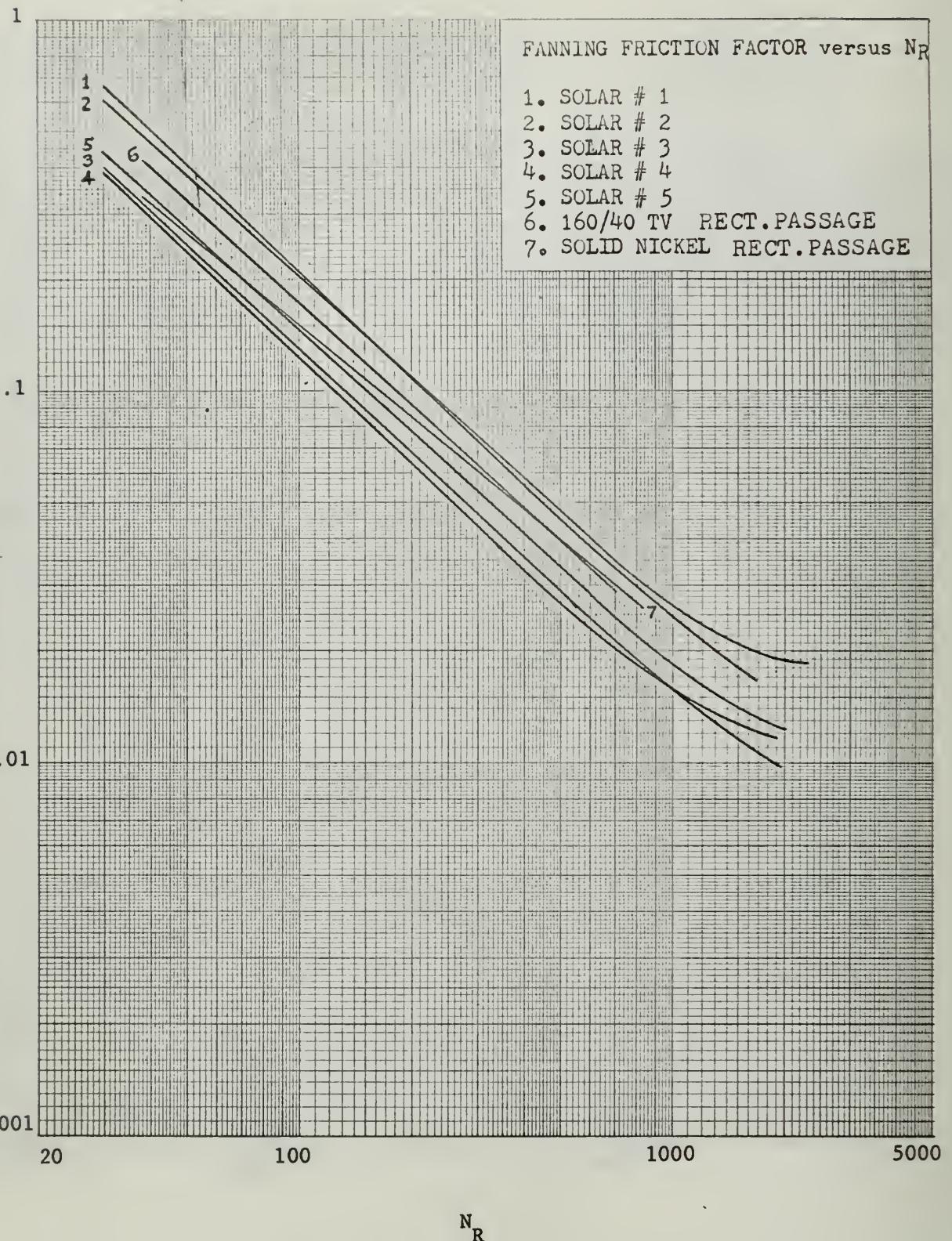
Figure 31.   Comparison of Flow Friction
             Characteristics for All Surfaces

72
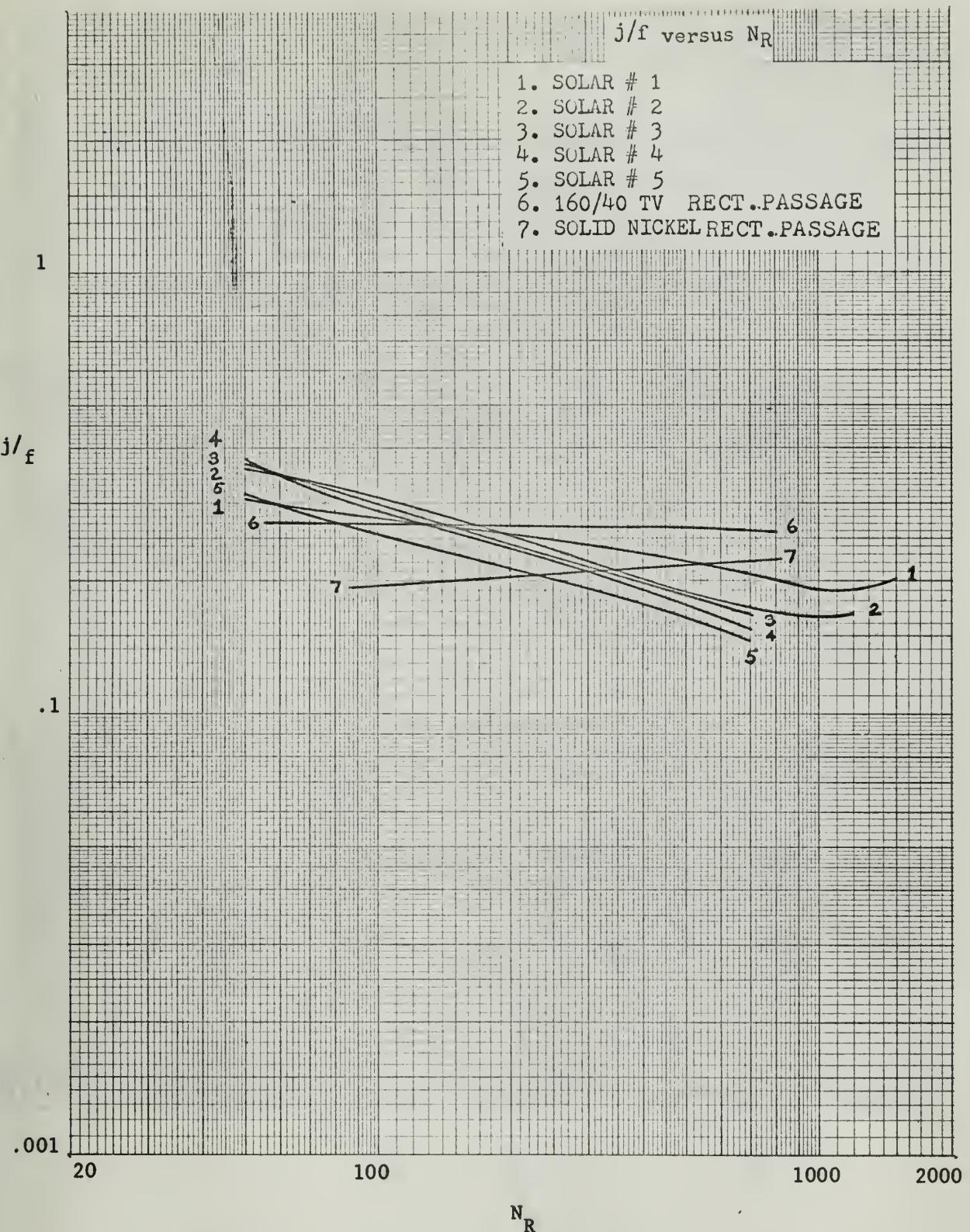
Figure 32.   Comparison of Flow Area Goodness
Factors for All Surfaces
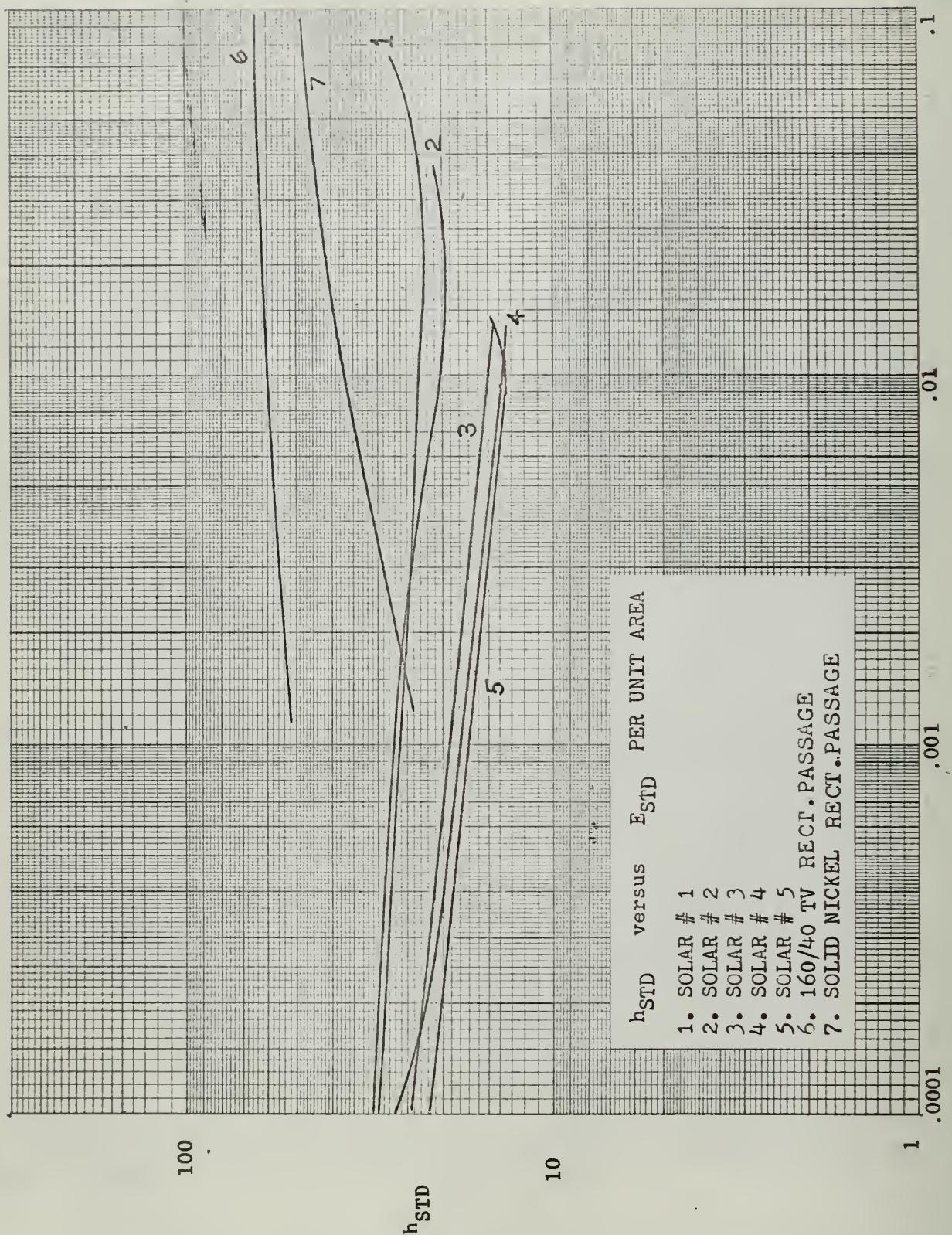
Figure 33.   Heat Transfer Power versus
             Flow Friction Power per Unit Area

74
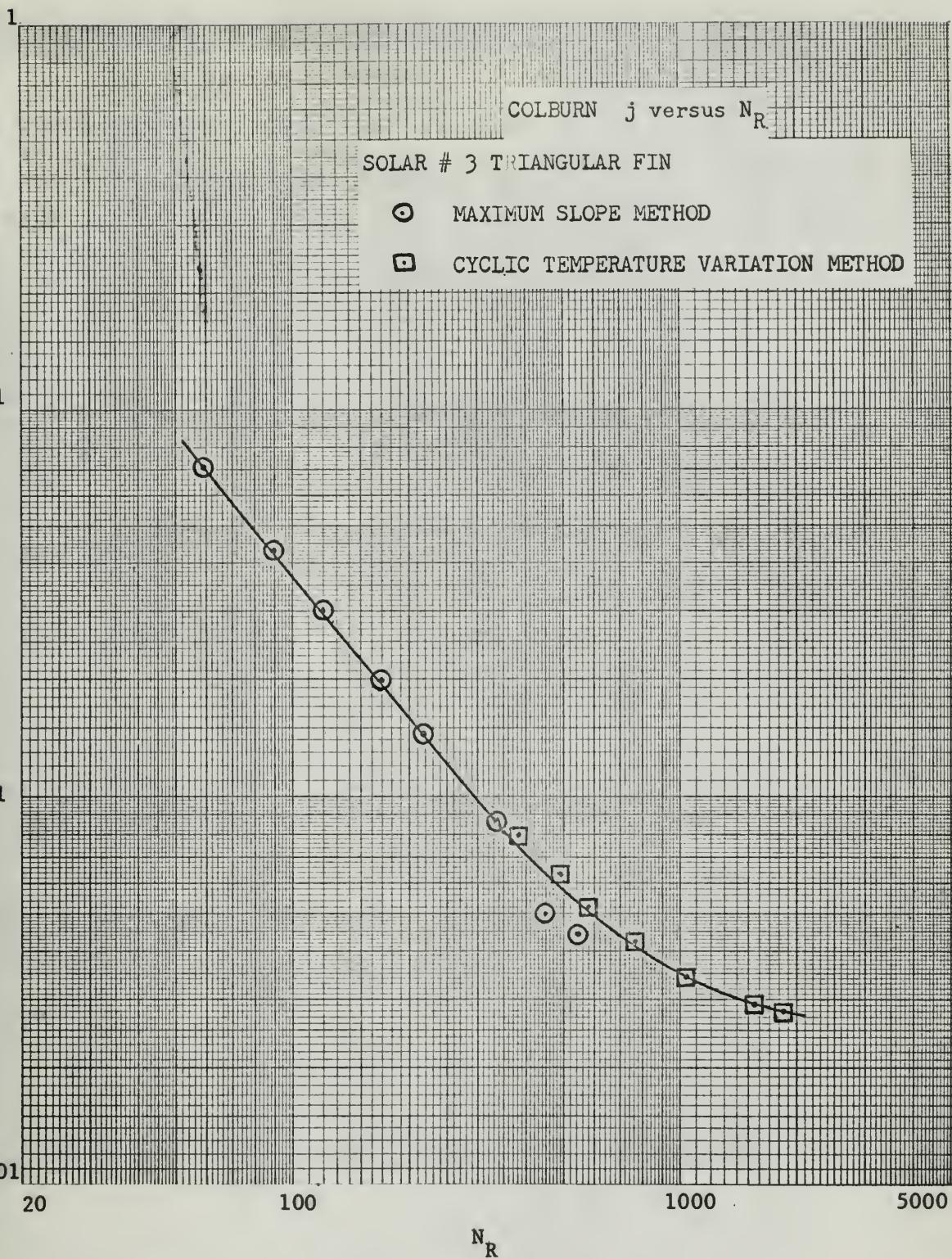
Figure 34.   Heat Transfer Data by Means of
Cyclic Technique Solar #3
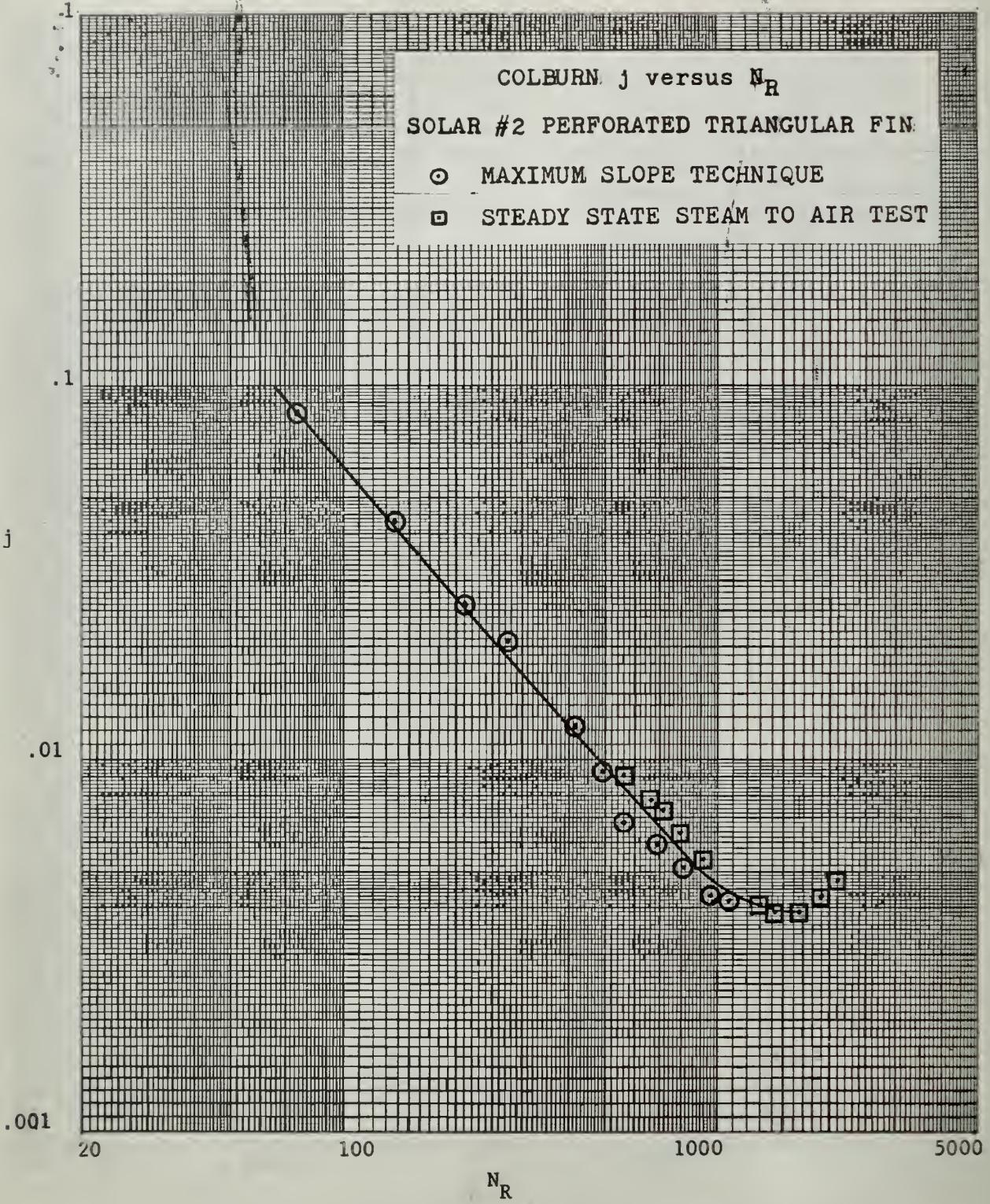
Figure 35. Heat Transfer Data by Means of Single Blow
and Steady State Steam to Air Test Solar #2

76
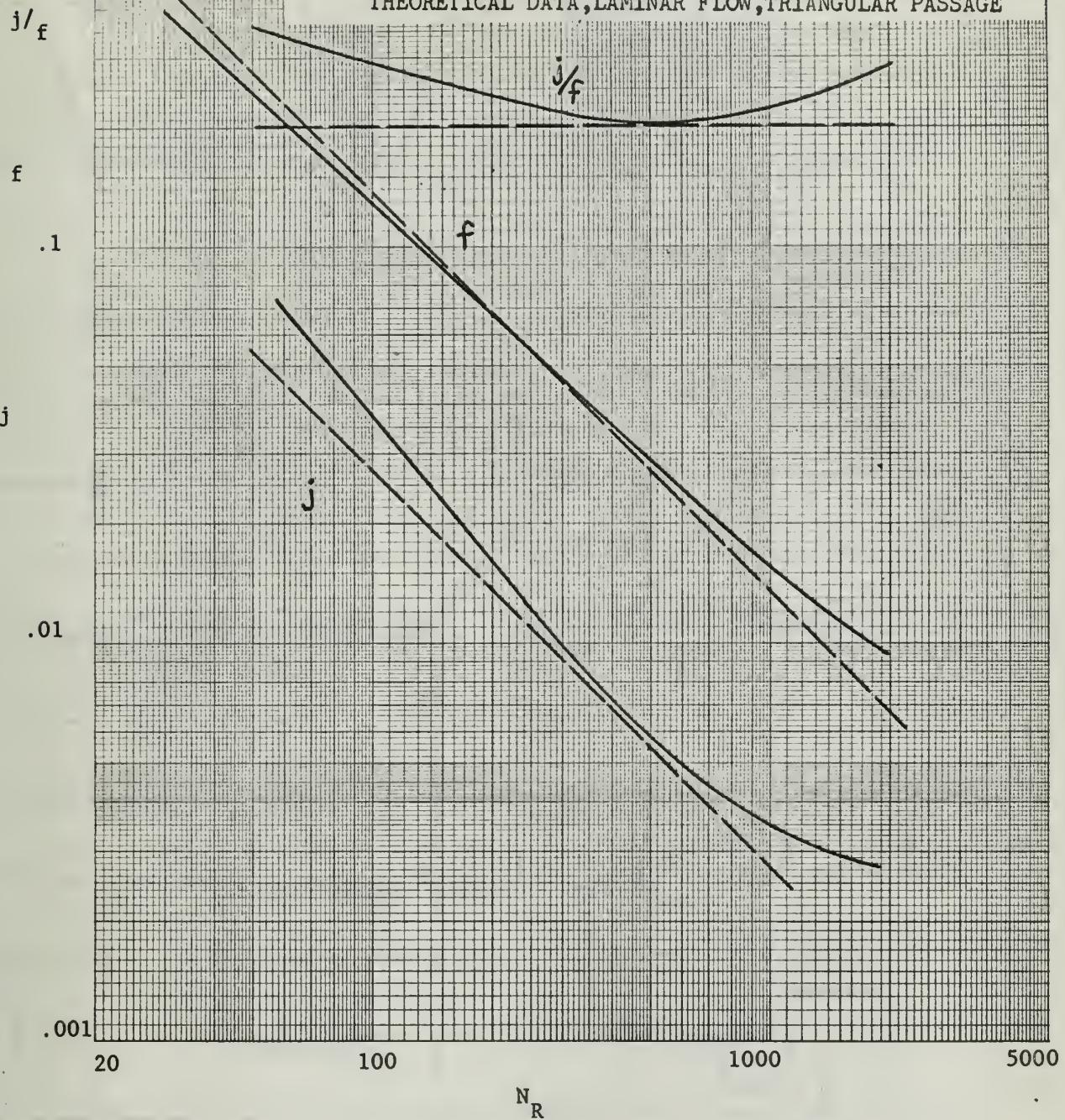
Figure 36. Comparison of Experimentally Determined
Heat Transfer and Friction Data with
Theory Solar #3
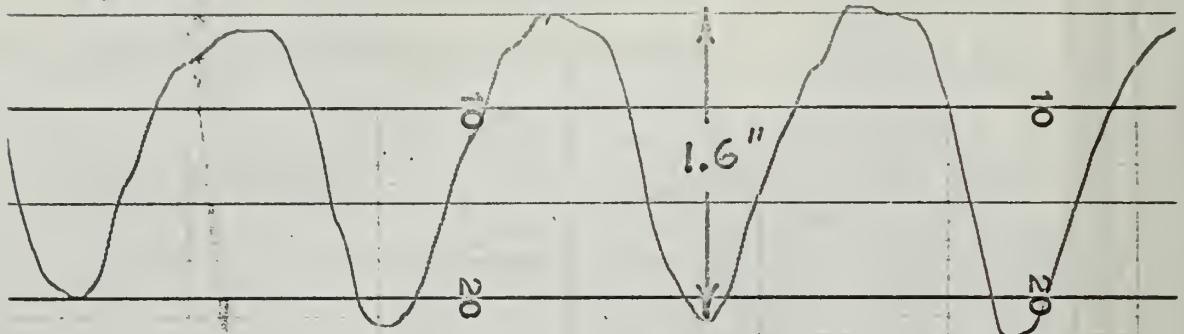
77
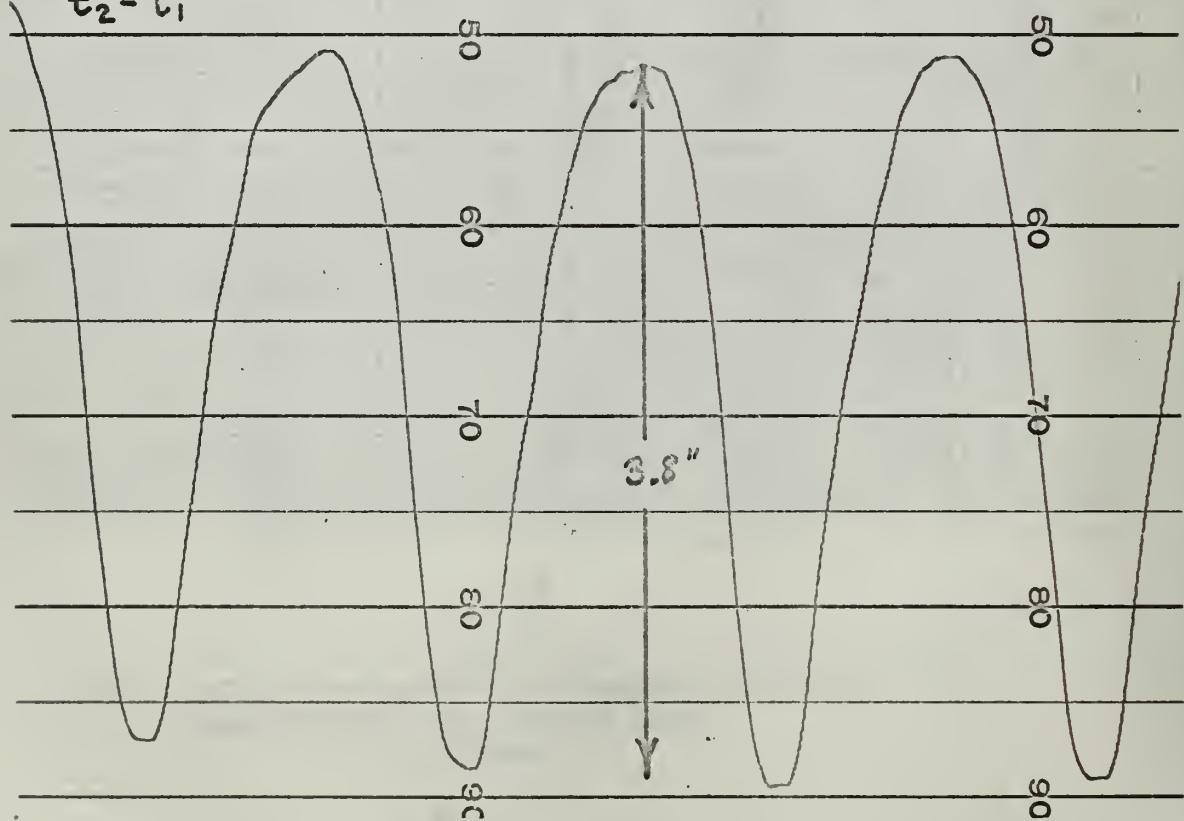
Figure 37. Chart Trace From Cyclic Test

78
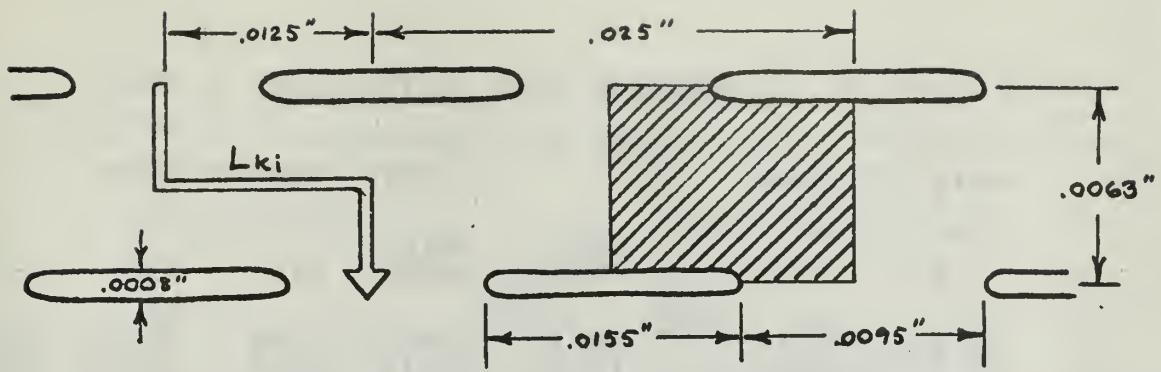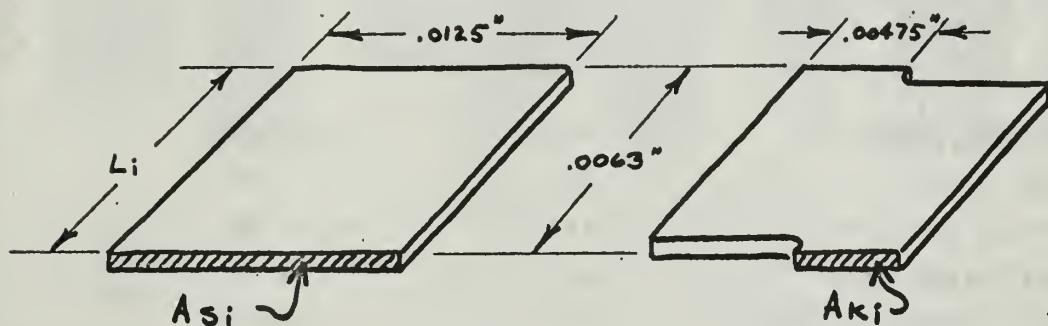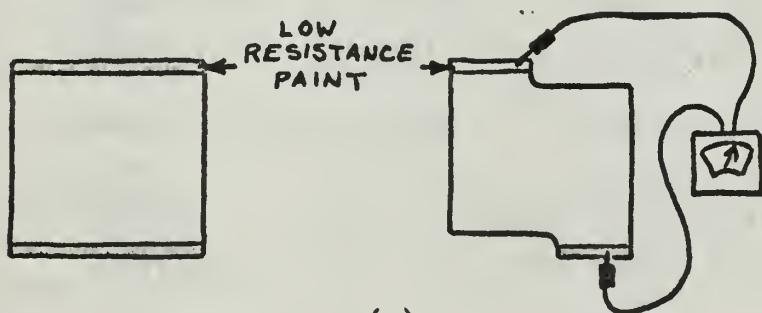
Figure 38. Conduction Parameter Analog

TABLE I. Summary of Heat Transfer and Friction Results

SCLAR NC.1 SINUSOIDAL FINS SOLID NICKEL 5 MILS

| FRICTION DATA | | | | HEAT TRANSFER DATA | | | |

RUN	NR	F	CONC PARAM	MAX SLOPE	NTU	NR	J
1	35.66	.58553	.32719	.92760	25.57	35.14	.09482
2	69.91	.30134	.16643	.93616	23.81	68.89	.08829
3	106.00	.20595	.10970	.92300	14.74	104.47	.05464
4	136.80	.15680	.08432	.88946	11.21	134.83	.04155
5	170.53	.12574	.06764	.86085	9.38	168.08	.03475
6	267.73	.08029	.04312	.72688	5.48	263.87	.02033
7	394.40	.05971	.02925	.63549	3.78	388.72	.01401
8	523.69	.04418	.02203	.56660	2.59	516.15	.00959
9	642.29	.03663	.01795	.54626	2.09	633.05	.00775
10	912.84	.02736	.01263	.49017	1.42	899.71	.00525
11	1164.10	.02248	.00990	.39251	1.06	1147.36	.00394
12	1293.89	.02064	.00892	.39769	1.08	1275.26	.00400
13	1432.01	.01873	.00805	.37934	1.03	1411.41	.00380
14	1557.13	.01773	.00741	.37751	1.02	1534.71	.00378
15	1678.22	.01681	.00688	.30071	.00	1654.05	.00000

FRONTAL AREA	AFR	.07022
FLOW LENGTH	L	.24917
MATRIX DENSITY	LB/FT3	86.13783
FREE FLOW AREA	AC	.05944
SOLID FRONTAL AREA	AS	.01078
PCROSITY	POR	.84640
HEAT TRANSFER AREA	A	12.76800
HYDRAULIC RADIUS	RH	.00116
AREA DENSITY (A/VM)	(BETA)	729.70260
CCNDUCTION PARAMETER RATIO (RS/RK)		1.00000
THERMAL CCNDUCTIVITY	KS	36.00
MATRIX HEAT CAPACITY	CS	.1060
ENTRANCE PRESS.LOSS CCEF.	KC	.93767
EXIT PRESSURE LOSS COEF.	KE	-.70431

TABLE II. Summary of Heat Transfer and Friction Results

SOLAR NO.2 80/20T SINUSOIDAL FINS SOLID NICKEL SPLITTERS 5 MILS

	FRICTION DATA			HEAT TRANSFER DATA			
RUN	NR	F	CCNC PARAM	MAX SLOPE	NTU	NR	J
1	38.67	.53389	.14025	.95455	25.60	38.12	.10087
2	75.32	.26494	.072C8	1.03187	21.88	74.24	.08623
3	110.81	.18811	.04926	.96874	13.84	109.21	.05455
4	139.0C	.15304	.03968	.91656	1C.98	136.98	.04330
5	212.84	.10594	.02560	.77382	6.60	209.78	.02602
6	276.05	.08185	.01996	.70906	5.24	272.04	.02066
7	421.28	.05593	.01290	.58821	3.09	415.24	.01217
8	497.17	.04840	.01096	.54974	2.35	490.02	.00926
9	570.53	.04258	.CC963	.53125	1.72	562.26	.00679
10	705.01	.03521	.00779	.50567	1.52	694.80	.00598
11	823.83	.03072	.00659	.46394	1.30	812.02	.00513
12	975.36	.02720	.00562	.39936	1.C9	961.25	.00428
13	1096.74	.02505	.005C0	.38556	1.05	1080.88	.00412
14	1368.82	.02142	.C0399	.00000	.00	1349.10	.00000
15	1538.31	.02057	.00355	.00000	.00	1516.14	.00000
16	2317.65	.01848	.00236	.00000	.00	2284.25	.00000

FRCNTAL AREA	AFR	.07022	
FLCW LENGTH	L	.25583	
MATRIX DENSITY	LB/FT3	70.30855	
FREE FLOW AREA	AC	.05989	
SCLID FRONTAL AREA	AS	.01034	
PCROSITY	POR	.85281	
HEAT TRANSFER AREA	A	12.09302	
HYDRAULIC RADIUS	RH	.00116	
AREA DENSITY (A/VM)	(BETA)	673.13967	
CCNDUCTICN PARAMETER RATIO (RS/RK)		.46730	
THERMAL CCNDUCTIVITY	KS	36.00	
MATRIX HEAT CAPACITY	CS	.1060	
ENTRANCE PRESS.LCSS CCEF.	KC	.07222	
EXIT PRESSURE LCSS CCEF.	KE	.02166	

TABLE III. Summary of Heat Transfer and Friction Results

SCLAR NO.3 SINUSOICAL FINS SOLID 430 STAINLESS MAX BRAZE 5 MILS

	FRICTION DATA			HEAT TRANSFER DATA			
RUN	NR	F	CONC PARAM	MAX SLOPE	NTU	NR	J
1	60.19	.20320	.07438	1.03852	23.30	59.32	.07076
2	91.18	.13761	.04907	.97702	14.24	89.87	.04325
3	121.78	.10327	.03673	.89137	9.98	120.03	.03031
4	172.54	.07288	.02593	.77241	6.57	170.06	.01995
5	221.36	.06223	.02021	.68751	4.82	218.18	.01464
6	342.40	.04132	.01308	.57362	2.81	337.48	.00853
7	456.46	.03125	.00980	.52398	1.65	449.90	.00502
8	567.42	.02574	.00789	.49362	1.44	559.26	.00438
9	672.09	.02200	.00666	.45011	1.25	662.44	.00379
10	902.44	.01737	.00496	.00000	.00	889.47	.00000
11	1194.66	.01378	.00375	.00000	.00	1177.47	.00000
12	1436.51	.01193	.00312	.00000	.00	1415.83	.00000
13	1921.60	.00975	.00233	.00000	.00	1893.93	.00000

FRONTAL AREA	AFR	.06803
FLOW LENGTH	L	.24833
MATRIX DENSITY	LB/FT3	94.26563
FREE FLOW AREA	AC	.05478
SOLID FRONTAL AREA	AS	.01325
POROSITY	POR	.80517
HEAT TRANSFER AREA	A	14.35884
HYDRAULIC RADIUS	RH	.00095
AREA DENSITY (A/VM)	(BETA)	849.89621
CONDUCTION PARAMETER RATIO (RS/RK)		1.00000
THERMAL CONDUCTIVITY	KS	12.80
MATRIX HEAT CAPACITY	CS	.1100
ENTRANCE PRESS.LOSS CCEF.	KC	.97439
EXIT PRESSURE LOSS CCEF.	KE	-.65449

TABLE IV. Summary of Heat Transfer and Friction Results

SOLAR NO.4 SINUSOIDAL FINS SOLID 430 STAINLESS MATL. 5 MILS

	FRICTION DATA			HEAT TRANSFER DATA			
RUN	NR	F	CONC PARAM	MAX SLOPE	NTU	NR	J
1	30.98	.37693	.13445	1.16696	2.00	30.53	.00611
2	59.13	.20381	.07044	1.07385	27.52	58.28	.08412
3	88.76	.14272	.04692	.97752	14.10	87.49	.04310
4	112.87	.11402	.03689	.89210	10.01	111.25	.03061
5	171.76	.07412	.02425	.74849	6.04	169.30	.01845
6	215.99	.05929	.01929	.68279	4.74	212.89	.01449
7	338.77	.03983	.01230	.56411	2.64	333.91	.008C6
8	447.77	.03100	.00929	.50780	1.53	441.35	.00467
9	557.45	.02546	.00747	.48585	1.40	549.45	.00429
10	664.38	.02172	.00627	.41536	1.13	654.85	.00346
11	888.19	.01741	.00469	.00000	.00	875.45	.00000
12	1162.42	.01426	.00358	.00000	.00	1145.75	.00000
13	1415.34	.01239	.00296	.00000	.00	1394.95	.00000
14	1908.14	.01161	.00219	.00000	.00	1880.66	.00000

FRONTAL AREA	AFR	.06713
FLOW LENGTH	L	.24417
MATRIX DENSITY	LB/FT3	88.59182
FREE FLOW AREA	AC	.05484
SOLID FRONTAL AREA	AS	.01229
POROSITY	POR	.81690
HEAT TRANSFER AREA	A	14.27694
HYDRAULIC RADIUS	RH	.00094
AREA DENSITY (A/VM)	(BETA)	870.99223
CONDUCTION PARAMETER RATIO (RS/RK)		1.00000
THERMAL CONDUCTIVITY	KS	12.80
MATRIX HEAT CAPACITY	CS	.1100
ENTRANCE PRESS.LOSS CCEF. KC		.96374
EXIT PRESSURE LOSS CCEF. KE		-.66901

TABLE V. Summary of Heat Transfer and Friction Results

SOLAR NO.5 TRIANGULAR FINS SOLID 430 STAINLESS MATL. 5 MILS

	FRICTION DATA			HEAT TRANSFER DATA			
RUN	NR	F	CONC PARAM	MAX SLOPE	NTU	NR	J
1	63.05	.22228	.06118	1.04806	21.15	62.15	.06573
2	96.54	.14597	.03995	.95656	12.62	95.15	.03924
3	121.54	.11431	.03172	.88205	9.54	119.79	.02967
4	183.46	.08385	.02101	.73707	5.81	180.83	.01805
5	231.11	.06594	.01667	.66779	4.48	227.80	.01393
6	360.72	.04488	.01068	.56045	2.57	355.54	.00800
7	482.55	.03439	.00798	.50007	1.48	475.63	.00460
8	600.21	.02846	.00642	.47897	1.37	591.59	.00426
9	708.74	.02472	.00544	.45696	1.28	698.57	.00396
10	964.34	.01907	.00401	.00000	.00	950.46	.00000
11	1247.65	.01548	.00310	.00000	.00	1229.68	.00000
12	1548.85	.01341	.00250	.00000	.00	1526.55	.00000
13	2040.53	.01207	.00190	.00000	.00	2011.13	.00000

FRONTAL AREA	AFR	.06781
FLOW LENGTH	L	.26417
MATRIX DENSITY	LB/FT3	81.93452
FREE FLOW AREA	AC	.05633
SOLID FRONTAL AREA	AS	.01148
POROSITY	POR	.83066
HEAT TRANSFER AREA	A	14.42340
HYDRAULIC RADIUS	RH	.00103
AREA DENSITY (A/VM)	(BETA)	805.13313
CONDUCTION PARAMETER RATIO (RS/RK)		1.00000
THERMAL CONDUCTIVITY	KS	12.80
MATRIX HEAT CAPACITY	CS	.1100
ENTRANCE PRESS.LOSS COEF.	KC	.95140
EXIT PRESSURE LOSS COEF.	KE	-.68569

TABLE VI· Summary of Heat Transfer and Friction Results

160/40 rv PERFORATED NICKEL FINS AND SPLITTERS

	FRICTION DATA			HEAT TRANSFER DATA			
RUN	NR	F	CCND PARAM	MAX SLOPE	NTU	NR	J
1	812.99	.02545	.00318	.55590	2.54	801.26	.00635
2	653.01	.03104	.00395	.59357	3.27	643.60	.00816
3	527.22	.03751	.00490	.65507	4.36	519.61	.01091
4	406.11	.04445	.00635	.69880	5.15	400.27	.01287
5	310.00	.06028	.00832	.77426	6.63	305.54	.01658
6	206.38	.08782	.01253	.89948	9.62	203.40	.02405
7	124.11	.13378	.02080	1.06826	15.73	122.32	.03932
8	69.91	.23837	.03694	1.17903	26.47	68.91	.06619
9	39.33	.42495	.06561	1.16650	2.00	38.76	.00500
10	69.29	.23339	.03736	1.21282	30.15	68.29	.07539
11	58.63	.27522	.04414	1.23549	2.00	57.78	.00500
12	48.89	.34594	.05293	1.22826	2.00	48.19	.00500
13	38.50	.41329	.06718	1.19438	2.00	37.94	.00500

FRONTAL AREA	AFR	.06264
FLOW LENGTH	L	.16670
MATRIX DENSITY	(LB/FT3)	70.51272
FREE FLOW AREA	AC	.05840
SOLID FRONTAL AREA	AS	.00424
POROSITY	PCR	.84000
HEAT TRANSFER AREA	A	18.59300
HYDRAULIC RADIUS	RH	.00048
AREA DENSITY (A/VM)	BETA	1604 ․5
COND.PARAMETER CORRECTION		.82844

TABLE VII.   Summary of Heat Transfer and Friction Results

.002 IN. SOLID NICKEL MOD.PARALLEL PLATE

	FRICTION DATA			HEAT TRANSFER DATA			
RUN	NR	F	COND PARAM	MAX SLOPE	NTU	NR	J
1	740.42	.02836	.00925	.57103	2.79	729.78	.00653
2	608.95	.03389	.01125	.58706	3.08	600.20	.00722
3	481.75	.04027	.01420	.61318	3.52	474.84	.00825
4	373.92	.04731	.01832	.67679	4.63	368.55	.01085
5	286.81	.05896	.02388	.71948	5.43	282.69	.01271
6	187.14	.08669	.03660	.81839	7.74	184.45	.01812
7	115.43	.12779	.05931	.86112	9.27	113.77	.02170
8	65.08	.21276	.10518	.81118	7.78	64.15	.01823
9	35.72	.37233	.19163	.77080	5.55	35.21	.01299

FRONTAL AREA	AFR	.06953
FLOW LENGTH	L	.16670
MATRIX DENSITY	(LB/FT3)	77.63067
FREE FLOW AREA	AC	.05939
SOLID FRONTAL AREA	AS	.01014
POROSITY	PCR	.85420
HEAT TRANSFER AREA	A	20.18750
HYDRAULIC RADIUS	RH	.00049
AREA DENSITY (A/VM)	BETA	1742.1
COND.PARAMETER CORRECTION		1.00000

Maximum Slope

Ntu \ λ	∞	10	1.0	.500	.100	.080	.060	.040	.035	.030	.025	.020	.015	.010	.005	0
1.0	.400	–	–	–	.384	.382	.380	.377	–	–	–	.374	–	–	–	.368
1.1	.445	–	–	–	.425	.420	.417	.413	–	–	–	.408	–	–	–	.403
1.2	.488	–	–	–	.459	.452	.447	.445	–	–	–	.440	–	–	–	.434
1.3	.529	–	–	.497	.487	.480	.475	.472	–	–	–	.467	–	–	–	.461
1.4	.568	–	–	.522	.511	.503	.498	.494	–	–	–	.489	–	–	–	.483
1.5	.603	–	–	.542	.530	.521	.517	.512	–	–	–	.507	–	–	–	.502
1.6	.637	–	–	.560	.544	.536	.530	.527	–	–	–	.522	–	–	–	.517
1.8	.697	–	–	.589	.561	.553	.547	.542	–	–	–	.539	–	–	–	.536
2.0	.748	.723	.646	.615	.571	.563	.556	.548	–	–	–	.545	–	–	–	.541
2.2	.791	.764	.677	.640	.582	.574	.566	.557	–	–	–	.549	–	–	–	.544
2.4	.827	.798	.703	.662	.592	.585	.577	.567	–	–	–	.557	–	–	–	.549
2.6	.857	.826	.726	.682	.603	.595	.587	.577	–	–	–	.566	–	–	–	.557
2.8	.882	.850	.745	.699	.615	.606	.598	.587	–	–	–	.577	–	–	–	.567
3.0	.903	.869	.761	.714	.626	.617	.608	.598	–	–	–	.587	–	–	–	.577
3.2	.920	.886	.775	.727	.637	.628	.619	.609	–	–	–	.598	–	–	–	.587
3.4	.934	.899	.787	.738	.647	.640	.630	.620	–	–	–	.610	–	–	–	.596
3.6	.946	.911	.798	.749	.658	.650	.641	.631	–	–	–	.621	–	–	–	.609
3.8	.956	.920	.807	.758	.668	.660	.652	.642	–	–	–	.632	–	–	–	.621
4.0	.964	.928	.815	.767	.678	.670	.662	.653	–	–	–	.643	–	–	–	.632
4.5	.978	.941	.831	.784	.701	.694	.687	.678	–	–	–	.670	–	–	–	.660
5.0	.987	.951	.843	.800	.722	.717	.711	.704	–	–	–	.697	–	–	–	.686
5.5	.992	.956	.852	.812	.742	.737	.733	.727	–	–	–	.722	–	–	–	.715
6.0	.995	.960	.859	.822	.760	.757	.753	.750	–	–	–	.746	–	–	–	.741
6.5	–	.962	.865	.830	.776	.774	.773	.771	–	–	–	.769	–	–	–	.767
7.0	1.000	.964	.870	.837	.792	.791	.791	.791	–	–	–	.792	–	–	–	.792
7.5	–	.965	.874	.844	.805	.806	.808	.810	–	–	–	.812	–	–	–	.816
8.0	–	.966	.877	.849	.817	.821	.824	.827	–	–	–	.832	–	–	–	.840
9.0	–	.967	.882	.858	.840	.847	.853	.861	–	–	–	.872	–	–	–	.885
10.0	1.000	.968	.886	.864	.860	.869	.880	.890	.893	.897	.901	.906	.911	.916	.922	.929
11.0	–	.968	.889	.870	.878	.888	.901	.917	.921	.927	.933	.939	.946	.953	.959	.970
12.0	–	–	–	.873	.893	.906	.922	.942	.948	.955	.962	.970	.979	.988	.998	1.010
13.0	1.000	–	–	.875	.907	.922	.941	.965	.973	.980	.990	.999	1.009	1.022	1.034	1.049
14.0	–	–	.893	.877	.921	.937	.958	.987	.996	1.005	1.016	1.027	1.039	1.053	1.068	1.085
15.0	–	–	–	.879	.932	.950	.975	1.007	1.017	1.028	1.040	1.053	1.068	1.085	1.102	1.121
16.0	–	–	–	.881	.942	.963	.990	1.026	1.037	1.049	1.063	1.077	1.094	1.112	1.133	1.156
18.0	–	–	–	.885	.960	.984	1.016	1.060	1.073	1.088	1.105	1.123	1.144	1.167	1.193	1.223
20.0	1.000	–	.894	.887	.975	1.003	1.039	1.089	1.105	1.123	1.143	1.164	1.189	1.217	1.249	1.286
22.0	–	–	–	.889	.987	1.018	1.059	1.116	1.134	1.154	1.177	1.202	1.231	1.264	1.302	1.347
24.0	–	–	–	.891	.997	1.032	1.077	1.140	1.160	1.182	1.208	1.237	1.269	1.308	1.352	1.404
26.0	–	–	–	.893	1.005	1.043	1.092	1.161	1.183	1.208	1.236	1.268	1.305	1.348	1.399	1.460
28.0	–	–	.895	.894	1.013	1.053	1.106	1.180	1.204	1.231	1.262	1.298	1.339	1.387	1.444	1.515
30.0	–	–	–	.895	1.019	1.061	1.118	1.198	1.224	1.253	1.286	1.325	1.370	1.423	1.487	1.565
32.0	–	–	–	–	–	–	–	1.214	1.241	1.273	1.309	1.351	1.399	1.458	1.528	1.617
34.0	1.000	–	–	–	–	–	–	1.228	1.258	1.291	1.330	1.374	1.427	1.490	1.568	1.665
36.0	–	–	–	–	–	–	–	1.242	1.273	1.308	1.349	1.397	1.453	1.521	1.605	1.712
38.0	–	–	–	–	–	–	–	1.254	1.287	1.324	1.367	1.418	1.478	1.551	1.641	1.757
40.0	–	–	–	–	–	–	–	1.266	1.300	1.339	1.384	1.437	1.501	1.579	1.676	1.801
45.0	–	–	–	–	–	–	–	1.292	1.328	1.372	1.422	1.481	1.554	1.643	1.757	1.908
50.0	1.000	–	–	–	–	–	–	1.313	1.353	1.400	1.455	1.520	1.601	1.702	1.833	2.010
55.0	1.000	–	–	–	–	–	–	1.332	1.375	1.425	1.483	1.555	1.644	1.756	1.902	2.107
60.0	1.000	–	–	–	–	–	–	1.347	1.392	1.445	1.508	1.585	1.680	1.803	1.967	2.199

TABLE VIII. Ntu as a Function of Maximum Slope and Longitudinal Conduction Parameter

APPENDIX A

DATA REDUCTION RELATIONSHIPS

GEOMETRY

Porosity = $\dfrac{\text{Matrix free flow area}}{\text{Matrix frontal area}}$

$$P = \frac{A_c}{A_{Fr}} \tag{A-1}$$

Hydraulic diameter = $\dfrac{4\text{x Free flow area}}{\text{Wetted perimeter}}$

$$D_H = \frac{4 A_c L}{A_b} \tag{A-2}$$

Area density = $\dfrac{\text{Heat transfer surface area}}{\text{Matrix volume}}$

$$\beta = \frac{A}{V_m} = \frac{A}{A_{Fr} L} \tag{A-3}$$

MASS RATE OF FLUID FLOW

The mass flow rate, $\dot{m}$, is calculated in accordance with references [21] and [23].

$$\dot{m} = 359\, k\, d_o^2\, F_a\, Y\, \sqrt{\Delta P_o\, \gamma} \qquad (lbm/hr) \tag{A-4}$$

Where:

$k = \dfrac{C}{\sqrt{1 - \beta^4}}$ the flow coefficient including velocity of approach

C = orifice coefficient of discharge from [21]

β = ratio of orifice diameter to inside pipe diameter

d_o = orifice diameter

F_a = thermal expansion factor

Y = expansion factor

$\gamma = \dfrac{P}{RT}$ the specific weight of the fluid flowing

P = absolute static pressure at the orifice (lbf/sq ft)

$R = 53.35\ \dfrac{\text{ft lbF}}{\text{lbm°R}}$, the universal gas constant for air

T = absolute temperature (°R) at the orifice

$\Delta P_o =$ Pressure drop across the orifice in inches of water

Making substitutions for K and Y, (A-4) becomes:

$$\dot{m} = \frac{359\, C\, d_o^2\, F_a\, Y}{\sqrt{1-\beta^4}} \sqrt{\Delta P_o \frac{P}{RT}} \qquad \text{(A-5)}$$

In accordance with [23] figures (38) and (40b):

$$F_a \approx 1.0$$
$$Y \approx 1.0$$

Also:

$$P = \left(P_{ATM} - \frac{P_o}{13.6}\right) .4912 \times 144 \qquad \text{(lbf/sq ft)}$$

Where: P_{ATM} is measured in inches of mercury

             P_o is measured in inches of water

and:

$$T = t_o + 459.7$$

where t_o is measured in degrees Fahrenheit

Introducing the values and expressions above into (A-5) produces the working formula:

$$\dot{m} = \frac{289.71\, C\, d_o^2}{\sqrt{1-\beta^4}} \sqrt{\Delta P_o \frac{\left(P_{ATM} - \frac{P_o}{13.6}\right)}{(t_o + 459.7)}} \qquad \text{(A-6)}$$

REYNOLD'S NUMBER

By definition:

$$N_R = \frac{D_H\, G}{\mu}$$

Substituting $\frac{4 A_c L}{A_b}$ for D_H, and $\frac{\dot{m}}{A_c}$ for G:

$$N_R = \frac{4 L \dot{m}}{\mu A_b} \qquad \text{(A-7)}$$

89
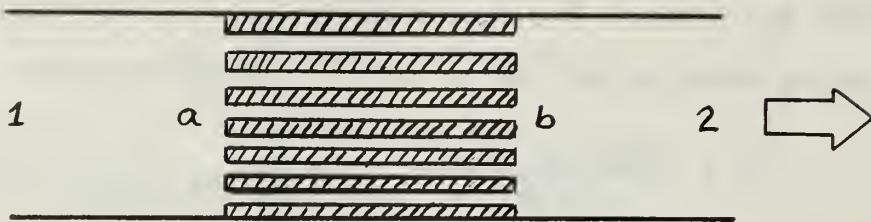
The following equation describes the flow through the matrix [12]:

$$\frac{\Delta P}{P_1} = \frac{G^2}{2g_c}\frac{v_1}{P_1}\left[\overset{\text{ENTRANCE}}{(k_c+1-P^2)} + \overset{\text{ACCELERATION}}{2\left(\frac{v_2}{v_1}-1\right)} + \overset{\text{FRICTION}}{f\frac{A_b}{A_c}\frac{v_m}{v_1}} - \overset{\text{EXIT}}{\left(1-P^2-k_e\right)\frac{v_2}{v_1}}\right]$$

where p = porosity ($\frac{A_c}{A_{Fr}}$)

It is assumed that $v_a \approx v_1$ and $v_b \approx v_2$ since the associated pressure changes are very small compared with the total pressure. It is also assumed that the perfect gas low applies ($v = \frac{RT}{P}$). Making the necessary substitutions and solving for f produces for the iso-thermal case:

$$f = \left[2\rho_m\frac{\Delta P}{G^2} - \left(\frac{P_1+P_2}{2}\right)\left(\frac{k_c}{P_1}+\frac{k_e}{P_2}\right) - \left(\frac{P_1+P_2}{2}\right)\left(\frac{1}{P_2}-\frac{1}{P_1}\right)(1+P^2)\right]\frac{r_H}{L} \qquad (A-8)$$

Since the first term within the brackets above is much larger than the other terms, the following approximation can be made:

$$\frac{P_1+P_2}{2} = P_m \approx P_1 \approx P_2$$

Thus equation (A-8) becomes:

$$f = \left[2g_c\rho_m\frac{\Delta P}{G^2} - (k_c+k_e) + \frac{\Delta P}{P_m}(1+P^2)\right]\frac{r_H}{L} \qquad (A-9)$$

k_c and k_e , the entrance and exit loss coefficients are functions of porosity, matrix configuration, and Reynold's number, and are obtained in accordance with reference [11].

MAXIMUM SLOPE

The maximum slope of the generalized cooling curve as previously mentioned, is a function of Ntu and conduction parameter, λ :

$$\left[\frac{d\left(\frac{t_{F_2}-t_i}{t_{F_1}-t_i}\right)}{d\left(\tau/Ntu\right)} \right]_{MAX} = \varphi(Ntu, \lambda) \tag{A-10}$$

where:

$$\tau = \frac{hA}{W_s c_s}\theta \qquad \text{and} \qquad Ntu = \frac{hA}{\dot{m}c_p}$$

Therefore:

$$\tau/Ntu = \frac{\dot{m}c_p}{W_s c_s}\theta$$

and:

$$d\left(\tau/Ntu\right) = \frac{\dot{m}c_p}{W_s c_s}d\theta = \frac{C_F}{C_s}d\theta \tag{A-11}$$

also:

$$\frac{t_{F_2}-t_i}{t_{F_1}-t_i} = \frac{t_{F_2}-t_{F_1}}{t_{F_1}-t_i} + 1$$

and:

$$d\left(\frac{t_{F_2}-t_i}{t_{F_1}-t_i}\right) = \frac{1}{t_{F_1}-t_i}d\left(t_{F_2}-t_i\right) \tag{A-12}$$

combining (A-11) and (A-12) yields:

$$\left[\frac{d\left(\frac{t_{F_2}-t_i}{t_{F_1}-t_i}\right)}{d\left(\tau/Ntu\right)} \right]_{MAX} = \frac{C_s}{C_F}\frac{1}{t_{F_1}-t_i}\left[\frac{d\left(t_{F_2}-t_{F_1}\right)}{d\theta}\right]_{MAX} \tag{A-13}$$

91

Now consider the following sketch of a generalized cooling curve:
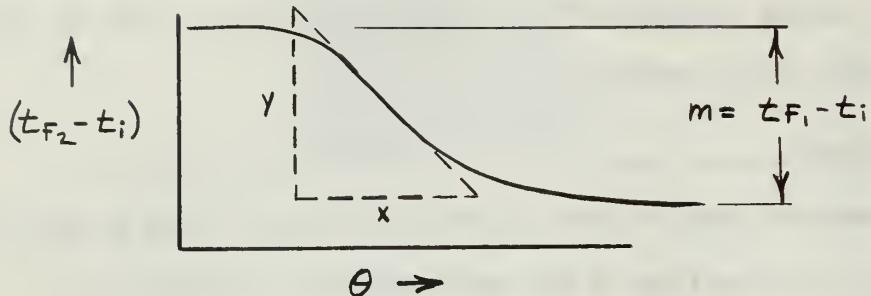
$$\left[\frac{d\left(t_{F_2} - t_{F_1}\right)}{d\theta} \right]_{MAX} = \frac{Y}{X}$$

$$d\theta = \frac{X}{CHART\ SPEED}$$

$$d\left(t_{F_2} - t_{F_1}\right) = Y$$

$$\left(t_{F_1} - t_i\right) = m$$

Combining the above produces the maximum slope:

$$\left[\frac{d\left(\frac{t_{F_2} - t_i}{t_{F_1} - t_i}\right)}{d\left(\tau / N_{tu}\right)} \right]_{MAX} = \frac{C_s}{C_F} \times \frac{1}{m} \times \frac{Y}{X} \times CHART\ SPEED \tag{A-14}$$

Ntu can now be determined from conduction parameter λ and maximum slope.

COLBURN j

Colburn's heat transfer parameter, j, is defined:

$$j = N_{st} \, N_{pr}{}^{2/3}$$

$$= \frac{h}{G \, c_p} \, N_{pr}{}^{2/3}$$

$$= \frac{hA}{\dot{m} \, c_p} \, \frac{A_c}{A} \, N_{pr}{}^{2/3}$$

(A-15)

thus:

$$j = N_{tu} \, \frac{A_c}{A} \, N_{pr}{}^{2/3}$$

(A-16)

From equations (A-1) and (A-3): $\quad P = \dfrac{A_c}{A_{Fr}} \quad and \quad \beta = \dfrac{A}{A_{fr} \, L}$

$$j = N_{tu} \, N_{pr}{}^{2/3} \, \frac{1}{L} \, \frac{P}{\beta}$$

(A-17)

From equation (A-17) it can be seen:

$$j \propto \frac{P}{\beta}$$

HEAT TRANSFER POWER

The heat transfer power per unit area per degree temperature difference is [12]:

$$h = \frac{c_p \, \mu}{N_{pr}{}^{2/3}} \, \frac{1}{D_H} \, j \, N_R$$

(A-18)

For dry air at standard conditions equation (A-18) becomes:

$$h_{sto} = .02195 \, \frac{N_R \, j}{D_H} \qquad Btu/(hr \; sq \; ft \; deg \, F)$$

(A-19)

93

FLOW FRICTION POWER

The flow friction power per unit area is defined as [12]:

$$E = \frac{1}{2g_c} \frac{\mu^3}{\rho^2} \left(\frac{1}{D_H}\right)^3 F \, N_R^3 \qquad \text{(A-20)}$$

For dry air at standard conditions equation (A-20) becomes:

$$E_{STD} = 1.11 \times 10^{-7} \left(\frac{1}{D_H}\right)^3 F \left(\frac{N_R}{1000}\right)^3 \quad HP/_{Sq. Ft} \qquad \text{(A-21)}$$

For comparison purposes the surface geometries were reduced to a common hydraulic diameter.

DESCRIPTION OF EQUIPMENT

PRIME MOVER:

Air as the working fluid is drawn through the system by means of a 30 HP, multistage, Spencer Turbo-Compressor. This compressor is designed for a flow rate of 550 cubic feet per minute.

FLOW METER:

Flow rates are measured by means of an ASME standard orifice section designed for convenient changing of orifice plates. Thin plate concentric orifices with throat diameters ranging from .308 to 2.31 inches are employed allowing for a wide range of flow rates. Pressure taps are located d upstream and d/2 downstream. Inside pipe diameter, d, is 3.08 inches.

HEATER SYSTEM:

The heater section is made up of 28 grid type nichrome wire heaters. Two heaters are wound to each bakelite frame and thus may be energized in pairs. A schematic wiring diagram for one heater frame is shown below:
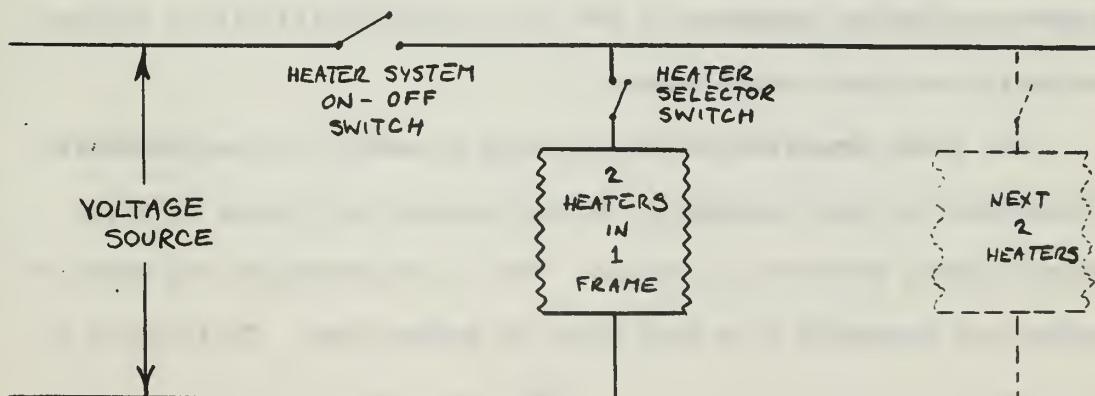
When energized, all heaters operate in parallel, the number of heaters in use depending upon flow rate.

For maximum slope operation the voltage source is 220 volts AC and can be varied by means of a General Radio Company "Variac" Autotransformer.

For cyclic operation the voltage source is a 1.5 KW General Electric Amplidyne connected in series with a D.C. source. The resulting input to the heaters is a sine wave voltage with an amplitude of 50 volts and an average value of 50 volts. Frequencies of .1 to 1.0 cycles per second are employed with a much wider range available.

MATRIX HOLDER AND TEST SECTION:

This section is constructed of polyethylene machined to close tolerances. The T_2 and T_4 thermocouple grids and the matrix upstream and downstream pressure taps are mounted in the frame. The T_3 thermocouple grid is mounted in the removable matrix holder. ½" sheet styrofoam inserts provide insulation and a snug fit for the test matrix. The flow channel measures 3-3/16" X 3-3/16" and matrices up to 3" in length may be accommodated in the test section. (See Figure 12)

TEMPERATURE MEASUREMENT:

The temperature at the orifice meter is measured by means of a copper-constantan thermocouple and read in millivolts with a Rubicon Portable Precision Potentiometer.

All other temperatures are measured by means of iron-constantan thermocouples, each temperature being measured by a group of five thermocouples connected in series. The T_1 thermocouples are bound together and insulated from each other by teflon tape. This bundle is

96

mounted at the throat of the intake cone, upstream of the wire screen flow straightener. The T_2, T_3, and T_1 grids are connected to a multiple barrel switch so that the emf generated by T_1 may oppose the emf generated by either T_2 or T_3. Thus the difference between ambient and matrix inlet or exit temperature can be read. These temperature differentials are recorded on a Minneapolis-Honeywell "Brown" Strip Chart Recorder with variable sensitivity and chart speed. For maximum slope operation, T_1 versus T_3 is recorded. For cyclic temperature variation, T_1 versus T_2, and T_1 versus T_3 are recorded.

PRESSURE MEASUREMENT:

The four pressure taps shown in Figure 8 are connected to Ellison draft gages by means of Imperial Company "Poly-flo" plastic tubing. The draft gages are a combination of inclined and vertical gages. They are shown in Figure 9. For small pressure differentials, Vernon Hill Company Type "C" Micromanometers are used. Pressures of 1.25" to 3.0" of water are read by means of the inclined draft gages. Pressures below this range are measured by means of the micromanometers; Pressure above 3.0" are read on vertical draft gages.

APPENDIX C

CONDUCTION PARAMETER FOR PERFORATED MATERIAL

The porous material used in the perforated plate matrices investigated in this report was made by Perforated Products, Inc. by means of an electro-depositing process.

For a solid plate or fin, the conduction parameter is defined as:

$$\lambda = \frac{k_s A_s}{LC}$$

where A_s is the solid cross-sectional area for conduction which is identical to the product of plate width and thickness, and L is the conduction path length which is identical to the matrix flow length.

For a perforated material such as the type 160/40 TV shown in Figure 38(a), the cross-sectional area for conduction varies in the flow direction, and the conduction path length is greater than the flow length.

The definition of conduction parameter is based upon a solid material, i.e.,

$$\lambda = \frac{k_s A_s}{LC} = \frac{1}{R_{Th} C}$$

where $R_{th} = \frac{L}{k_s A_s}$ the matrix thermal conduction resistance.

Using the above definition for a perforated material, an "equivalent" conduction parameter, λ_k , can be evaluated by determining the thermal resistance $(R_{th})_k$. By defining a relative shape factor S', the conduction parameter of a perforated material, λ_k , can be related to the conduction parameter of the same material as if it were unperforated:

$$\lambda_k = S'\lambda = S' \frac{k_s A_s}{LC}$$

or:

$$R_{Th} = S' (R_{Th})_k$$

By the analogy between conduction heat flow and electric current, note that for similar shapes, the ratio of electrical resistances:

$$\frac{r}{r_k} = \frac{R_{Th}}{(R_{Th})_k} = S'$$

In Figure 38(b) are shown two shapes, each representing the shaded portion of Figure 38(a). The shape on the left represents an unperforated material, and the shape on the right is an incremental model for the 160/40 TV material. The relative shape factor is determined from the ratio of the electrical resistances of these two models. Since the material is of uniform thickness, two dimensional models can be constructed from electrically conducting paper (such as Teledeltos paper) as shown in Figure 38(c), with low resistance silver paint applied as indicated. The electrical resistances are then measured with an ohm-meter. This analog method produced the following results for the type 160/40 TV perforated nickel material:

$$S' = \frac{R_{Th}}{(R_{Th})_k} = \frac{r}{r_k} = \frac{8.5}{27} = .315$$

thus: $\lambda_k = .315\,\lambda$

Whereas, $\lambda_k = .127\,\lambda$ as determined in reference [22] using:

$$\lambda_k = \lambda \frac{A_k}{A_s} \frac{L}{L_k}$$

where:
$$A_k = \sum A_{ki}$$
$$L_k = \sum L_{ki}$$

and: A_{ki} and L_{ki} are approximations indicated in Figures 38(a), and (b).

The effects of these approximations upon Ntu and j are shown in Figure 15.

99

APPENDIX D

EXPERIMENTAL UNCERTAINTY INTERVALS

According to reference [13], the uncertainty interval for a result is:

$$W_R = \left[\left(\frac{\partial R}{\partial V_1} W_1 \right)^2 + \left(\frac{\partial R}{\partial V_2} W_2 \right)^2 + \ldots + \left(\frac{\partial R}{\partial V_n} W_n \right)^2 \right]^{1/2} \qquad (D-1)$$

w_1, w_2, ... w_n are the uncertainty intervals of the factors making up the result.

R is the expression for the result

V_1, V_2, ... V_n are the factors making up the result.

The expression for Colburn j is:

$$j = N_{tu} \frac{A_c}{A} N_{Pr}^{2/3}$$

The uncertainty interval for Colburn j is:

$$W_j = \left[\left(\frac{\partial j}{\partial N_{tu}} W_{N_{tu}} \right)^2 + \left(\frac{\partial j}{\partial A_c} W_{A_c} \right)^2 + \left(\frac{\partial j}{\partial A} W_A \right)^2 + \left(\frac{\partial j}{\partial N_{Pr}^{2/3}} W_{N_{Pr}^{2/3}} \right)^2 \right]^{1/2}$$

$$W_j = \left[\left(\frac{A_c}{A} N_{Pr}^{2/3} W_{N_{tu}} \right)^2 + \left(\frac{N_{tu}}{A} N_{Pr}^{2/3} W_{A_c} \right)^2 + \left(\frac{N_{tu}}{A^2} A_c N_{Pr}^{2/3} W_A \right)^2 + \left(\frac{2}{3} \frac{N_{tu}}{A} A_c N_{Pr}^{-1/3} W_{N_{Pr}^{2/3}} \right)^2 \right]^{1/2}$$

$$\frac{W_j}{j} = \left[\left(\frac{W_{N_{tu}}}{N_{tu}} \right)^2 + \left(\frac{W_{A_c}}{A_c} \right)^2 + \left(\frac{W_A}{A} \right)^2 + \left(\frac{2}{3} \frac{W_{N_{Pr}^{2/3}}}{N_{Pr}^{2/3}} \right)^2 \right]^{1/2}$$

For Ntu = 3.0; λ = 0 etc:
$$\frac{W_j}{j} = 7.5\%$$

For Ntu - 25.0; λ = .05 etc:
$$\frac{W_j}{j} = 10.2\%$$

100

APPENDIX E

DIGITAL COMPUTER PROGRAM FOR DATA REDUCTION

Included herein is a computer program for a CDC 1604 digital computer. By means of this program all necessary calculations were made to produce the heat transfer and flow friction data appearing in the tables and graphs of this report.

A data reduction program was written by Bannon [1]. This program was then further sophisticated by Piersall [22], producing conduction parameter λ , maximum slope, and friction factor as well as other flow information from geometric and experimental data inputs.

The present program will now produce all necessary heat transfer and flow friction data in table form from a minimum of input. When data from the single-blow technique is processed, a curve-fitting interpolation subroutine is utilized to determine Ntu from maximum slope and conduction parameter. The input for this subroutine is Howard's [9] maximum slope data (Table VIII). For the cyclic technique, Ntu is determined from equation (2-33) by means of an iteration process.

The program will process data obtained by means of either the single-blow or cyclic technique and data from more than one matrix can be reduced in each computer run.

```
      PROGRAM NUELC B
5000  DIMENSION MRUN(50),D(50),C(50),CD(50),CCE(50),S(50),RT(50),F(50),
     1RF(50),E(50),H(50),TU(50),COL(50),R(50),CPA(16),TUN(51),SL(16,51),
     2T(51),LABEL(10)
      COMMCN CPA,TUN,SL
      READ 1,(CPA(I),I=1,16)
      READ 1,(TUN(I),I=1,51)
      READ 1,((SL(J,I),J=1,16),I=1,51)
    1 FORMAT(16F5.0)
      L=5
      K=1
   30 READ 301,LABEL
  301 FORMAT(10A8)
  311 READ 300,XML,AS,RH,POR,AC ,A  ,WM
  300 FORMAT(7F10.0)
  400 READ 400,EK,SK,CM,RATIO,N
  400 FORMAT(5F10.0,I2)
    C KC,KE FCR TRIANGULAR FINS LAMINAR FLCW NR UNDER 2000
  900 IF(RATIO-1.0)901,902,902
  901 XKC=1.0
      GO TO 903
  902 XKD=1.43
  903 CC =.611+.045*POR  +.34*(POR **5.7)
      CK =(1.-2.*CC+(CC*CC)*(2.*XKD)-1.))/(CC*CC)
      EK =1.-2.*XKC +POR **2.
  401 DO 704 M=1,N
   10 READ 7,CC,BETA,CS,ICVOLTS,CELPO,PO,CELH,HS,DTIME,DTEMP,TSPAN,ATMPFR,RB
    7 FORMAT(2F10.0,2F10.0,2F10.0,2F5.0)
    8 TEMPC=(TOVCLTS-0.608)*15.0/0.336+60.0
    9 SLC=DTEMP/(DTIME*TSPAN)
      P3=(ATMP-(PC/13.6))**.4912
      TO=TEMPO+459.7
      UFR=0.0395+0.64167E-4*TEMPO
      TB=TEMPO+10.0
      UH=0.0395+0.64167E-4*TB
```

```
11   IF(ABSF(BETA-.75)-.0000001)27,27,12
12   IF(ABSF(BETA-.64)-.0000001)26,26,13
13   IF(ABSF(BETA-.50)-.0000001)25,25,14
14   IF(ABSF(BETA-.40)-.0000001)24,24,15
15   IF(ABSF(BETA-.25)-.0000001)23,23,16
16   IF(ABSF(BETA-.15)-.0000001)22,22,17
17   GO TO 80
21   X2=0.59225
     DELX=0.01916
     ASSUM=0.6000
     GO TO 28
22   X2=0.59171
     DELX=0.01691
     ASSUM=0.6000
     GO TO 28
23   X2=0.59184
     DELX=0.01622
     ASSUM=0.6000
     GO TO 28
24   X2=0.59448
     DELX=0.01867
     ASSUM=0.6000
     GO TO 28
25   X2=0.59850
     DELX=0.02125
     ASSUM=0.6000
     GO TO 28
26   X2=0.60575
     DELX=0.02595
     ASSUM=0.6000
     GO TO 28
27   X2=0.60691
     DELX=0.03839
     ASSUM=0.6000
28   COR=ASSUM
     NC=0
331  B1=1./SQRTF(1.-EETA**4)
     NC=NC+1
29   IF(NC-4)29,29,60
     D(M)=589.81*CC*DO*SQRTF(DELPO*P3/TO)*CCR*B1
     RNUM=(4.961*C(M)/UFR)/EETA
     CORA=X2+DELX*SQRTF(1000C./RNUMO)
32   COR=CORA
     GO TO 331
60   PR=0.8017-.82353E-4*TEMFC
```

```
      C1=PR*AC /A
      CP=0.24
  615 RNUMP=5.09*C(M) /UFR
  616 RT(M)=(4.0*XML*C(M))/(A  *UH)
  617 RF(M)=RT(M)*UH/UFR
  618 C(M)=D(M)*CP/3600.0
  619 CAPS=WM*CM
  620 S(M)=(CAPS*SLC)/(C(M)*CS)
  621 CD(M)=(SK*AS)/(XML*D(M)*CP)
  622 CDE(M)=CD(M)*RATIO
      B=CK+EK
      C=1.0+PCR**2
  623 G=C(M)/(AC **36CC.0)
      CELP=DELH*.03613
      PS=HS*.03613
      PA=ATMP*.4912
      PT=PA-PS
      P2=PT-DELP
      PM=(P1+P2)/2.
      RHOM=(PM*144.0)/(53.3*(TEMPO+460.0))
      FF1=((64.4*RT+CM*CELP*144.0)/(G*G))
      FF2=(C*DELP/PM
      FF3=FF1-FF2-E
  624 F(M)=FF3*RH/XML
  625 CONST=COR*H1
  626 STDI=(0.02195*RT(M)*C1)/(4.**RH)
  627 E(M)=1.11E-7*(1.0/(4.**RT))**3*F(M)*(RF(M)/1000.)**3
      MRUN(M)=M
      CP=CCE(M)
      SM=S(M)
```

```
      IF(FR-.001)61,61,69
   69 EM=(D(M)*.24)/(WM*CM*6.2832*FR*3600.0)
      CALL CYCLE (RB,EM,P)
      TU(M)=P
   60 TO 702
   61    CALL  INTER(CP,SM,TU)
         TU(M)=TU
  702 COL(M)=C1*TU(M)
  704 R(M)=COL(M)/F(M)
  704 H(M)=STDH*TU(M)
  714 PRINT715,LABEL
 7150FORMAT(1H1,20X,10A8
     1,////,     120H RUN    MDOT        C AIR   LAMDA   LAMDA K    SLOPE
     2 NTU              NR    F-T   F FAN  NR      FR       J/F      E
     3H    //)
      DO 717 I=1,N
 7170PRINT 718,MRUN(I),C(I),CD(I),CDE(I),S(I) ,TU(I),CCL(I),RT(I),
     1F(I),RF(I),R(I),E(I),H(I)
 7180FORMAT(I3,F9.2,3F8.5,F10.5,F10.3,F9.5,F10.2,F8.5,F9.2,F9.5,F8.5,
     1F11.5)
  914 PRINT915
 9150FORMAT(1H1,
     160H           FRICTICN DATA                 HEAT TRANSFER DATA     ///
     260H                                        COND     MAX
     360H RUN            NR         F            PARAM     SLOPE    NTU     NR      J   //
     4)
      DO 919 I=1,N
  919 PRINT 920,MRUN(I),RF(I),F(I),CDE(I),S(I),TU(I),RT(I),COL(I)
  920 FORMAT(I3,F9.2,F7.5,F13.5,F8.5,F7.2,F9.2,F7.5)
  601 RO=WM/(AFR*XML)
  602 AD=A/(AFR*XML)
```

```fortran
603 PRINT 604,AFR,XML,RO,AC,AS,PCR,A ,RH,AD,RATIO
6040 FORMAT(//,37H FRCNTAL AREA              AFR        F10.5//
     1       37H FLCW LENGTH         L                F10.5///
     2       37H MATRIX DENSITY      LB/FT3           FF100.5///
     3       37H FREE FLCW AREA      AC               FF100.5///
     4       37H SCLID FRONTAL AREA  AS               FF100.5///
     5       37H PCRCSITY            POR              FF100.5///
     6       37H HEAT TRANSFER AREA  A                FF100.5///
     7       37H HYDRAULIC RACIUS    RH               FF10.5//
     8       37H AREA DENSITY (A/VM)                  F10.5
     9       37H CCNCUCTION PARAMETER RATIC (RS/RK)            )
905 PRINT 906,SK,CM,CK,EK
9060 FORMAT(//,37H THERMAL CCNDUCTIVITY     KS        F1C.2
     1       37H MATRIX HEAT CAPACITY     CS        FF10.4
     2       ///,37H ENTRANCE PRESS.LOSS COEF. KC       FF10.5
     3       ///,37H EXIT PRESSURE .LOSS COEF. KE       FF10.5 )
607 K=K+1
608 IF(L-K)20,30,30
 80 PRINT 81,K
 81 FORMAT(1H1,17H BETA ERRCR RUN  ,I2 )
 82 BETA=0.5
 83 GO TO 25
 20 STOP
    END
    SUBROUTINE CYCLE (RB, EM, P)
    COMMON RB, EM, P
    P = 0.0
 62 RC = EXPF(-P/(1.0+(EM*P)**2))
    IF(RC-RB)64,64,63
 63 P = P + .002
    60 TO 62
 64 RETURN
    END
```

INITIAL DISTRIBUTION LIST

No. Copies

1. Defense Documentation Center   20
   Cameron Station
   Alexandria, Virginia 22314

2. Library   2
   U. S. Naval Postgraduate School
   Monterey, California

3. Naval Ship Systems Command   1
   Navy Department
   Washington, D. C. 20360

4. LT Stuart F. Ball, Jr, USN   1
   Ship Repair Facility
   Box 34
   FPO
   San Francisco, Calif. 96650

5. Prof. P. F. Pucci   10
   Mechanical Engineering Department
   U. S. Naval Postgraduate School
   Monterey, California

DOCUMENT CONTROL DATA - R&D

(Security classification of title, body of abstract and indexing annotation must be entered when the overall report is classified)

1. ORIGINATING ACTIVITY (Corporate author)	2a. REPORT SECURITY CLASSIFICATION
U. S. NAVAL POSTGRADUATE SCHOOL MONTEREY, CALIFORNIA	Unclassified
	2b. GROUP N.A.

3. REPORT TITLE

Experimental Determination of Heat Transfer and Flow Friction Characteristics for Several Plate Fin Type Compact Heat Exchanger Surfaces

4. DESCRIPTIVE NOTES (Type of report and inclusive dates)
N.A.

5. AUTHOR(S) (Last name, first name, initial)

BALL, Stuart Franklin, Jr., LT, USN

6. REPORT DATE	7a. TOTAL NO. OF PAGES	7b. NO. OF REFS
May 1966	110	29

8a. CONTRACT OR GRANT NO. N.A.	9a. ORIGINATOR'S REPORT NUMBER(S) N.A.
b. PROJECT NO.	
c. N.A.	9b. OTHER REPORT NO(S) (Any other numbers that may be assigned this report) N.A.
d.	

10. AVAILABILITY/LIMITATION NOTICES

~~Qualified requesters may obtain copies of this report from DDC~~ *Npunuhen 199/68*

This document has been approved for public release and sale; its distribution is unlimited

11. SUPPLEMENTARY NOTES N.A.	12. SPONSORING MILITARY ACTIVITY U. S. Navy

13. ABSTRACT

In this report, the heat transfer and isothermal flow friction characteristics for seven compact heat exchanger surfaces are presented and compared. Five of the surfaces were of a similar triangular fin configuration, differing in material and method of construction, and two of the surfaces, having been tested previously, were of a modified rectangular passage configuration. The modified rectangular passage surfaces showed better overall performance than the triangular fin surfaces, and matrices constructed from perforated material showed better overall performance than similar surfaces constructed from non-perforated material. For similar matric configurations, small variations in manufacturing procedure had little effect upon heat transfer and flow friction performance.

The heat transfer data was obtained by means of the single-blow transient testing technique. A cyl&c method of transient testing was also investigated, and found to be both reliable and useful in that the additional method of testing extends the Reynolds number range for the experimental apparatus.

DD FORM 1 JAN 64 **1473**

14. KEY WORDS	LINK A		LINK B		LINK C	
	ROLE	WT	ROLE	WT	ROLE	WT
Compact Heat Exchangers Heat Transfer Characteristics for Compact Heat Exchangers Transient testing techniques for compact Heat Exchangers						

INSTRUCTIONS

1. ORIGINATING ACTIVITY: Enter the name and address of the contractor, subcontractor, grantee, Department of Defense activity or other organization (corporate author) issuing the report.

2a. REPORT SECURITY CLASSIFICATION: Enter the overall security classification of the report. Indicate whether "Restricted Data" is included. Marking is to be in accordance with appropriate security regulations.

2b. GROUP: Automatic downgrading is specified in DoD Directive 5200.10 and Armed Forces Industrial Manual. Enter the group number. Also, when applicable, show that optional markings have been used for Group 3 and Group 4 as authorized.

3. REPORT TITLE: Enter the complete report title in all capital letters. Titles in all cases should be unclassified. If a meaningful title cannot be selected without classification, show title classification in all capitals in parenthesis immediately following the title.

4. DESCRIPTIVE NOTES: If appropriate, enter the type of report, e.g., interim, progress, summary, annual, or final. Give the inclusive dates when a specific reporting period is covered.

5. AUTHOR(S): Enter the name(s) of author(s) as shown on or in the report. Enter last name, first name, middle initial. If military, show rank and branch of service. The name of the principal author is an absolute minimum requirement.

6. REPORT DATE: Enter the date of the report as day, month, year; or month, year. If more than one date appears on the report, use date of publication.

7a. TOTAL NUMBER OF PAGES: The total page count should follow normal pagination procedures, i.e., enter the number of pages containing information.

7b. NUMBER OF REFERENCES: Enter the total number of references cited in the report.

8a. CONTRACT OR GRANT NUMBER: If appropriate, enter the applicable number of the contract or grant under which the report was written.

8b, 8c, & 8d. PROJECT NUMBER: Enter the appropriate military department identification, such as project number, subproject number, system numbers, task number, etc.

9a. ORIGINATOR'S REPORT NUMBER(S): Enter the official report number by which the document will be identified and controlled by the originating activity. This number must be unique to this report.

9b. OTHER REPORT NUMBER(S): If the report has been assigned any other report numbers (either by the originator or by the sponsor), also enter this number(s).

10. AVAILABILITY/LIMITATION NOTICES: Enter any limitations on further dissemination of the report, other than those imposed by security classification, using standard statements such as:

(1) "Qualified requesters may obtain copies of this report from DDC."

(2) "Foreign announcement and dissemination of this report by DDC is not authorized."

(3) "U. S. Government agencies may obtain copies of this report directly from DDC. Other qualified DDC users shall request through

_____."

(4) "U. S. military agencies may obtain copies of this report directly from DDC. Other qualified users shall request through

_____."

(5) "All distribution of this report is controlled. Qualified DDC users shall request through

_____."

If the report has been furnished to the Office of Technical Services, Department of Commerce, for sale to the public, indicate this fact and enter the price, if known.

11. SUPPLEMENTARY NOTES: Use for additional explanatory notes.

12. SPONSORING MILITARY ACTIVITY: Enter the name of the departmental project office or laboratory sponsoring (paying for) the research and development. Include address.

13. ABSTRACT: Enter an abstract giving a brief and factual summary of the document indicative of the report, even though it may also appear elsewhere in the body of the technical report. If additional space is required, a continuation sheet shall be attached.

It is highly desirable that the abstract of classified reports be unclassified. Each paragraph of the abstract shall end with an indication of the military security classification of the information in the paragraph, represented as (TS), (S), (C), or (U).

There is no limitation on the length of the abstract. However, the suggested length is from 150 to 225 words.

14. KEY WORDS: Key words are technically meaningful terms or short phrases that characterize a report and may be used as index entries for cataloging the report. Key words must be selected so that no security classification is required. Identifiers, such as equipment model designation, trade name, military project code name, geographic location, may be used as key words but will be followed by an indication of technical context. The assignment of links, roles, and weights is optional.